An experimental comparison of thermal-mechanical properties of freshwater and saline ice in Arctic environments

Elizabeth Jean McMaster   December 15, 2021

TUDelft   NTNU   EWEM   UNIS
The University Centre in Svalbard

An experimental comparison of thermal-mechanical properties of freshwater and saline ice in Arctic environments

by

Elizabeth Jean McMaster

This report is submitted to obtain the degrees of
Master of Science in Offshore Engineering at Delft University of Technology
&
Master of Science in Wind Energy Technology at Norwegian University of Science and Technology,
under the **European Wind Energy Master** programme.

To be defended publicly on December 21, 2021.

Faculty of Mechanical, Maritime and Materials Engineering, Delft University of Technology
Department of Civil and Environmental Engineering, Norwegian University of Science and Technology

Project duration:	January 15, 2021 – December 15, 2021		
Thesis committee:	Prof. Dr. A. Marchenko	UNIS	Supervisor
	Prof. Dr. K. V. Høyland	NTNU	Supervisor
	Prof. Dr. H. Hendrikse	TU Delft	Supervisor
	Prof. J. Hoving	TU Delft	Examiner
	Dr. P. O. Moslet	Dr.techn	External Censor

An electronic version of this thesis is available at `http://repository.tudelft.nl/`.

Abstract

Thermal ice pressure is one of the eight ice loads to consider for the support structure design of bottom-fixed offshore wind turbines defined by international standard IEC 614000-3-1. Temperature changes in ice drive its deformation and cause structures restricting expansion to experience loading. The effective coefficient of thermal expansion (ECTE) can be used to quantify the difference in sea versus fresh ice behavior under thermal action. Since the thermal expansion of fresh ice is generally well understood, fresh ice thermal expansion experiments can be compared to sea ice, which has a more complex structure consisting of a solid ice matrix containing liquid and gas. Fiber Bragg Grating (FBG) strain and temperature sensors enabled measurements of thermal expansion in fresh and saline ice samples under different boundary conditions in the cold laboratory. Experiments were compared amongst fresh and saline ice samples for three distinct applied thermal actions: air temperature change, floating in water, and flooding the ice surface. Fieldwork on fresh and sea ice under the same meteorological conditions was performed to compare thermal stresses. The thermal expansion air experiments yielded no significant differences in ECTE values for fresh, granular, and columnar saline ice. However, it was observed during the unconfined ice floating experiments that granular saline ice resulted in a larger ECTE than fresh ice. Negative values for ECTE were obtained for columnar sea ice air temperature change experiments and during granular saline ice floating experiments, both occurring during heating cycles. Flooding experiments described the thermal response of latent heat release during water freezing on the ice surface, and it was observed that fresh ice showed stronger hysteresis in results than saline ice. Thermal stresses monitored for approximately one month during winter in the Vallunden lake sea ice attached to Van Mijenfjorden and in a nearby freshwater lake demonstrated higher values for fresh ice than sea ice and increased over the depth for both ice sheets which experienced the same meteorological conditions.

i

Acknowledgements

Contents

List of Tables

List of Figures

1

Introduction

1.1. Industry Relevance

Saline and fresh ice expands and contracts when experiencing heating and cooling, respectively. This thermally initiated alteration in ice volume occurs on rivers, seas, lakes, and reservoirs and can cause loading on man-made structures, which is applicable for civil engineering design. Recent development in the Arctic, as well as offshore structures such as wind turbines in cold-climate regions, demand critical analysis of ice actions during the design process. Thermal expansion loading from ice is recognized as a necessary design criterion by international standards, including IEC 614000-3-1 [4] for fixed offshore wind turbines, and ISO 19906 [1] for Arctic infrastructure.

The demand for renewable energy is rapidly growing, and offshore wind energy is becoming an increasingly profitable solution [24]. Wind energy projects are developing in colder regions due to their high wind potential and space availability [7]. When the offshore wind energy industry moves towards cold regions such as the Baltic Sea, ice loads become the main technological challenge for the foundation design [34]. Understanding ice thermo-mechanical properties for ice loads assessment is necessary for offshore wind turbine foundation longevity in waters susceptible to ice-cover. The effect of ice loads and icing on wind turbines in cold climate regions is a significant issue for the industry [7]. By expanding international standards on ice actions on structures, such as thermal expansion loading, ice-induced design loads on wind turbine foundations can be more comprehensively understood.

An additional industrial application of this work is maritime transport in ice-covered waters. Ice in Arctic regions is experiencing rapid melting in recent years due to climate change [32]. Maritime routes are opening up for part of the year, where solid ice previously blocked the channels year-round. These routes offer quicker shipping times, and hence greater resource availability [23], than conventional routes such as the Suez Canal route. Understanding the design loads on maritime vessels traveling through Arctic regions as the ice starts to melt will be crucial in this transportation transition.

1.2. Fixed Offshore Wind Turbine Design Standard, IEC 614000-3-1

According to the International Electrotechnical Commission standard IEC 614000-3-1:2019 [4] standard, thermal ice pressure is one of the eight ice loads to consider for the support structure design of fixed offshore wind turbines. Appendix D of the standard states fast ice cover can exert a horizontal load caused by temperature fluctuations on the support structure. Applicable locations for this thermal loading include lakes and brackish seas, and the standard remarks ice pressure in open seas with higher salinity levels, such as the North Sea, can be neglected. The important support parameter for the ultimate limit state design from thermal ice loads (DLC D1) is the unit force acting on the width of the support structure, which is mentioned to be 300 kN/m for both standalone support structures or for peripheral support structures in a wind farm [4].

1.3. Arctic Offshore Structures Standard, ISO 19906

The International Organization for Standardization's ISO 19906:2010 outlines the design requirements for offshore structures constructed in Arctic and cold regions, subject to sea ice, iceberg, and icing phenomena. Section A.8.2.4.11 of the standard describes potential thermal action effects on structures. Field measurements in the Russian and Canadian seas were conducted, concluding sea ice does not expand appreciably for ice temperatures warmer than -10°C corresponding to salinities higher than 3 ppt or above -7°C for salinities higher than 1 ppt [1]. Thermal actions for fresh ice are stated to be higher in magnitude than sea ice loads. Greater details on sea and fresh ice thermal expansion could be added to improve the content of the ISO19906 standard, such as a range of ice pressure conditions resulting from temperature fluctuations for the ultimate limit state design of arctic offshore structures.

1.4. Report Objectives

The research question motivating this study is: how do thermal deformations compare for fresh and saline ice caused by thermal actions of different types? In order to reach this goal, the following objectives were created for this study:

- Provide an overview of past research on thermal expansion of sea and fresh ice and introduce why further experiments are needed.

- Compare thermal deformations measured in laboratory experiments where thermal actions were performed by controlled air temperature changes for saline and fresh ice samples.

- Compare thermal deformations measured in laboratory experiments where thermal actions are initiated by unconfined ice floating in water for saline and fresh ice samples.

- Compare thermal deformations measured in laboratory experiments where thermal actions were performed by water flooding on the ice surface for saline and fresh ice samples.

- Compare thermal stresses measured in fieldwork experiments for freshwater lake ice and saline lagoon ice in close proximity with similar meteorological conditions.

- Build a finite element model in COMSOL Multiphysics for select cold laboratory tests to confirm thermal expansion measurement results.

Overall, the laboratory experiments where the ice is resting on a table exposed to air on all sides should give an answer as to how much fresh ice deforms compared to saline ice over a certain time when the air temperature changes. Experiments with unconfined floating ice should give the answer to the same question, but when the ice has different boundary conditions. When ice is floating, it is only exposed to air temperature change from the top surface exposed to air, and the bottom surface of the ice equates to the freezing point. Experiments where ice is flooded with water on the surface aim to compare fresh and saline ice deformations when air temperature is constant and thermal action is caused by the radiation of latent heat due to the water freezing at the surface. This answer is not yet known or accepted in the field. The fieldwork is related to quantifying the difference in confined sea and fresh ice thermal stresses in the Vallunden lake attached to Van Mijenfjorden and in a nearby freshwater lake with the same meteorological conditions.

1.5. Limitations

Adjustments to the initial plan of laboratory experiments were required after UNIS Cold Laboratories 2 and 3 became inoperable towards the end of the study. The software used to control the temperature in the laboratories became inoperable and took several months to replace. The original plan consisted of testing the saline ice brought back from Svea in Cold Lab 2, which houses the water tank, however COVID-19 related travel limitations prevented regular trips to Svea from occurring. Therefore, floating ice experiments could not be performed for the Svea columnar saline ice. Experiments took place in Cold Lab 4 to compromise, which did not have a water tank for floating ice experiments. Freshwater ice was also not brought back from Svea for any laboratory testing to due to lack of time on the fieldwork site.

1.6. Structure of the Report

The report is structured as follows: Chapter 2 gives an introduction to the background of thermal expansion experiments for fresh and sea ice, as well as the theory behind current measurement techniques used in the laboratory experiments. Chapter 3 presents the methodology for the laboratory and fieldwork experiments as well as the specifications for building the COMSOL finite element model. Chapter 4 outlines the results achieved from the cold laboratory experiments, the fieldwork, and the theoretical model. Chapter 5 summarizes the meaning of the results and analyzes areas for future work to develop the understanding of sea and fresh ice thermal expansion.

<div style="text-align: right; font-size: 3em;">2</div>

Background and Theory

2.1. Previous Work

In this section, the literature on thermal expansion experiments of saline and freshwater ice is reviewed to understand the current motive behind the stated research objectives of this work. Different research approaches are discussed to measure thermal expansion. Research gaps and remaining questions in past thermal expansion experimental techniques are identified in order to motivate the research objectives of this work.

2.1.1. Fresh ice thermal expansion

Thermal expansion of the hexagonal freshwater ice (Ih) has been extensively studied in the 20th century with dilatometric and X-ray techniques [30].

Jakob & Erk, 1929

The works of Jakob & Erk [9] contained one of the first accurate calculations of linear thermal expansion of freshwater ice. The experiment utilized a dilatometer to measure expansion of polycrystalline ice cylinders frozen externally and radially in paper tubes from a large temperature range of 0 to -250°C. The orientation of the polycrystalline ice was unknown at the time of the experiment. The results obtained from the fresh ice thermal expansion experiments are displayed in Table 2.1.

T [°C]	LCTE [$\times 10^{-6}$ 1/°C]
0	**52.7**
-100	33.9
-200	0.8
-250	-6.1

Table 2.1: Results obtained from Jakob & Erk's dilatometrically measured fresh ice thermal expansion experiments. [9]

From the results, it can be observed that negative linear coefficients of thermal expansion (LCTE) were found at low temperatures less than -200°C, and LCTE decreases as the temperature cools. The LCTE for 0°C is highlighted in Table 2.1 because it is the most relevant obtained result for the temperature ranges used in this thesis report.

Butkovich, 1959

Performed in the cold laboratories of USA SIPRE in Wilmette, Illinois, thermal expansion experiments on fresh ice were conducted by Butkovich in 1959 [3]. Butkovich utilized a Statham displacement transducer calibrated with a fused quartz rod to conduct his experiments with a narrower temperature variation of 0 to -30°C. Butkovich's goal of the tests was to find the influence of crystal orientation on single and polycrystalline ice thermal expansion and experiments were hence performed on a multitude of artificial and natural ice samples. The obtained values displayed a general trend of decreasing LCTE

as the temperature also decreased and concluded a mean LCTE value of 52.52×10⁻⁶ 1/°C for 0°C temperatures, agreeing with the results of the same applied temperature from Jakob & Erk [9]. Another notable conclusion from this work is that the thermal expansion coefficient of ice samples reduces over the duration of additional runs on the same sample. Butkovich analyzed the potential explanations for this result observation to be either deformation due to stresses on the sample, or the creation of lattice vacancies in the ice structure but inferred further research was required to prove these conditions.

Lonsdale, 1958, Hamblin, 1958, and La Placa & Post, 1960

Lonsdale [14] attempted prove that Ih ice displays a more anisotropic thermal expansion behavior at decreasing temperatures. The results also proclaimed that the c-axis ice thermal expansion is less than the expansion along the a-axis of the crystalline structure, deviating from measurements from various dilatometric thermal expansion experiments. One such dilatometric experiment on bulk ice was conducted by Hamblin and reported by Powell in 1958 [28]. This experiment agreed with the results of Jakob & Erk [9] and Butkovich [3], who also worked with monocrystilline ice. Although Butkovich did not find any notable anistophy in his ice thermal expansion experiments, Hamblin reported a small anistrophy in the thermal expansion, as α_c measured larger than α_a.

Lonsdale's unprecedented finding led to a reevaluation from La Placa & Post [12], who conducted ice thermal expansion estimations on a diffractometer modified to operate at low temperatures. This X-ray technique used a powder ice crystal sample to measure diffraction. Temperatures ranged in the experiment from -180°C to -10°C and results found anomalous behavior at around -150°C (displayed in Figure 2.1 around 125 K), but otherwise confirmed similar values indeed exist for different experimental methods: X-ray diffraction and previously conducted dilatometric determinations [3] of ice thermal expansion.

Röttger et al., 1994

Röttger et al. [30] employed a synchrotron radiation to achieve ice crystal powder diffraction to examine the thermal expansion of H_2O and D_2O (heavy water) isotopes. Temperature ranges of -260°C to -8°C were implemented in the experiments, and the ice LCTE demonstrated a strong temperature dependency. Negligible anistrophy was found in the expansion comparisons, agreeing with the results of Butkovich [3], but contradicting the findings of Hamblin, reported by Powell [28], bringing the conclusion that there may be discrepancies of measurement techniques used (X-ray and dilatometric) and thus the anistrophy of thermal expansion of ice requires further research. An estimated error margin for determining ice LCTE of 4×10⁻⁷/°C was reported for measured variables, but the actual variation between runs was recorded to an even greater magnitude, 2×10⁻⁶/°C. In temperatures lower than -200°C (alternatively 73 K as displayed in Figure 2.1), negative LCTE were found for both the H_2O and D_2O isotopes, consistent with the works of Jakob & Erk [9].
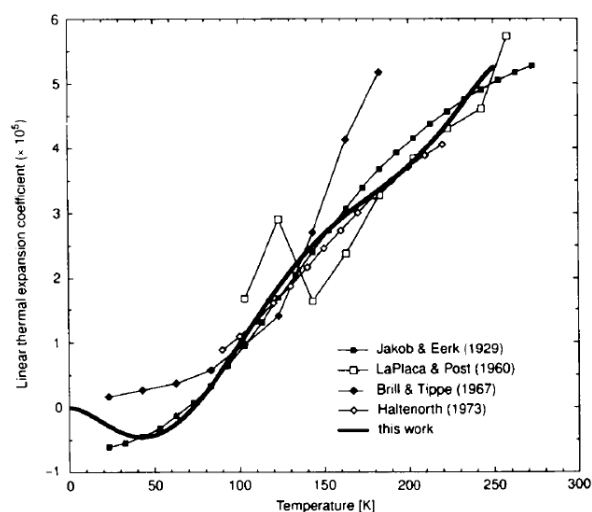
Figure 2.1: Comparison of Röttger et al. LCTE results to previous work for different temperatures [30].

2.1.2. Saline ice thermal expansion

Sea ice, unlike fresh ice, is a composite material consisting of a solid ice matrix with liquid and gas inclusions [19]. Pure ice grains aligned in columns or platelets, and brine pockets and channels are the components of sea ice. Brine can migrate through the porous channels in sea ice when pressure is applied, changing the structure of sea ice under the action of thermal and mechanical loads [22]. When cooling temperatures occur, brine can solidify into ice, and ice can yield water when heated, altering the permeability of the ice. These phase changes can lead to atypical behavior in thermal expansion for sea ice since, when brine freezes, the density of the ice is reduced, as sea ice is less dense than water. Thus in contrast to freshwater ice, sea ice can expand when cooled and contract when heated. A summary of supporting literature to lead to current sea ice thermomechanical property understandings is presented in this section.

Pettersson, 1883, and Malmgren, 1927
The coefficients of sea ice thermal expansion were first identified from laboratory experiments conducted at the same university by Pettersson [26] in 1883 and Malmgren [16] in 1927. The method utilized to obtain results consisted of submerging a saline ice block in a liquid and calculating the difference in liquid volume while the temperature of the ice block altered. Malmgren assumed the ice is impermeable, where all brine stayed confined in the sample. The difference in the volume of the liquid was used to find thermal expansion coefficients for sea ice. Johnson and Metzner [10] later point out that this experimental approach does not account for the chance that brine and air may be discharged into the enclosing liquid, and that the enclosing fluid may be forced into the sample, affecting the thermal expansion coefficient calculation. The saline ice thermal expansion coefficients were found by Malmgren to be larger compared to freshwater ice and can be either negative or positive, depending on the temperature and salinity of the sample [16].

The saline ice thermal expansion coefficients determined by Petterson and Malmgren in laboratory conditions were found to be higher than the first field measurements of linear coefficients of thermal expansion determined by Legenkov and Uglev (reported by Doronin and Kheisin [6] in 1977). The difference in results was due to narrow changes in ice temperature and the time lag in the temperature changes in the field work. The field measurements also found salinity changes with depth for the ice floe considered in the analysis, which also caused their calculated thermal coefficients to be lower than Pettersson's and Malmgren's. Hence, Doronin and Kheisin reported deeper ice layers opposed the thermal deformation of the higher layers, and vice-versa [6].

Cox 1983
Cox [5] added onto Malmgren's assumption that all brine stayed enclosed in the ice sample, but treated the ice as infinitely permeable. Unlike the assumption in Malmgren's work, Cox assumed the components of sea ice, brine and fresh ice, act independently of each other, having no effect on the thermal expansion coefficient. In addition, Cox concluded coefficients of thermal volume expansion for saline ice must be equal to freshwater ice coefficients for all types of temperature changes, around 1.5×10^{-4} K^{-1}. The approach used by Cox [5] did not include sufficient supporting measurements to disprove Petterson's [26] and Malmgren's [16] results at the time of publication. However, Johnson and Metzer [10] later determined thermal linear expansion coefficients for saline ice samples to further test Cox's 1983 investigation.

Johnson and Metzner, 1990
Johnson and Metzner [10] measured the linear thermal expansion coefficients of sea ice from cylindrical samples from first-year ice in Harrison Bay, Alaska. The dimensions of the cylindrical ice samples were both 38 mm in diameter, with distinct lengths corresponding to different salinity values. For the ice samples with 2 ppt, the sample was 71.25 mm in length, and for 4 ppt ice, 69.33 mm in length. The experiments, utilizing an interferometer and temperature control unit, achieved accepted results for the coefficient of thermal expansion for sea ice: 5×10^{-5}/°C. This result was notably comparable to the freshwater ice coefficient of thermal expansion. The sample with 4 ppt salinity demonstrated a lag in temperature change when the temperature decreased then increased, which occurred subsequent to the original temperature increase experiment, confirming experimental hysteresis. This phenomenon was also observed in the experiments of Butkovich [3], where freshwater ice samples exhibited lower thermal expansion coefficient values over the duration of ensuing tests. The works of Johnson and

Metzner ultimately disproved the results of Pettersson [26] and Malmgren's experiments [16], and confirmed the analytical description of Cox [5], which predicted similarity in the coefficients of thermal expansion for sea ice and freshwater ice. The hystersis during temperature cycling, due to thermal ice-stress-related dislocation movement, was concluded to require future examination.

Marchenko, 2012 to 2018
In years 2012 to 2018, a wide range of experiments on the thermal-mechanical properties of sea ice have been conducted in cold laboratories in the University Centre in Svalbard in northernmost Norway, and the University College London in the UK [13, 17–20, 22, 33]. The methodical studies can now test samples with greater dimensions and in various size configurations. In addition, floating samples submerged in water can now be analyzed. An adaptable experiment methodology was implemented to achieve these new research capabilities, consisting of Fiber Bragg Gratings-based fiber optic strain and temperature sensors, rendering a state-of-the-art research technology to examine ice thermal expansion.

In 2016, Marchenko [22] analyzed the thermal expansion of sea ice induced by the movement of fluid brine within the ice, and created a theoretical model of the process. The model assumed deformation in the ice sample will occur as temperature varies, due to the process of closed brine pockets eventually converting into permeable brine channels. Cold laboratory experiments with FBG sensor technology were performed on sea and fresh ice. By comparing the laboratory experiments to the model forecasts, results confirmed ice samples with 6 ppt, 8 ppt, and 9.4 ppt had negative thermal expansion coefficients, and the sample with less salinity demonstrated a positive coefficient. Ice samples experienced unconventional thermal expansion behavior, contracting during warming, when temperatures warmed more than -8°C for 6 ppt and 8 ppt ice and -11°C for 9.4 ppt ice [22]. Also recognized by Butkovich [3] and Johnson and Metzner [10], hysteresis effects were witnessed during thermal expansion when the temperature was increased then decreased.

Results additionally concluded ice confinement can influence the coefficient of thermal expansion. Specifically when ice is submerged in water, floating in a tank, and growing ice freezes to the tank walls, hence causing confinement as the ice is unable to expand horizontally. The ice, therefore, is in a state of compression within the four tank walls when expanding, initiating deformation in the sample. In this case, water below the confined ice exerts pressure on the bottom of the sample, pushing the brine migration upwards. In actual conditions such as tidal changes, confined sea ice can also experience pressure from the water underneath the ice when it is constrained and cannot simply move vertically, as it would if unconfined. Hence, unconfined floating ice experiments need to be performed without ice freezing to the tanks walls.

The confined floating ice experiment results additionally concluded normal (positive) thermal expansion behavior: sea ice expanded when heated. The process of vertical brine migration is responsible for this effect: the brine located at the base of the ice layer, where the ice temperature is the greatest, causes the surface layers of the ice to increase in temperature when the brine moves upwards. The brine at the base of the sample is of similar temperature to the encompassing ice due to the brine and ice being in a state of thermodynamic equilibrium. The conclusion is that thermal expansion in the sea ice will occur if brine migrates upwards, creating a vertical temperature gradient in the ice.

2.2. Theory

This section of this thesis focuses on the theory behind the laboratory measuring techniques used to determine ice thermal expansion. The report audience is assumed to be technically well-versed in ice physics and rheology, heat transfer and thermodynamics. Background information on the thermodynamics necessary to understand this report can be found in *Introduction to Heat Transfer* [2]. *The Physics of Ice* [27] gives a comprehensive overview of the mechanical and thermal properties of sea and fresh ice.

2.2.1. FBG sensors for strain and temperature measurement

The experimental technique in this work to calculate thermal expansion of ice utilizes Fiber Bragg Grating sensors to measure temperature and strain. The FBG system was designed by Advance Optic Solutions GmbH in Germany. When undisturbed, the sensors represent a periodic fluctuation in the refractive index of the optical fiber core from exposure to two interfering UV laser beams [11]. When the index modulates, the distributed grating pattern on the fiber reflects part of the propagating light wave on the core back to the UV origin [22] as demonstrated in Figure 2.2. Outputted in wavelength domain, the stain or temperature readings along the distance of the optical sensor is registered as modifications in the spectra reflected [29]. The reflected light waves interfere constructively when the fiber is undisturbed (without any non-uniform strain or temperature changes). The wavelength of the reflected light is expressed as:

$$\lambda_B = 2n_{eff}\Delta, \tag{2.1}$$

where λ_B corresponds to the Bragg wavelength, n_{eff} the effective refractive index of the optical fiber core, and Δ the period of the grating [11]. When the fiber core is either experiencing strain or compression, the Bragg wavelength will output a different value, while the effective refractive index corresponds to the properties of the material which are highly dependent on temperature variation. Hence, the wavelength dependency of temperature with regards to thermal and mechanical loads allows FBG sensors to measure strain and temperature accurately [25].
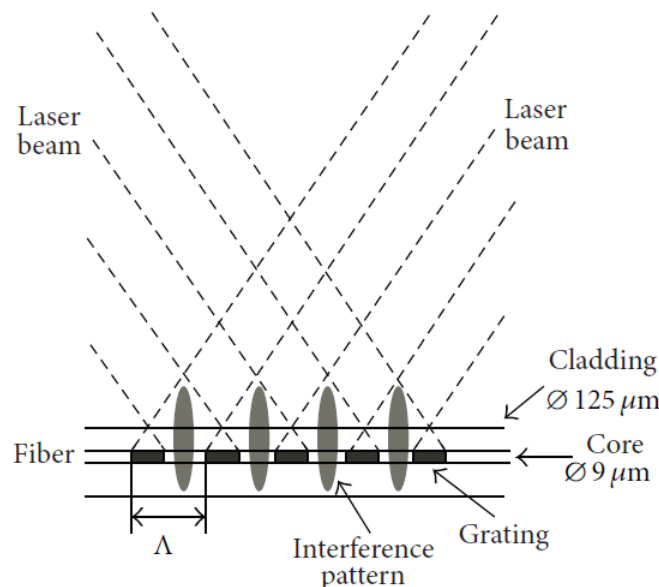
Figure 2.2: UV light source interference schematic for a FBG optical sensor [22]

In contrast to previously discussed dilatometer measurement techniques, FBG sensors can be installed directly into the ice sample, allowing for larger sample sizes and geometries [22]. Any deviation in axial strain or temperature along the sensor length will issue a deviation in the period of the grating, hence changing the Bragg wavelength [29].

2.2.2. ECTE calculation

The optical FBG strain sensors measure the Bragg wavelength, and the temperature is directly measured with a thermistor string consisting of twelve evenly spaced temperature sensors. Thermal expansion depends on local temperature, as the change in temperatures at different depths along the cross section of the ice has different expansions [15], requring the thermistor string sensor. A thermistor string and strain sensor can be used together to measure thermal expansion of ice. Any ice temperature variation causes a change of thermal stress. The resolution for stain measurements in FBG sensors is in the order of 10^{-6} with an accuracy of $5 \cdot 10^{-6}$, comparable to the resolution of the X-ray measuring technique implemented by Röttger [30] and the dilatometer used by Johnson and Metzer [10].

FBG sensors can measure the temperature, T, and linear deformation, ϵ_L of the samples over time [22]. The linear deformation, or strain, is defined as:

$$\epsilon_L = \frac{L - L_0}{L_0},$$ (2.2)

where L is the new length of the sample, L_0 is the initial length of the sample, and t is the time. The effective coefficient of linear thermal expansion (ECTE) of a saline ice sample can be found with the following formula:

$$\kappa_{si,L} = \frac{d\epsilon_L}{dt} \left(\frac{dT}{dt} \right)^{-1},$$ (2.3)

where the temperature is measured at a point inside the sample. However, temperature gradients within the sample can make it difficult and inaccurate to analyze just a single point for this calculation. Thus, the temperature should be read with a thermistor string at several points within the ice sample in order to accurately represent the temperature gradient over the sample [22].

The relation of strain to thermal expansion can be equated as:

$$\epsilon = \frac{\Delta L}{L} = \frac{\Delta \lambda}{\lambda} \frac{1}{GF} - \frac{TK\Delta T}{GF},$$ (2.4)

where GF is the gauge factor from the FBG sensors and is equal to 0.719, TK is the linear temperature coefficient, equal to $5.5 \cdot 10^{-6}$, which are both constants achieved from FBG sensors calibration [22]. The variation of the peak wavelength, $\Delta \lambda$ is found with a spectrometer that receives the reflected signal from the FBG sensor. The temperature change, ΔT, should be measured at the strain sensor's position with a temperature sensor in each block of ice.

The effective linear temperature coefficient can be calculated from the formula:

$$ECTE = \frac{1}{L} \frac{dL}{dT},$$ (2.5)

after the strain and change in temperature is found from data processing.

3

Methods

This chapter is divided into three sections, outlining the steps taken to complete the cold laboratory experiments, fieldwork, and COMSOL numerical modeling.

3.1. Cold laboratory experimental design

The fresh and saline ice thermal expansion experiments were conducted in the Cold Laboratory at the University Centre in Svalbard (UNIS). Administered in the same cold laboratory, the experimental methods of Marchenko (2016) [22] inspired the laboratory procedures in this report. There were three main experiments conducted for the purpose of this analysis:

- Air temperature change experiments

- Floating unconfined ice experiments

- Ice flooding experiments

The air temperature change experiments were conducted with columnar fresh ice, columnar sea ice, and granular saline ice. Whereas the floating unconfined ice experiments were conducted with columnar fresh ice and granular saline ice. Granular saline ice was used in the floating tests rather than columnar sea ice due to collection limitations.

3.2. Air temperature change experiments

The purpose of this experiment was to have a controlled ice sample stationary on a table subject to air temperature changes to compare to the floating ice sample in the same environment and temperature changes. The experiment was performed with both fresh and saline ice, using the same sensor installation setup. Figure 3.1 illustrates the experimental setup for the fresh ice sample.
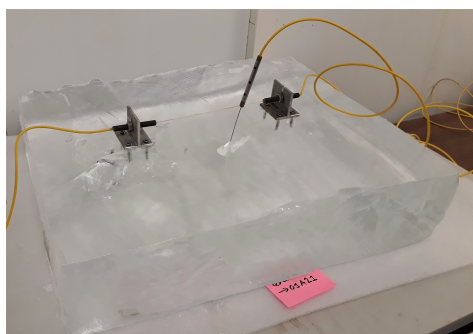
(a) Experimental lab setup with a strain and temperature sensor installed on the fresh ice sample
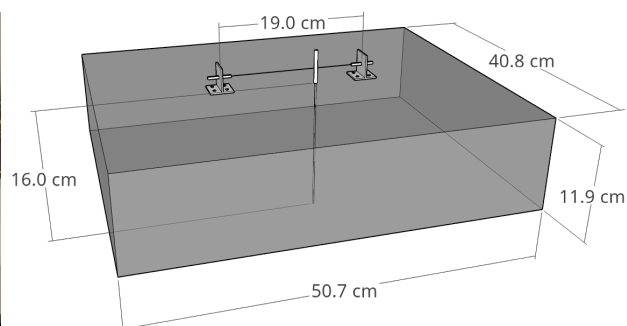
(b) Fresh ice sample and sensor setup modelled for illustration purposes. The thermistor string measured 16 cm in length.

Figure 3.1: Fresh ice air temperature change thermal expansion experimental set-up

3.2.1. Collection of ice Samples: fresh ice

Fresh ice samples were retrieved from a freshwater lake near Mine 7 (Gruve 7 in Figure 3.2) at the end of January 2021. The lake was chosen due to its close proximity to the UNIS cold laboratory in Longyearbyen.
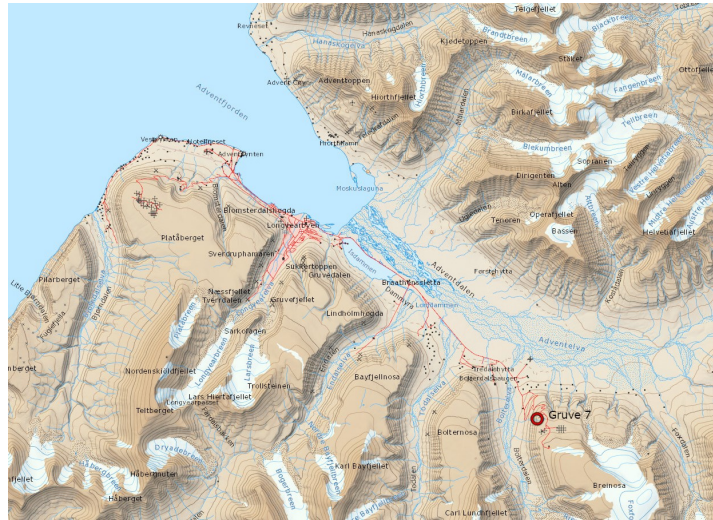
Figure 3.2: Location of the fresh ice sample extraction: a freshwater lake next to Mine 7 (Gruve 7)

Ice samples were taken out of the lake by cutting out pieces with a chainsaw as shown in Figure 3.3. First, a pit was made, then pieces were cut out by sawing the edges and then making an undercut. The undercut method is demonstrated in Figure 3.3b.

(a) Creating initial pit to retrieve freshwater ice samples

(b) Chainsaw undercut method

Figure 3.3: Fresh ice sample collection for the air temperature change thermal expansion experiments

The ice samples were strapped directly onto a sled used for snowmobiles, which was pulled by an all-terrain vehicle equipped to drive in Arctic conditions. Once the all-terrain vehicle reached Mine 7, the ice was transported with a truck. The snowmobile sled was winched onto a trailer and pulled by the vehicle. Once arrived at UNIS, a crane was utilized to lift the heavy sled off of the trailer illustrated in Figure 3.4.

(a) All-terrain vehicle with snowmobile sled attached to back, used for ice sample transport from the freshwater lake to Mine 7 over rough terrain.

(b) Vehicle (back), trailer(right), and snowmobile sled (left) used to transport ice samples from Mine 7 to the laboratory.
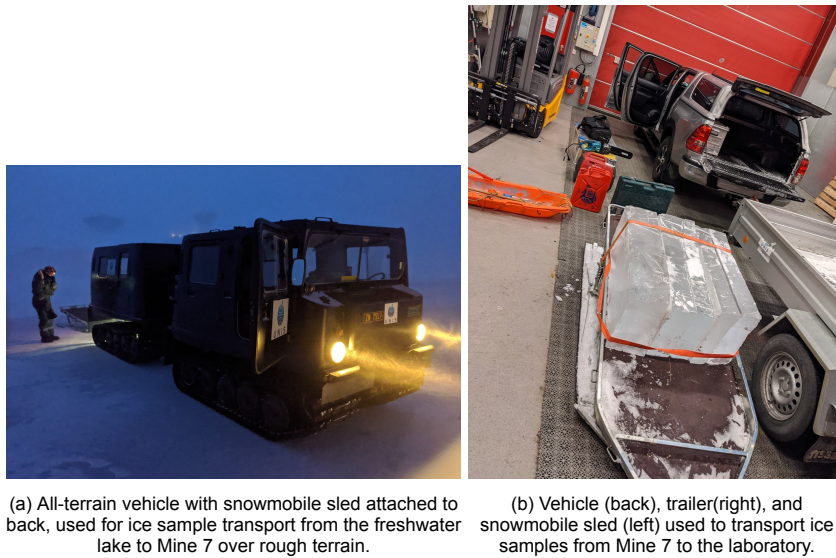
Figure 3.4: Fresh ice sample transportation methods

3.2.2. Collection of ice samples: saline ice

Saline ice samples were collected during low tide from the coast behind Svalbard Adventures in Adventfjorden displayed in Figure 3.5. The ice block was extracted from a beached floe onshore. Due to the close proximity to UNIS, the ice block was transported via truck directly to the cold laboratory.

Figure 3.5: Location of saline ice sample extraction: shore behind Svalbard Adventures

An overview of all fresh and saline ice samples from the cold laboratory experiments is listed in Table 3.1.

Sample ID	Latitude	Longitude	Type	Date of Collection	Length [cm]	Width [cm]	Height [cm]
01A1	78.15682	16.03255	Fresh	25/01/2021	50.7	40.8	11.9
02A1	78.22329	15.66971	Saline, granular	05/02/2021	57.5	38.5	17
01B1	78.15682	16.03255	Fresh	25/01/2021	91.6	43.0	15.1
03A1	77.87792	16.79060	Saline, columnar	27/04/2021	50.2	40.0	30.3

Table 3.1: Overview of ice sample collection location, dimensions, and dates.

3.2.3. Air temperature change experiment: fresh ice

The unconfined fresh ice block thermal expansion experiment consisted of a stationary rectangular ice sample placed on a table in the cold laboratory (sample 01A1 from Table 3.1). The ice sample was instrumented with a similar mechanism used in [22] to measure the horizontal extension or compression with an optical fiber FBG strain sensor with a distance of 19 cm from bracket-to-bracket. The fiber was fixed to the steel brackets by two anchor bolts made of brass, fastened with nuts and washers (Figure 3.6a). Each bracket was installed by drilling four holes and then screws.

By fastening the optical fiber, which houses the FBG, to the ice sample, the thermal expansion or contraction of the ice sample is transferred to the fiber [22]. The optical fiber was prestrained to approximately 0.3% by tightening the nuts on the anchor bolts.

(a) Sample 01A1 and FBG strain and temperature sensor set-up.   (b) Plastic casing used to limit evaporation.

Figure 3.6: Fresh ice sample air temperature change experiment

An FBG thermistor string housed in a 1 mm stainless steel capillary tube was installed to detect the air temperature above the surface of the ice as well as the ice temperature profile. To insert the FBG thermistor string with 12 sensors into the sample, a vertical hole was first drilled in close proximity to the strain sensor (without disturbing its path). To calculate thermal expansion, an average of the readings from the thermistor sensors in the ice was taken, neglecting the thermistors in the air, which reflect air temperature changes rather than ice internal temperature. The strain and temperature sensors were programmed to record measurements every 1s.

A plastic sheet was put over all samples including this ice block to prevent sublimation (Figure 3.6a). The temperature in the cold laboratory was changed in several iterations of -10°C to -2°C, and then back to -10°C over the course of three days. The time between each temperature change was at least 6 hours. A cooling system in the laboratory consisted of an air circulation system controlled in a LabView program on a PC in an adjacent room outside of the cold lab. The actual air temperature in the lab varied slightly from the set temperature with an adjustment period of 12 minutes.

3.2.4. Air temperature change experiment: granular saline ice

The rectangular ice sample corresponds to sample 02A1 in Table 3.1. The ice block was instrumented the same as previously described for fresh ice and is shown in Figure 3.7. The lab air temperature

for this experiment started at -2°C and was cooled to -20°C, and then warmed back to -2°C, with temperature changes applied in increments of 5 to 8 degrees with at least 5 hours between changes.
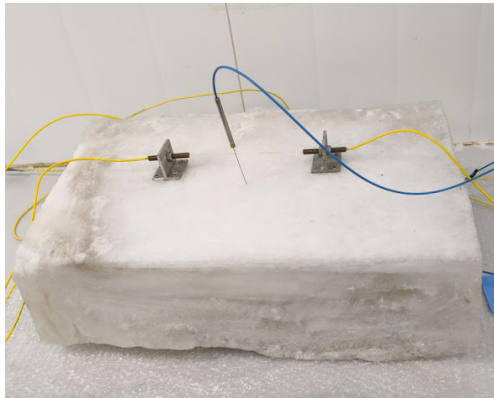
(a) Saline ice experiment, sample 02A1. Temperature sensor (blue wire) and strain sensor (yellow wires) installed in sample.
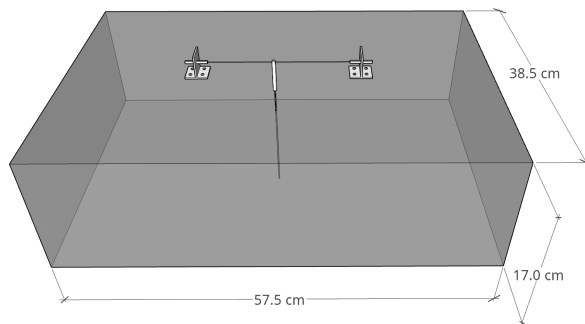
(b) Saline ice sample modelled for illustration purposes

Figure 3.7: Unconfined saline ice thermal expansion experiment.

Salinity profile
The salinity was measured on 02/09/2021 to be between 6 and 8 ppt with a Mettler Toledo Seven Pro conductivity meter SG7, consisting of a resolution of 0.01 ppt. Salinity samples were taken from another ice block from the granular saline ice batch obtained from the same location. This block measured 16 cm thick, and four samples were taken of 4 cm thickness each. Each ice sample was placed in small plastic jars to melt. The jar numbers were pre-assigned but were chosen to occur in ascending order as ice layer depth increases.
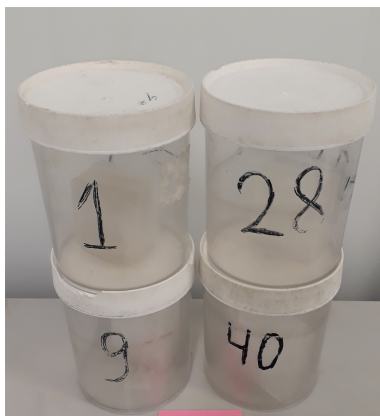
(a) Ice samples melting in salinity plastic jars.

Salinity Jar Number	Ice Layer	Salinity
1	0 to 4 cm	7.76 ppt
9	4 to 8 cm	7.14 ppt
28	8 to 12 cm	6.57 ppt
40	12 to 16 cm	6.34 ppt

(b) Salinity measured from melted saline water.

Figure 3.8: Salinity measurements for saline ice sample.

3.2.5. Air temperature change experiment: Svea columnar sea ice

This experiment was implemented to have sensors at different depths along the saline ice block, in order to determine the thermal expansion occurring at different locations along the ice. Salinity changes with depth, hence the experiment demonstrates how thermal expansion depends on salinity.

Sample collection: columnar sea ice
The ice block was brought back from fieldwork on the Vallunden lagoon in Van Mijen Fjord, near Svea, Svalbard. Students from UNIS course AT-211 assisted in extracting ice by first sawing the edges with a chainsaw (done by the professor), then hand-sawing remaining ice, and lastly collectively lifting the thick ice block out with ice screws. The ice thickness measured at the date of extraction in the Vallunden lagoon was 68 cm.

The ice was brought back to UNIS by strapping it down to a snowmobile sled. Once at UNIS an ice block with dimensions detailed for sample 03A1 in Table 3.1 was cut from the large sample. The remainder of the ice was stored for future projects.

(a) Ice sample extraction process on Vallunden lagoon.

(b) Sawing sample at UNIS before cold lab experiment.

Figure 3.9: Svea saline ice sample collection and preparation.

Experiment description

The lab temperature was changed gradually in cycles from -10°C, to -5°C, to -2°C, to -5°C and back to -10°C. The ice block was elevated off the lab table by two 2x4 wood blocks in order for the air temperature to reach the ice block surface directly (Figure 3.10a). The ice block was covered in plastic housing as in previous experiments to prevent sublimation.
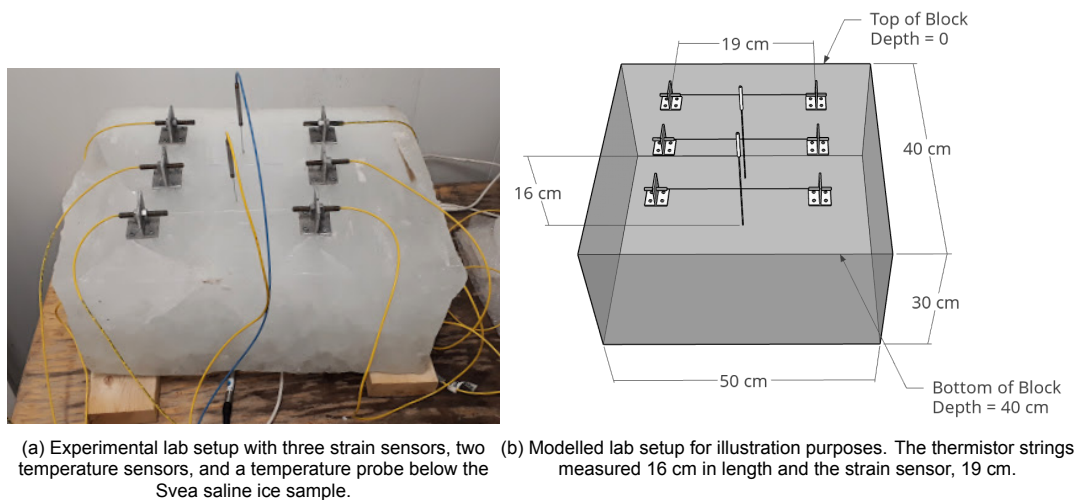
(a) Experimental lab setup with three strain sensors, two temperature sensors, and a temperature probe below the Svea saline ice sample.

(b) Modelled lab setup for illustration purposes. The thermistor strings measured 16 cm in length and the strain sensor, 19 cm.

Figure 3.10: Unconfined Svea ice thermal expansion experiment.

Three strain sensors were installed along the depth of the ice block. The first was installed 10 cm from the top of the ice block (where depth is 0), then at depths of 20 cm, and 30 cm from the top of the block (labeled in Figure 3.10b). Two temperature thermistor strings were installed into the ice sample, each 16 cm in length and each having 4.5 cm of the sensor above the ice surface.

Salinity profile

To measure the salinity during the fieldwork on April 28th, 2021, a vertical core was drilled out of the ice with a 70 mm diameter core barrel. The core was divided into seven plastic jars onsite and brought back

to the lab for salinity analysis. The ice samples were allowed to melt and the salinity was measured with the Mettler Toledo Seven Pro conductivity meter SG7 (Figure 3.11b).

Salinity Jar Number	Ice Layer	Salinity
1	0 to 13 cm	6.80 ppt
17	13 to 20 cm	4.90 ppt
21	20 to 30 cm	4.08 ppt
39	30 to 40 cm	4.06 ppt
103	40 to 50 cm	3.87 ppt
106	50 to 60 cm	4.19 ppt
111	60 to 68 cm	8.79 ppt

(a) Salinity measurement method.   (b) Salinity measured from melted saline water.

Figure 3.11: Salinity profile from vertical saline ice core extracted from Vallunden lagoon on April 27, 2021. Local ice thickness was measured as 68 cm.

3.3. Floating unconfined ice experiments

These experiments tested the expansion and contraction from air temperature variations for floating fresh and saline ice blocks. The fresh ice block (Figure 3.12) was tested first, using a new block (sample 01B1) from the same batch (Figure 3.4b) extracted from the freshwater lake near Mine 7. The saline ice sample (02A1 from Table 3.1) was reused from the previous unconfined ice experiment. Both the fresh and saline ice samples were instrumented the same as the previous experiments with FBG strain and temperature sensors. Not attached to the tank walls, the ice samples floated in hydrostatic equilibrium.

(a) Experimental lab setup with a strain and temperature sensors installed on the freshwater ice sample.
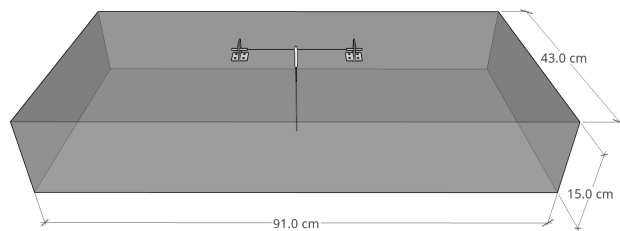
(b) Ice sample submerged in water modelled for illustration purposes.

Figure 3.12: Floating unconfined freshwater ice thermal expansion experiment.

3.3.1. Floating unconfined experiment: fresh ice

At the start of the experiment on 01/29/21, the ice sample had dimensions of 91.6 by 43.0 by 15.1 cm (sample 01B1 from Table 3.1). The ice tank has internal dimensions of 100 cm by 50 cm. Freshwater was filled with a hose into the tank, and then the ice block was manually lifted and lowered into the water. The sample in the tank was initially left exposed to allow the surface to freeze for approximately one hour, and then the plastic cover was applied (Figure 3.13).

Figure 3.13: Plastic covering over ice tank to prevent evaporation.

The lab temperature was changed gradually in cycles from -10°C, to -5°C, to -2°C, to -5°C and back to -10°C. Every 24 hours new ice growth on the sides of the block was hand-sawed off to ensure the block remained floating and unconfined. The sensors were also reinstalled every 24 hours due to the water on the surface of the ice causing them to displace. The thermistor string sensor was also pushed upwards out of the ice sample, and the brackets were displaced with the screws pushed upwards out of the ice. The displacement of the brackets caused the optical fiber to decrease in tension (Figure 3.14), which caused the measurements to become unreliable, hence requiring the re-installation of the sensors.

Figure 3.14: Displacement of sensors after 24 hours of installation. Sensors were reinstalled in an adjacent position on the ice every 24 hours of experimentation.

3.3.2. Floating unconfined experiment: saline ice

The saline ice sample (02A1 from Table 3.1) was submerged into the tank, which was filled with seawater coming from the nearby fjord. The fjord sea water is easily accessed from the tap in the saline laboratory at UNIS. The salinity of the seawater was approximately 38 ppt. The ice sample was reused after the unconfined ice experiment. The lab temperature variation and sensor installation procedure

was identical to the freshwater ice floating experiment. A notable thing about this experiment is that the saline ice sample was reused, and as illustrated in Figure 3.15, has a square-shaped indentation around the sensors, which may affect results. This indentation is from a previous saline ice pool experiment, where ice was melted with a heated steel plate to mimic tidal flooding on the ice surface. This pool was later filled with saline water and frozen to obtain a level surface again. The salinity profile matched Figure 3.11.

(a) Saline ice sample floating in tank.   (b) Enlarged view of saline ice sample.
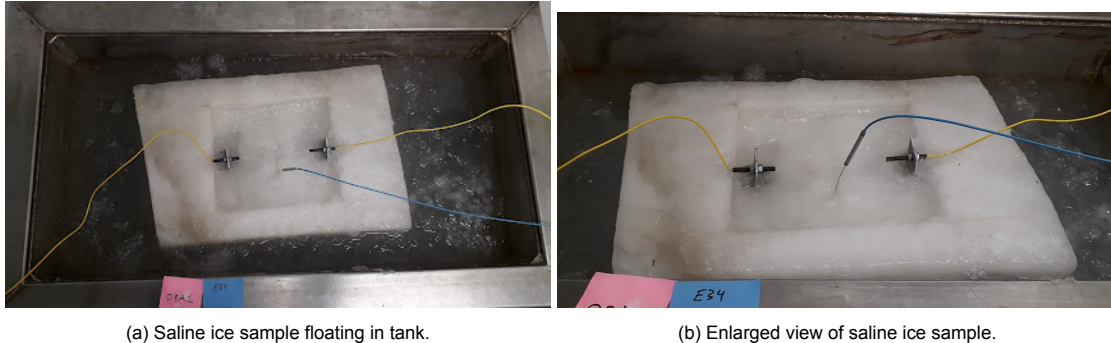
Figure 3.15: Floating unconfined saline ice thermal expansion experiment.

3.4. Flooding ice experiments

The ice flooding experiments measured deformations for sea and fresh ice samples under the influence of latent heat radiation from water freezing on the surface of the ice blocks, while air temperature remained constant. The fresh ice block sample corresponded to sample 01B1 and was used for this experiment after the floating tests. The saline ice sample corresponded to sample 02A1.

To create a pool to house water on the ice surface, a metal hot plate with dimensions 25 cm x 28 cm x 2.5 cm was utilized to melt the fresh ice sample as shown in Figure 3.16. A different technique was used to create the saline ice pool, by use of cutting the ice with a chainsaw as demonstrated in Figure 3.17.

Water was added to the ice surfaces into the cut-out pools once it reached respective freezing points for freshwater and seawater. Seawater had a salinity of 31.7 ppt at the initial start of the test and was added to the saline ice pool about one hour after the freshwater was added to the fresh ice pool. The weights of the water in the pools were measured to be 544.09 g for fresh ice and 1344.1 g for saline ice.
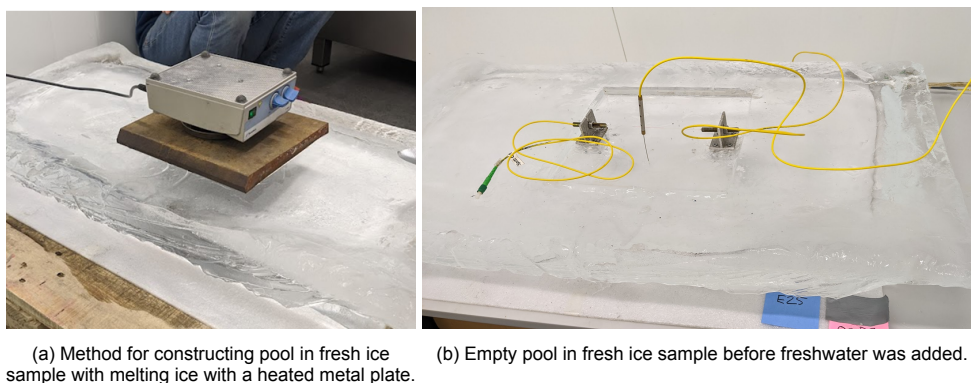
(a) Method for constructing pool in fresh ice sample with melting ice with a heated metal plate.   (b) Empty pool in fresh ice sample before freshwater was added.

Figure 3.16: Fresh ice pool creation methodology.

(a) Method for constructing pool in granular saline ice sample with chainsaw.

(b) Empty pool in saline ice sample before seawater was added.

Figure 3.17: Saline ice pool creation methodology.

3.5. Fieldwork

Fieldwork installation occurred in Svea, Svalbard on the 16th and 17th of March, 2021, and de-installation occurred on the 27th and 28th of April 2021. The aim of this work was to install pressure sensors in the ice in both a freshwater lake and lagoon adjacent to each other with similar meteorological conditions. The location of the Vallunden lagoon and adjacent freshwater lake where pressure sensors were installed is displayed in Figure 3.18.

(a) Fieldwork location on the island of Spitsbergen, Svalbard.

(b) Location of fieldwork in Svea, Svalbard. Vallunden lagoon (top marker) and freshwater lake (bottom marker).

Figure 3.18: Location of fieldwork in Svea, Svalbard (Map data taken from TopoSvalbard).

3.5.1. Instrumentation installation

The main equipment installed in both the freshwater lake and the saline lagoon included four Model 4800 Geokon Pressure Cells rated to 700 kPa (two per location) and two Geokon LC-2×4 dataloggers (one per location). The pressure sensors and datalogger are both pictured in Figure 3.19a. To secure and house the equipment to the ice, two wooden pallets and two custom-made wooden boxes (one per location) were installed. To read the data, a field laptop registered data acquisition during the initial equipment installation. The following instrumentation installation procedure was implemented for both the freshwater lake and the lagoon.

(a) Geokon pressure cells (bottom) and datalogger attached to wooden enclosure box shelf.

(b) Wooden enclosure box housing datalogger.
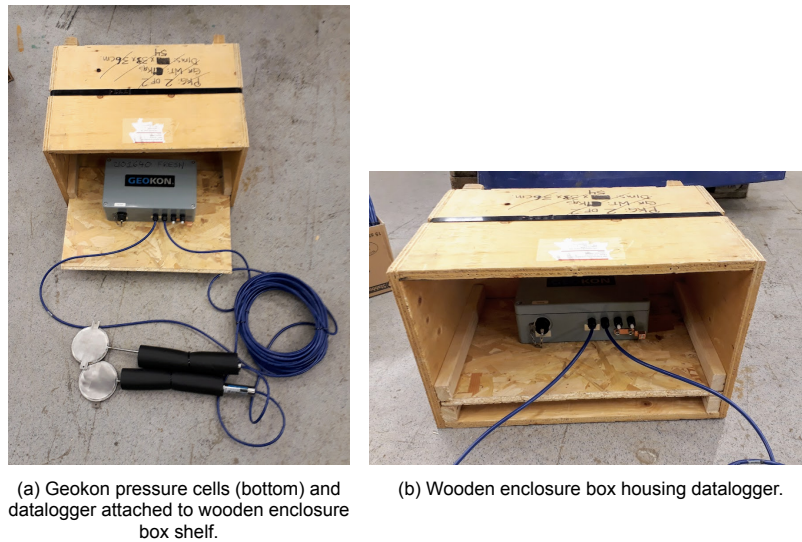
Figure 3.19: Geokon pressure cells, datalogger and wooden box enclosure.

Once located at each determined fieldwork installation site, a trench was cut for the pressure sensors and the top sensor was installed so that the transducer unit was near the ice surface. The deeper pressure sensor was installed with the aim that the transducer is at the level of the upper sensor's pressure plate. On the Vallunden saline lagoon, the local ice thickness was measured to be 65 cm while the ice thickness of the freshwater lake was unable to be measured due to time limitations. Pressure sensor installation location data is documented in Table 3.2. Pressure sensors were installed to measure the stresses in the top layer and mid-layer of the ice.

Site Location	Latitude	Longitude	Depth of top pressure sensor	Depth of bottom pressure sensor	Ice thickness
Vallunden Saline Lagoon	77.87792	16.79060	17 cm	35 cm	65 cm
Freshwater Lake	77.87607	16.79626	17 cm	36 cm	not measured

Table 3.2: Coordinates and depths of pressure sensor installations for the saline and freshwater site locations. Installation and ice thickness measurement occurred on March 16th and 17th.

The datalogger was installed by first inserting batteries into the unit, which had a capacity of recording data for approximately 74 days, then depositing silica gel packs inside the datalogger enclosure to absorb any moisture, and lastly closing the datalogger enclosure with screws. The data logging was then initiated with the field laptop on-site using a Geokon-designed LabView program. After waiting about 15 minutes for the sensors to reach equilibrium with in situ temperature readings, the field laptop was connected and initial readings were taken with zero loadings (the sensors were in position but were not in direct contact with the ice) as shown in Figure 3.20a.

Once a positive reading was registered on the field laptop, the sensor installation was finalized by pouring water into the trench housing both sensors to freeze the sensors into place (Figure 3.20b).

(a) Using the field laptop to confirm initial readings were successfully transferred from the pressure cells to the datalogger and lastly to the laptop.

(b) Freezing sensors in position by pouring water into the trench.

Figure 3.20: Svea fieldwork equipment installation.

A wooden pallet was utilized as a foundation for the equipment and was moved over to the location where sensors were installed in the ice to cover them. A custom-made open-faced wooden box was placed upside down on top of the pallet, enclosing and protecting the datalogger (Figure 3.19a). The box was equipped with a sliding wooden shelf that the data logger was attached to, keeping the datalogger in place (Figure 3.19b). The wooden enclosure was elevated above the pallet with two 2x4 wood pieces to clear snow and allow air to circulate, as well as to enable the datalogger to be higher off of the ice, in case of flooding. The cables from the pressure cells passed through the wooden pallet were grouped together and stored inside the enclosure box (Figure 3.21a).

Cargo straps and ice screws were installed to secure the wooden pallet and box into the ice (Figure 3.21b). This mechanism was selected to reduce the chance of the wooden housing and foundation being tipped over by extreme weather or polar bears.

(a) The cabling for the pressure sensors ran through the gaps of the wooden pallet and was grouped together and stored inside the wooden enclosure along with the datalogger.

(b) Final fieldwork data collection set-up on the saline lagoon near Svea. The same final configuration was installed on the nearby freshwater lake.
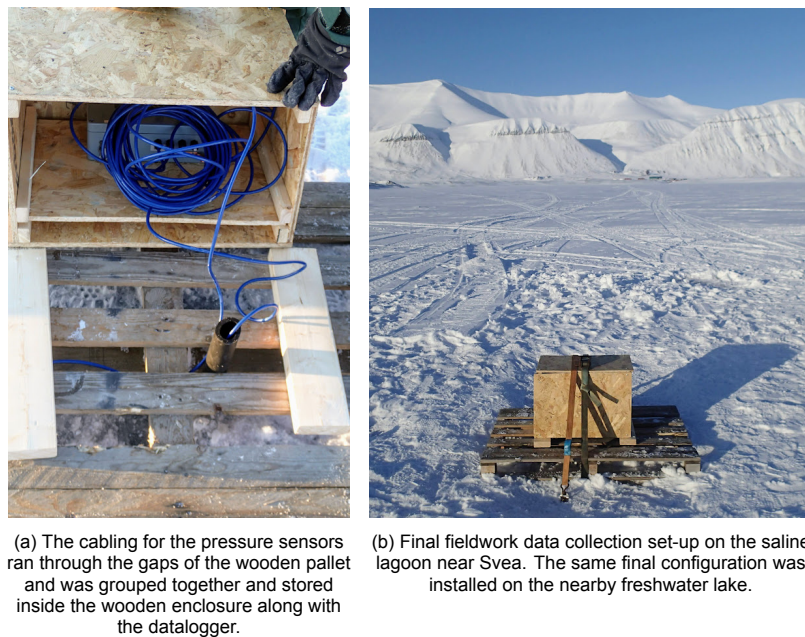
Figure 3.21: Final data acquisition set-up on the saline lagoon.

3.5.2. Valluden salinity profile

Salinity was measured on March 30th, 2021, and is displayed in the following table. The salinity core was taken in the immediate proximity of the Valluden sensor installation location. While the vertical ice core is usually hand-sawed into smaller pieces to store in plastic jars, no hand-saw was available so the core was divided into pieces using a metal ice pick. This caused the cut surfaces to not be completely orthogonal to the vertical axis and also not planar, which could result in some inaccuracy in results.

Salinity Jar Number	Ice Layer	Salinity
1	0 to 10 cm	5.23 ppt
16	10 to 22 cm	4.54 ppt
21	22 to 30 cm	4.31 ppt
25	30 to 41 cm	4.44 ppt
39	41 to 51 cm	5.39 ppt
42	51 to 65 cm	5.26 ppt

Table 3.3: Salinity measurements of Valluden saline site location.

3.5.3. Instrumentation recovery

On the 27th and 28th of April 2021, the pressure sensors and data loggers were recovered from the ice. A shovel was used to remove snow from each of the data logging stations. Snow filled in the wooden enclosure boxes through the gaps in the wooden pallet (Figure 3.22b) but did not affect data logging capabilities. The field laptop was connected to the datalogger and all data was collected from the recording period. Then, the generator was used to power a chainsaw to remove the pressure sensors from the ice. After the chainsaw was used to cut around the sensors, a heavy metal ice pick was used to break the remaining ice.
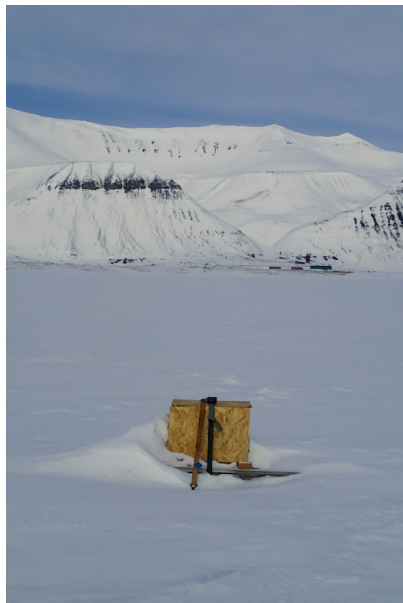
(a) Valluden saline site on April 27 fieldwork.

(b) Snow that filled in the wooden enclosure box (which occurred on both sites).

Figure 3.22: Valluden saline site instrumentation recovery fieldwork

An additional salinity profile was measured on the Valluden lagoon (previously documented in Figure 3.11b). Local ice thickness was measured to be 68 cm on April 27th and 28th fieldwork, a 3 cm increase from the previously measured thickness of 65 cm on March 16th and 17th that was presented in Table 3.2.

3.6. Numerical Modeling: COMSOL model set-up

The air temperature change experiment for fresh ice was modelled in COMSOL Multiphysics software in order to validate general trends observed in laboratory experiments. Differences between theory and practice were to be identified, as errors could have likely caused practical results to become slightly different than theoretical due to imperfections in the ice samples, experimental procedures, or inconsistencies in the air circulation cycles in the cold laboratory.

3.6.1. Air temperature change thermal expansion modeling

The model of the fresh ice sample resting on the lab table was inputted into COMSOL to confirm accuracy in laboratory results. The model consisted of the fresh ice block and two vertical aluminum brackets (shown in Figure 3.23a) which were used to hold the fiber optic FBG strain sensor in tension.

(a) COMSOL model of freshwater ice sample.

(b) Freshwater ice sample (01A1 from Table 3.1)
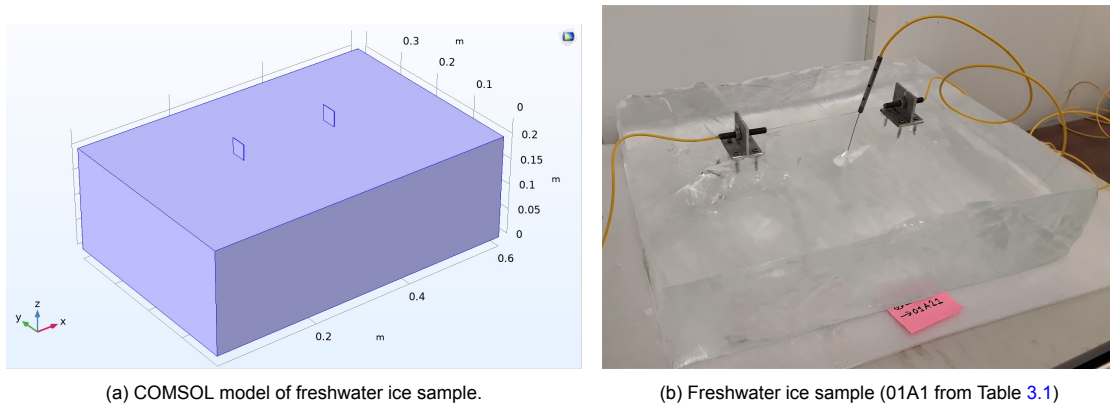
Figure 3.23: Numerical modelling of unconfined ice thermal expansion experiment.

The following material properties for the aluminum brackets and fresh ice (Table 3.4 and Table 3.5, respectively) were entered into the model parameters. The computation domain representing the fresh ice sample is a rectangular block with sizes matching the respective ice sample dimensions listed in Table 3.1, with the length along the x-axis, the width along the y-axis, and the height along the z-axis. The origin of the domain was assigned to the lower corner of the rectangular block, where the vertical coordinate z is pointing upwards. Two aluminum square brackets were added on top of the ice block model, halfway along the y-axis, or width of the ice block, where sensors were typically installed on each sample. The fresh ice sample was created in a Structural Mechanics module implementing a linear elastic material with creep and thermal expansion. The elastic modulus and Poisson's ratio used were 9 GPa and 0.33, respectively.

Property	Variable	Value	Unit
Heat capacity at constant pressre	C_p	904	J/(kg·K)
Density	ρ	2700	kg/m^3
Thermal conductivity	k_{iso}	237	W/(m·K)
Young's modulus	E	70.0e9	Pa
Poisson's ratio	ν	0.34	-
Coefficient of thermal expansion	α	23.1e-6	1/K
Tangent coefficient of thermal expansion	α_t	5e-6	1/K
Volume reference temperature	T	TS(0)+273.15	K

Table 3.4: Aluminum bracket material properties used in COMSOL model.

Property	Variable	Value	Unit
Thermal conductivity	C_p	2090	J/(kg·K)
Density	ρ	916.8	kg/m3
Thermal conductivity	k	2.2	W/(m·K)
Young's modulus	E	9.0e9	Pa
Poisson's ratio	ν	0.33	-
Tangent coefficient of thermal expansion	α_t	5.27e-5	1/K

Table 3.5: Material properties for fresh ice (user-inputted).

An initial temperature was applied to all bodies in the model, which corresponds to the ice surface temperature from the thermistor string in the lab and was converted to Kelvin units. The following mesh was generated in the finite element model.
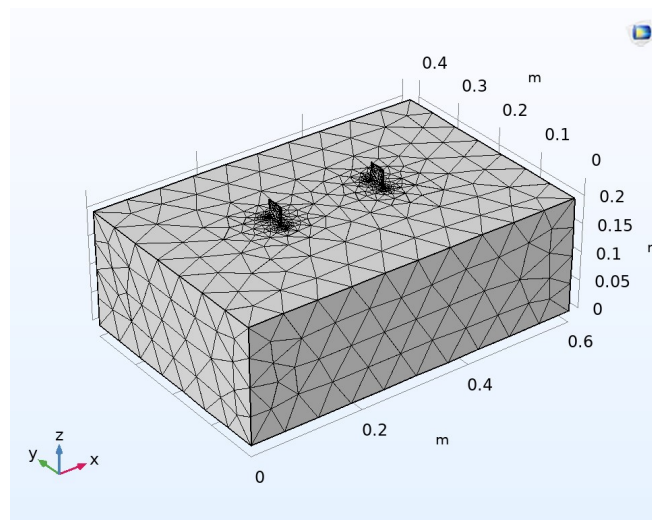
Figure 3.24: Chosen meshing method for COMSOL model.

<div style="text-align: right; font-size: 4em;">4</div>

Results

The results and discussion of the cold laboratory experiments and fieldwork are presented in this section. We compare the thermal deformation of both fresh and saline ice in three types of thermal action experiments.

- **Air experiments** The unconfined ice block is placed on a table in a cold laboratory, the air temperature is altered.

- **Floating experiments**: The ice block is unconfined and floating in a water tank, the air temperature is altered.

- **Flooding experiments**: Water is applied to the ice surface, air temperature remains constant. The thermal action is caused by the radiation of latent heat due to the water freezing at the surface.

All three tests were performed with fresh lake and saline (granular) spray ice. For the columnar sea ice retrieved from fieldwork at Svea, only the air experiment was conducted due to COVID-19 related limitations. In the air experiments, we extracted the ECTE constant for the three different types of ice (summarized in subsection 4.1.2). For the floating and flooding experiments, we compare thermal strains instead of ECTE, due to temperature gradients in the ice sample.

The first section of this chapter (section 4.1) presents the results of the air experiments for fresh and saline (both granular and columnar) ice. section 4.2 describes the floating experiment for fresh and granular saline ice. The flooding experiment results are shown in section 4.3. Lastly, the results from the fieldwork are presented in section 4.4. All of the individual plots for the experiments are documented in Appendix A.

4.1. Air temperature change experiments

Thermal deformations of ice samples of two different types, granular saline ice, and fresh ice, when unconfined on the lab table, are compared to each other in this section. The fresh ice sample was taken from a lake near Mine 7 outside of Longyearbyen, Svalbard, Sample 01A1 from Table 3.1. The saline ice sample was taken from a washed-up ice floe on the shore behind the University Centre in Svalbard (sample 01B1 from Table 3.1). The tests setup is described in the Methods chapter, section 3.2. The fresh ice and saline ice samples used for this comparison were placed next to each other in the same cold laboratory and underwent the same air temperature changes. The mean ice temperature was cooled from -5°C to -16°C and warmed to approximately -7°C with increments of 4 to 6 degrees for each of the three tests in this comparison.

The individual results from the three tests shown in Figure 4.1, and the additional ice-air experimental data is outlined in Appendix A: Figures A.1-A.10 for fresh ice, Figures A.11-A.13 for granular saline ice, and Figures A.14-A.16 for columnar saline ice. The Appendix plots demonstrate air and ice temperature over time measured by the thermistor string in the ice sample, the ice temperature gradient, strain over time, and strain over the mean ice temperature. In addition, the methodology used to find respective ECTE values for each test is shown over several plots for each experiment.

The top plot in Figure 4.1 demonstrates the strain, calculated from the wavelength output from the Fiber Bragg Grating (FBG) sensor against time for the fresh and saline ice samples, samples 01B1 and 02A1, respectively. The time-dependent strain is then plotted against time-dependent mean ice temperature, where the slope of the lines represents the ECTE of the ice. The strain-temperature relation for each test can be characterized by two distinct parts which correlate to the cooling and heating periods of the experiment. The linear behavior in these individual parts is used to fit the thermal expansion coefficients for each test.

For both the fresh and saline ice experiments, the heating period, corresponding to the upper part of each curve in the strain-temperature relation plot for each sample, shows a lesser value of deformation than the cooling period. This hysteresis effect was also observed by Butkovich [3] with fresh ice, who concluded the linear coefficient of thermal expansion decreased through the cycles of tests. Hysteresis in the strain-temperature curves with succeeding runs was also observed by Johnson and Metzner [10]. In the results from Figure 4.1 below, the fresh ice tests experience a greater hysteresis effect than the saline tests, as there is a greater difference in deformations from the cooling and heating cycles.
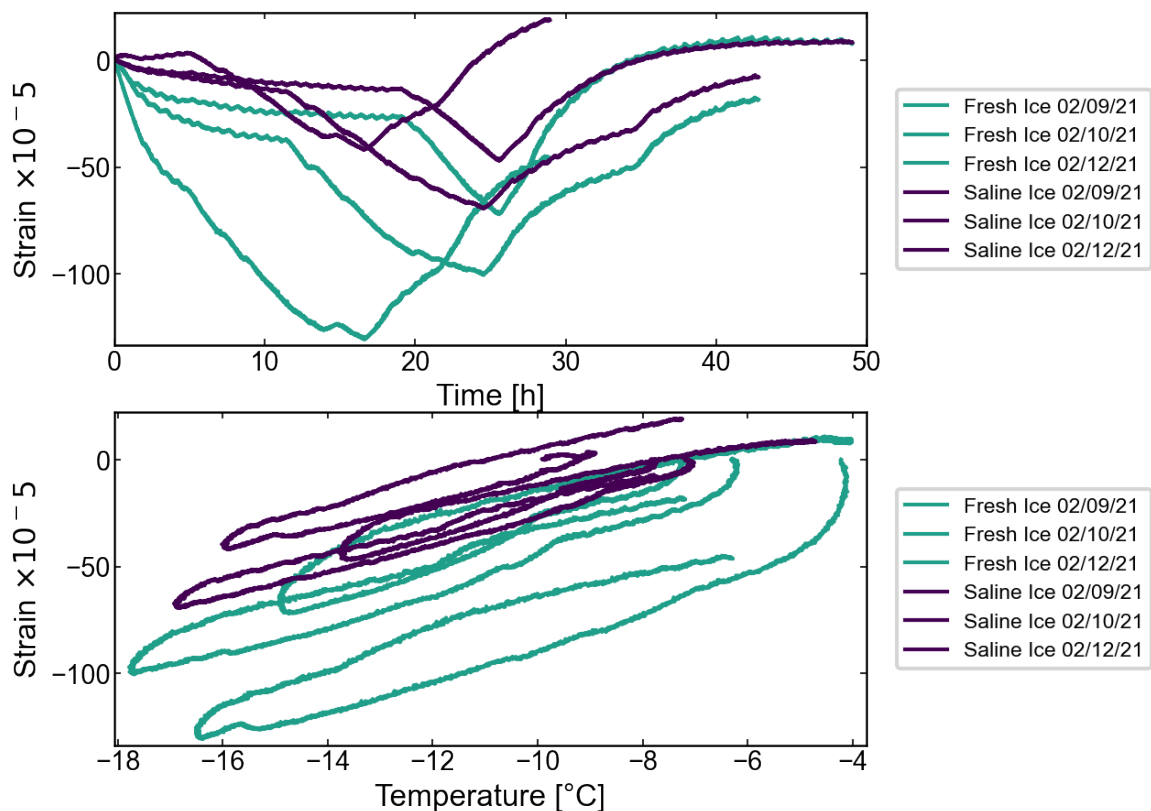
Figure 4.1: Strain against time and strain against mean ice temperature for the saline and fresh ice unconfined thermal expansion experiments, where air temperature conditions remained the same.

From the bottom plot of Figure 4.1, the ranges of mean temperature change in fresh ice can be observed to be wider than that of saline ice, while the air temperature of the cold laboratory was kept the same for both samples. This observation can be explained from the different dimensions of the saline and fresh ice blocks. The fresh ice block was approximately 30 cm longer in length, requiring more time to be cooled to a certain temperature than the smaller saline sample when the initial ice temperature is the same. Another explanation follows that the fresh ice sample was tested in these experiments after being previously used in the floating fresh ice experiments. This is important to mention, as some cracks in the ice that formed during sensor installation were filled with water from the tank, possibly affecting the thermal behavior of the fresh ice sample during freezing, after the floating tests were performed in the tank.

The different ranges in temperature change for the fresh and sea ice samples can also be attributed

to the fact that the ice sample temperature range shrinks when specific heat capacity is increased. Specific heat is an important parameter for calculating the heat energy content of an ice field. From Figure 4.1, fresh ice has an ice temperature range of approximately -18°C to -4°C, whereas saline ice has a range of approximately -16°C to -7°C. Each test for saline ice shows a smaller temperature range than the corresponding fresh ice test for the same lab air temperature conditions. The specific heat of water is approximately 4200 J/kg·K whereas the specific heat for freshwater ice is half, 2100 J/kg·K. The specific heat capacity of saline ice can be much higher than in fresh ice because of the latent heat used for melting and refreezing of the brine in pockets in the ice [31]. As saline ice is composed of pure ice, brine, solid salt crystals, and air bubbles, the freezing of internal brine causes a major heat-absorbing process [31].

Hence, with the saline samples possessing a higher specific heat capacity than fresh ice, Figure 4.1 demonstrates this correlates to a narrower ice temperature range in which thermal deformations occur. While ECTE values, corresponding to the slope of the strain against the mean ice temperature plot, are similar for both fresh and saline ice, it can be concluded the ice experienced different temperature ranges during thermal deformations.

From the upper graph in Figure 4.1, it can also be concluded that the deformation for fresh ice was larger, especially during cooling when strain increases in the negative direction, in comparison to saline ice, i.e. it experienced more contraction than the saline ice sample. Brine pockets, which can act as a suspension for thermal expansion, can explain why the saline ice block underwent less deformation than the fresh ice block.

ECTE Analysis

ECTE is an important parameter for this analysis because it is a constant characterizing material behavior under thermal action. A summary of ECTE values obtained from all ice-air experiments is displayed in Table 4.1. In these experiments, ice was exposed to air temperature change on all lateral sides, as well as the top surface, whereas the bottom face was resting on top of a table. The results corresponding to the tests displayed in Figure 4.1 are from samples 01B1 and 02A1. Comparing the results for these samples, the granular saline ice sample demonstrates a similar ECTE value to the fresh ice sample, $6.11 \times 10^{-5} K^{-1}$ and $5.56 \times 10^{-5} K^{-1}$, respectively. Fresh ice sample 01A1 demonstrates a higher ECTE value than the saline ice sample 02A1, however, this set of experiments took place at the beginning of tests, when uncertainty in the results may be higher due to initial human error when drilling the screws into the fresh ice sample to secure the aluminum brackets, causing cracks around the brackets to form as shown in Figure 4.2. Sea ice samples are more porous due to brine channels and salinity, causing fewer cracks to form during the drilling of the sensor screws. The FBG strain sensor is nearly a thin cable, where the tension in the cable translates to strain values and is highly sensitive to movement. Therefore, it is possible the FBG strain sensors could have measured additional displacement from the brackets moving in screw holes for fresh ice sample 01A1, hence fresh ice results from sample 01B1 will mainly be considered.

Type of Experiment	Sample	ECTE [1/K] (x10^{-5})		
		mean μ	max M	min m
Fresh ice on table	01A1	6.18	7.98	5.50
Fresh ice on table	01B1	5.56	7.58	5.06
Spray ice (granular) on table	02A1	6.11	7.83	5.04
Sea ice (columnar) on table	03A1	7.61	12.09	4.68

Table 4.1: Mean, maximum, and minimum ECTE results for applicable experiments.

The granular saline ice sample gives a slightly higher result for the ECTE than fresh ice sample 01B1 in Table 4.1, however, it can be argued that the difference between these two values is negligible and within error margins of the experiment. In saline ice, when the temperature is altered, phase changes ensue along the boundaries of the closed brine pockets, initiating adjustments in local deformations and

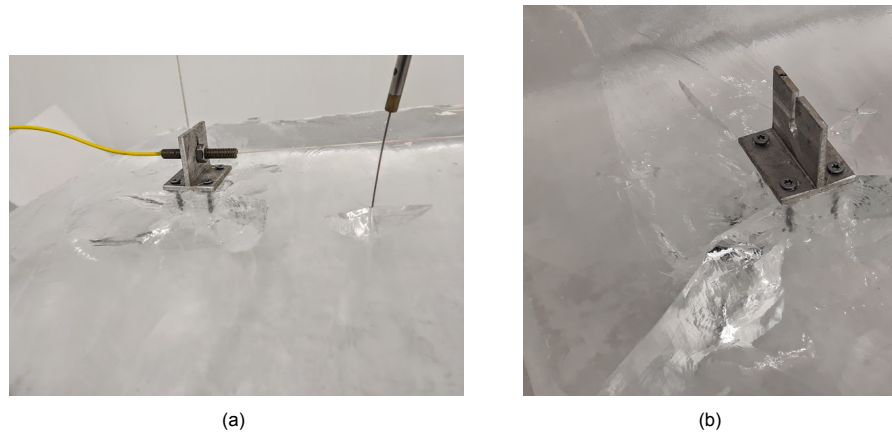(a)   (b)

Figure 4.2: Cracks formed during sensor installation for fresh ice sample 01A1.

pressure, as ice is 10% less dense than brine [20]. From Malmgren's 1927 experiments on thermal expansion [16], it was concluded that the freezing and melting of brine makes sea ice expand less than fresh ice, as it was assumed no brine was allowed to escape the ice sample, making the ice sample effectively impermeable. Volumetric effects due to phase changes exist only within the ice matrix, thus justifying the atypical behavior observed in sea ice, where ice can expand during cooling. In more recent works, Cox argued in 1983 [5] that sea and fresh ice should have the same LCTE and that sea ice is not a closed system; brine and ice can experience volumetric effects independently, and the ice sample is fully permeable. The brine can drain out of the ice sample, and phase changes have no effect on thermal expansion, leading to the thermal expansion coefficient of sea ice being the same as for fresh ice.

Therefore, if we accept that the ECTE values for fresh and saline ice are similar, it can be reasoned that the similarity in values for the saline and fresh ice ECTE results is in agreement with Cox [5]. The brine likely drained during expansion for the saline ice sample, as the lower parts of the ice were subjected to small temperature variations when resting on the table. Since saline ice ECTE values are slightly higher than fresh ice values, the results are less consistent with Malmgren's [16] assumption that sea ice expands less than fresh ice. The results are more consistent with Cox's analysis that sea and fresh ice should have the same coefficient of thermal expansion, and that sea ice is a permeable system [5].

4.1.1. Svea columnar sea ice experiment

This experiment aimed to study thermal stresses along the depth of the columnar sea ice block, which originated from the Valluden lagoon in Svea, Svalbard (sample 03A1).

The two thermistor strings installed on the ice sample measured the temperature profile in the ice in the horizontal direction, and these results are recorded in section A.3. The strain sensors are installed along the depth of the ice, where the top layer of the ice sample is facing the wall of the lab in the test (schematically shown in subsection 3.2.5). Thus with the thermistor strings inserted into the side of the sample, they are measuring temperature parallel to the ice surface, representing a horizontal temperature profile. The two thermistor strings measured almost identical temperature gradients and the ice temperature results quickly follow the air temperature changes.

Unlike granular sea ice, columnar sea ice has flat and elongated crystals, where brine is trapped in these layers in brine channels. When ice is warmed, these channels can widen and connect, and brine can escape from the lower end of the ice. In addition, in columnar sea ice, permeability can be different in various layers, and salinity also does not have a constant profile along the depth of the ice [8].

In the Svea ice thermal expansion experiment, strain sensor 1 was installed near the ice surface at a depth of 10 cm, strain sensor 2 was installed at 20 cm, and sensor 3 was installed near the bottom of the ice sample at a depth of 30 cm. Sensor 3 was installed in the ice layer that had a salinity greater than 7 ppt, and sensor 1 was in the range of 4-5 ppt.

From Figure 4.3 below, during the initial stage of cooling from -9°C to -13°C, strain sensors 1 and

2 demonstrate similar deformations, and strain sensor 3 shows a larger deformation and strain rate. Then, during the next stage of heating from -13°C to -2.5°C, the ECTE of sensor 1 contains a positive value, and the ECTE of sensor 2 is negative when the temperature is greater than -7°C, and the ECTE of sensor 3 is negative when the mean ice temperature is greater than -10°C. During the last stage of cooling from -2.5°C to -13°C, all of the strain sensors demonstrated similar deformation patterns, with positive ECTE values.
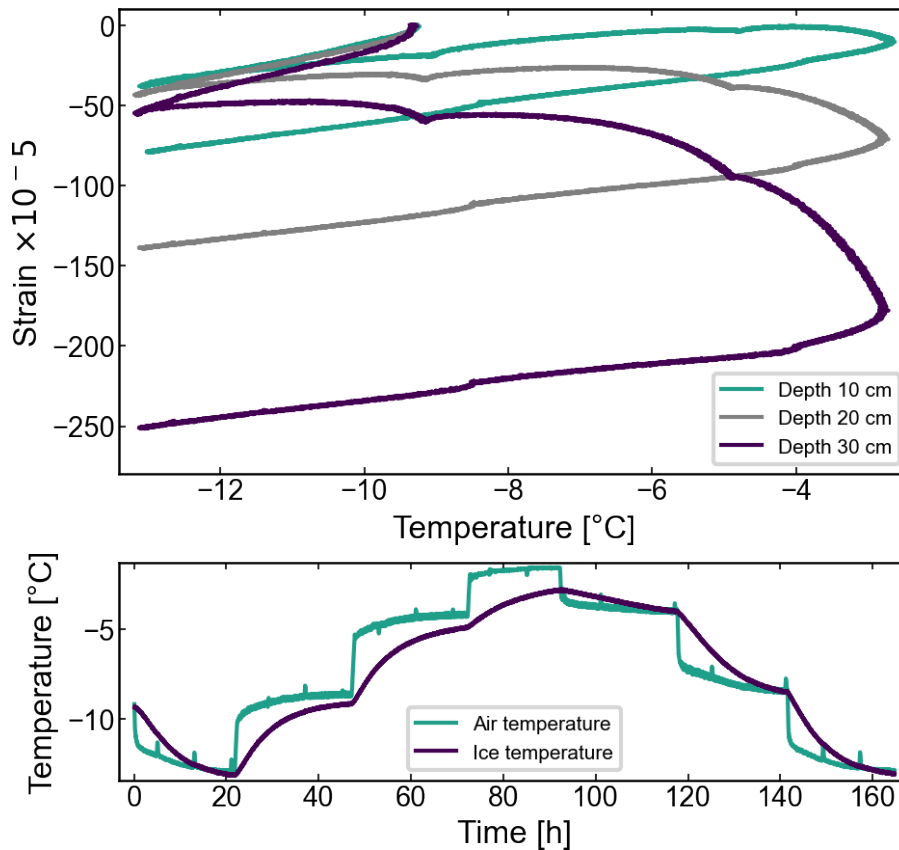
Figure 4.3: Svea columnar sea ice experimental comparison of deformations over the depth of the sample, when resting stationary on a table exposed to air temperature change.

The average ECTE value for this experiment is displayed in Table 4.1, excluding negative values of thermal expansion. All ECTE values from the experiment are recorded in Table 4.2.

It can be concluded from Figure 4.3 that ECTE values increase over the depth of the sample, equating to $8.5 \times 10^{-5} \text{K}^{-1}$ for sensor 1 during the first cooling cycle, compared to $12.09 \times 10^{-5} \text{K}^{-1}$ for sensor 3 during the first cooling cycle of the deepest layer. These results indicate that the properties of sea ice such as salinity participate in influencing thermal expansion results.

As the cooling and warming tests were repeated in this experiment, cyclic thermal loading demonstrated strong hysteresis in deformations, visible by the difference in strain values for each strain sensor after each warming and cooling period. This hysteresis effect was demonstrated to be stronger than the columnar fresh ice hysteresis previously shown in the report.

4.1.2. Summary of ECTE results

The following table summarizes all obtained values for ECTE for the non-floating, ice-air experiments with fresh ice, granular saline ice, and columnar sea ice. The corresponding plots outlining the methodology for obtaining these ECTE results can be found in Appendix A. Thin section images are included in the summary table below to illustrate the crystalline structure of the ice sample examined.

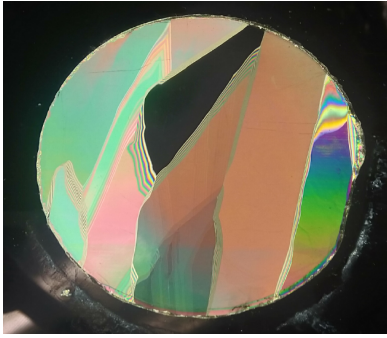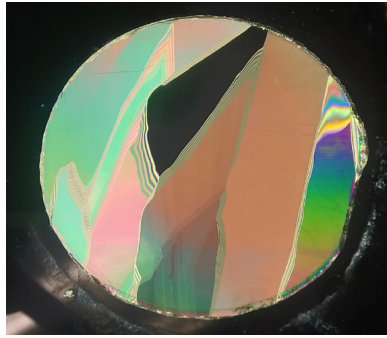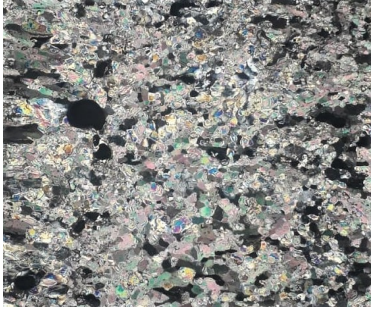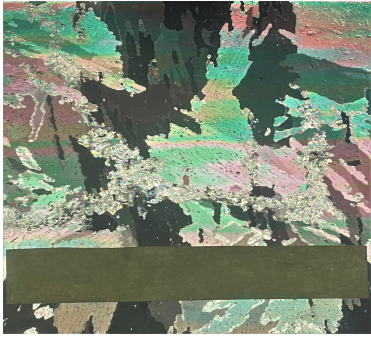| Test	ECTE [1/K] $(\times 10^{-5})$	ΔT_{Ice}, [°C] ECTE	ΔT_{Ice}, [°C] Test	Process	Thin Section Image	Sample/ Type/ Salinity
E01	5.50	-5.4 to -4.3	-4.2 to -5.1	Cooling		
	6.81	-7.8 to -5.5	-5.3 to -7.9	Cooling		
	5.63	-7.2 to -5.3	-7.9 to -4.2	Heating		
E02	6.47	-5.9 to -4.3	-4.0 to -6.0	Cooling		01A1, Fresh
	7.98	-9.1 to -7.0	-6.0 to -9.0	Cooling		
	5.82	-8.6 to -5.0	9.1 to -4.6	Heating		
E03	5.65	-10.0 to -7.8	-4.2 to -10.0	Cooling		
	5.61	-8.8 to -5.8	-9.8 to -4.9	Heating		
E04	7.58	-15.0 to -7.5	-4.8 to -16.0	Cooling		
	5.30	-11.0 to -6.0	-16.0 to -6.1	Heating		
E05	5.68	-17.6 to -12.9	-6.1 to -17.6	Cooling		
	5.29	-11.0 to -7.0	-17.6 to -7.5	Heating		
E06	5.59	-10.0 to -8.0	-6.9 to -15.0	Cooling		01B1, Fresh
	5.16	-13.0 to -5.0	-14.9 to -4.7	Heating		
E07	6.15	-13.0 to -10.0	-3.9 to -13.8	Cooling		
	5.06	-13.0 to -4.0	-14.0 to -4.0	Heating		
E08	5.28	-14.1 to -9.0	-3.8 to -14.1	Cooling		
	5.23	-13.8 to -10.4	-14.1 to -7.6	Heating		
E09	5.26	-13.1 to -8.3	-2.6 to -13.1	Cooling		
	5.12	-9.0 to -4.9	-13.1 to -2.5	Heating		
E10	6.38	-14.4 to -9.5	-9.9 to -16.0	Cooling		
	6.23	-15.1 to -7.0	-16.0 to -7.0	Heating		
E11	6.33	-16.9 to -9.3	-7.5 to -16.9	Cooling		02A1, Sea ice, grannular, 7.76 ppt
	5.04	-11.0 to -7.9	-17.0 to -7.9	Heating		
	5.58	-16.0 to -12.0	-17.0 to -7.9	Heating		
E12	7.83	-13.8 to -8.0	-7.9 to -13.8	Cooling		
	5.36	-13.3 to -7.8	-13.8 to -4.8	Heating		
E13	8.59	-13.1 to -9.3	-9.0 to -13.1	Cooling		03A1, Sea ice, columnar, 4.08 ppt, depth = 10 cm
	4.68	-13.0 to -6.0	-13.1 to -5.3	Heating		
	6.30	-12.9 to -3.2	-3.2 to -12.9	Cooling		
	9.59	-13.2 to -9.4	-9.2 to -13.2	Cooling		3.87 ppt, depth = 20 cm
	-13.65	-5.0 to -2.8	-5.0 to -2.8	Heating		
	6.06	-13.6 to -2.9	-2.9 to -13.6	Cooling		
	12.09	-13.2 to -9.1	-9.1 to -13.2	Cooling		8.79 ppt, depth = 30 cm
	-4.90	-13.7 to -5.1	-13.7 to -5.1	Heating		
	6.00	-12.9 to -3.1	-3.1 to -12.9	Cooling		

Table 4.2: ECTE results for all experiments where ice is stationary on a laboratory table, with no flooding on the surface.

The fresh ice thin section image was captured through a UNIS course one year prior to the experiments, from fresh ice extracted from the same freshwater lake near Mine 7.

4.2. Floating experiments

The next section describes the results from the experiments where saline and fresh ice samples (02A1 and 01B1, respectively) were floating in the tank, submerged in either saline or freshwater depending on the type of sample. Floating, unconfined ice thermal expansion experiments have not been performed in laboratory settings, and these experiments aim to answer the question of how much ice deforms over a certain time when the air temperature of the lab is altered. The temperature of the floating ice can only change from one side (the top surface) as the bottom surface is always at the freezing point. The lateral sides of the ice sample have a temperature that is equal to the freezing point at the bottom depth of the sample, and to the ice surface temperature at the top of the sample, which is close to the air temperature.

The linear coefficient of thermal expansion characterizes the deformation of ice when the ice temperature changes by 1°K in all of the volume of the ice. The linear coefficient assumes that all of the samples have the same temperature, but the temperature profile in this sample is not constant, due to the boundary conditions causing a temperature gradient. Hence only thermal strains are considered and ECTE is not determined quantitatively for the floating tests.

Due to there being only one tank present in the lab, these tests were not performed at the same time and had slightly different air temperatures applied for each test. However, general trends can still be inferred from the results, when experiments are compared for fresh and saline floating samples. It should be mentioned that the floating saline ice sample was used for these tests after the flooding experiments had already been performed on this sample, where a square indentation was melted on the surface of the sample and water was flooded on the surface, which may increase the uncertainty of results.
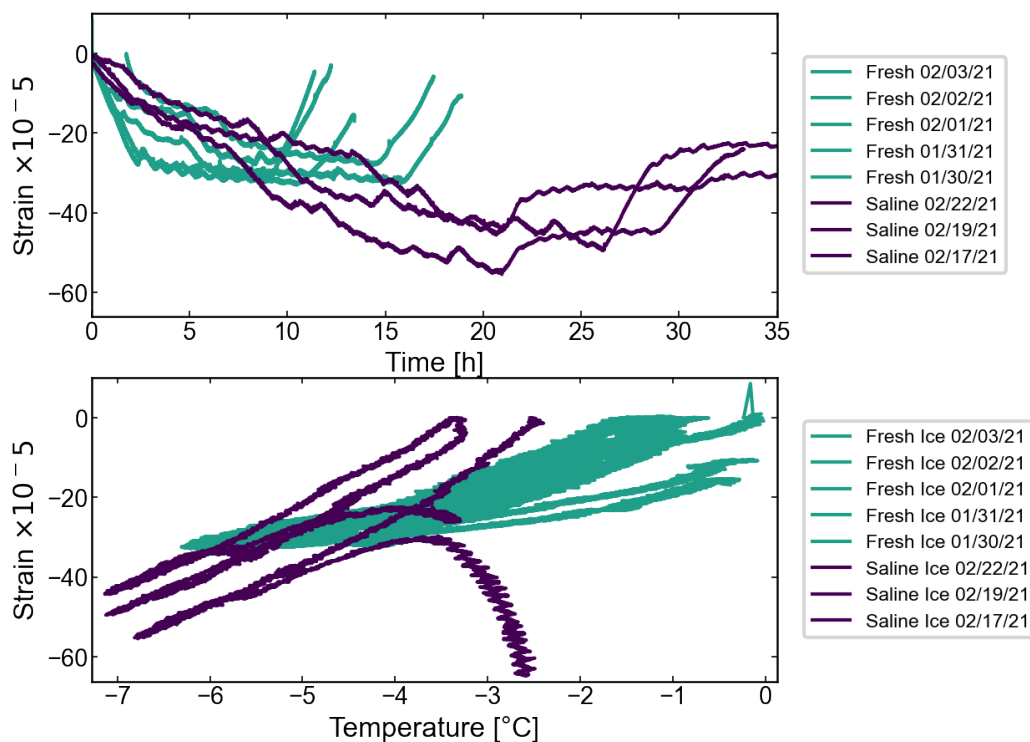

Figure 4.4: Strain against time and strain against mean ice temperature for the saline and fresh ice unconfined floating thermal expansion experiments.

Figure 4.4 demonstrates the FBG sensor strain against time, and strain against mean ice temperature. In these tests, the samples underwent cooling and then heating. The bottom plot displays different

temperature ranges for the saline and fresh ice samples (approximately -7°C to -3.5°C for saline ice, and -6.1°C to -0.2°C for fresh ice). This difference is due to the saline samples being tested for a longer duration of time with greater air temperature ranges. However, it can be concluded that the fresh ice samples display a larger range in these temperatures than saline ice, which is consistent with the temperature range results from the non-floating ice experiments previously discussed. Having a greater specific heat value than fresh ice, saline ice samples demonstrate a shrinkage in temperature ranges during thermal deformations. In saline ice, thermodynamic characteristics depend on temperature and salinity stronger than fresh ice. Therefore, the range of temperature change also may influence the thermal expansion of saline ice to be different than fresh ice.

From the bottom sub-figure in Figure 4.4, it follows that the ECTE of saline ice is greater than for fresh ice. This trend is prevalent from the steeper slope of the saline ice strain-temperature data compared to the slope of the fresh ice tests, as the coefficient of linear thermal expansion of a material is formally equal to the tangent of the slope angle for each value of the temperature.

A negative ECTE value for saline ice is also visible from these results during the higher temperatures at the end of the test, during heating. Negative coefficient of thermal expansion values for saline ice have been recorded previously [16] [20]. Marchenko reported for 6 ppt or higher, negative values of thermal expansion were observed when ice temperature is higher than -8°C. The results are consistent with this finding, as they occurred with a salinity of 7.76 ppt for temperatures higher than -4°C. This corresponds to atypical thermal behavior when contraction occurs when the temperature rises. In granular sea ice, the crystalline structure includes small and rounded crystals where numerous pockets of trapped brine exist. The thin section of this ice sample is displayed in E11 to E13 in **??** where the granular structure is visible. Negative ECTE values stem from brine migration. When the temperature rises, the ice at the phase boundary between ice and brine starts to melt, decreasing the brine salinity and altering the local phase ratio. The brine pockets increase in size and can join together, creating permeable channels within the sea ice matrix. When the phase ratio is changed, the density of the ice can also increase with temperature change, as the brine is denser than ice, which occurs when contraction caused by the change of phase is greater than thermal expansion. Thus, the ECTE can become negative when sea ice temperature increases.

4.2.1. Saline floating ice experiments compared to non-floating experiments

Now, we can compare saline experiments for two cases: floating and on the table. Figure 4.6 demonstrates the difference between saline floating and non-floating tests, where Figure 4.5 shows the mean ice temperatures and air temperatures of the tests over time.
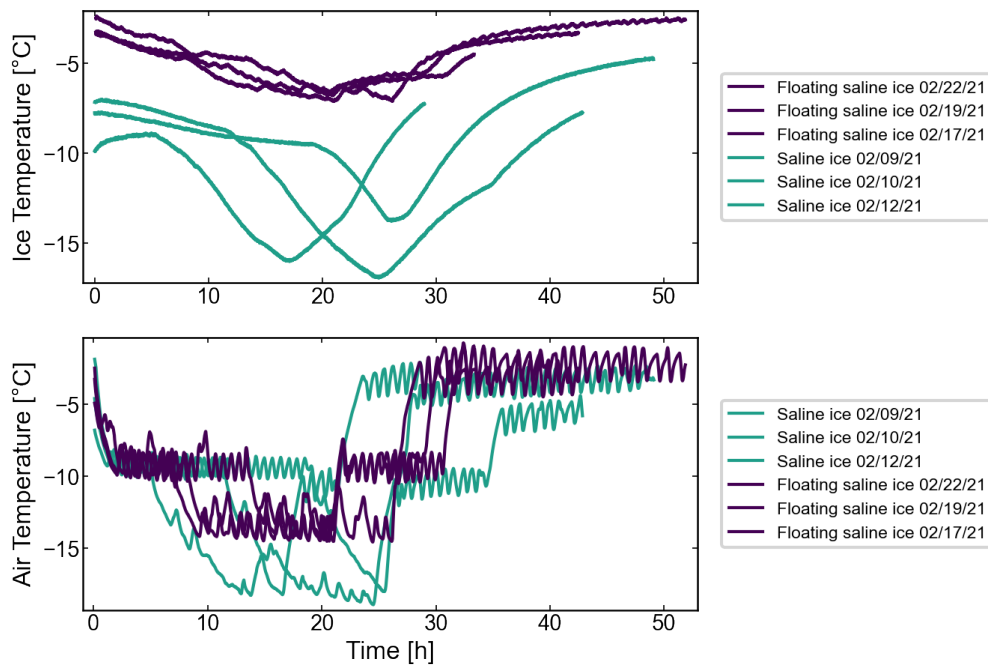
Figure 4.5: Saline ice on table and saline ice floating experimental comparison.

Figure 4.5 demonstrates that the floating ice takes longer to cool down or heat up, due to the insulation effect of the water in which the floating block of ice is submerged in, which delays the effect of a temperature change as the ice is only exposed to the air temperature at the top surface. Thus, the ice temperature range becomes much larger for the non-floating experiment.

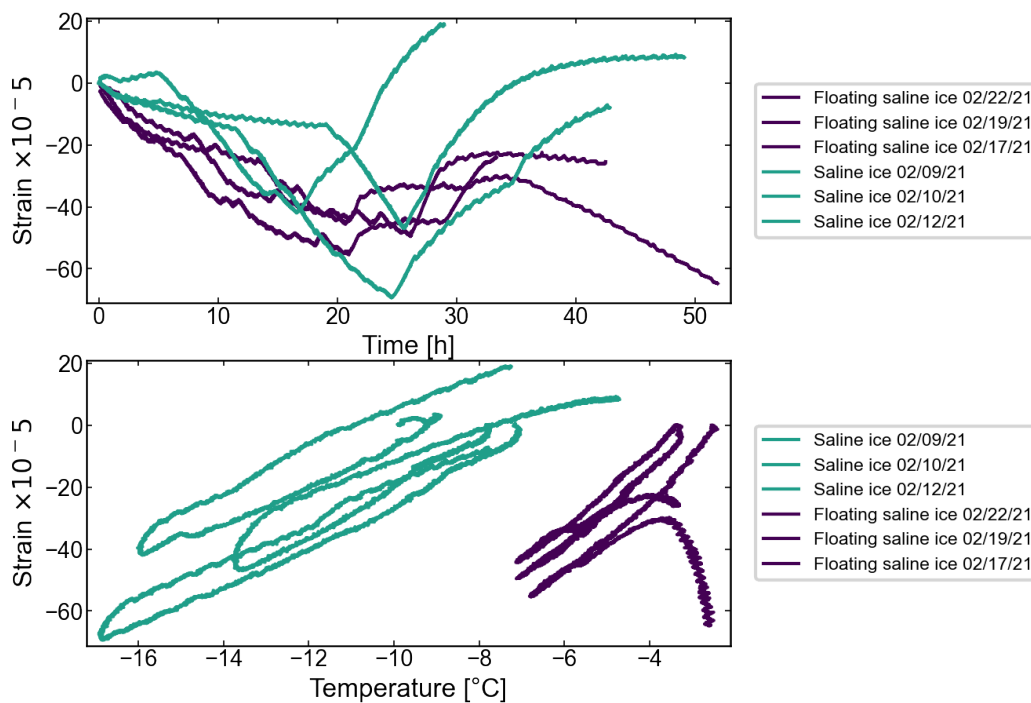Figure 4.6: Saline ice on table and saline ice floating experimental comparison.

Figure 4.6 illustrates that similar values of strain are reported from the tests, however, the saline ice

on a table experiment had a much greater range of temperature change. It is worth noting the similarity in the patterns between the recorded mean ice temperature over time in Figure 4.5 to the deformation over time in Figure 4.6. The similar shape in the deformation over time plot, especially for non-floating saline ice, indicates a strong relationship between ice temperature and strain. Decreasing temperatures cause a negative strain result, and increasing temperature yield an increasing strain result, often having a less linear slope. The dependence of strain from the mean ice temperature is different in saline ice in the floating tests compared to the non-floating tests for two reasons: the difference in air temperature rates, and the difference in boundary conditions. Temperature rate is the driving force for thermal expansion. Internal stresses in the ice sample decrease when the temperature change decreases. Also having an effect, the buoyancy force applied to the floating ice block may influence deformations in addition to thermal deformations.

4.3. Flooding experiments

The ice surface flooding, or pool experiments, aim to characterize the difference in thermal action between fresh and saline ice samples when the air temperature is held constant, and the thermal action is initiated by the radiation of latent heat occurring from the water freezing on the surface of the ice samples.

The two experiments for fresh and saline ice were performed at the same time with the same air temperature conditions, where either distilled water for the fresh ice sample or seawater for the saline ice sample was added to a cut-out pool on the surface of the ice samples. The fresh ice sample had 544.1g of freshwater added to the ice surface, whereas the saline ice sample had 1344.1g of seawater of 31.7 ppt salinity contained in the pool. The added water masses are different due to the methodologies in which the pools were created for each ice sample. A hot plate was used to melt a square-shaped pool into the surface of the fresh ice sample, whereas a chainsaw was used to carve out a pool in the saline ice sample, creating different sizes in the pools and thus different volumes of liquid at the surface. Future tests should utilize the same technique for creating the pools to ensure the same volume of water can be added to the surface. The seawater was added about one hour after the freshwater to the ice samples, explaining the delay in strain maxima in Figure 4.7 between fresh and saline ice tests. The ice blocks were different in size, causing a slight difference in temperature gradients in the ice blocks, which is visible in Figure A.27 and Figure A.28 of section A.6.

Figure 4.7 describes how the temperature of the ice changed compared to how the air temperature changed in the cold laboratory, for both fresh and saline samples. The initial ice temperature of fresh ice was around -9°C, and in the saline ice, it was around -8°C. When the liquids were cooled to the freezing points, 0°C and -1.9°C for fresh and seawater, respectively, they were added to the pools. As a result, the strain sensor in the saline ice sample demonstrated an expansion of 0.00015 and in fresh ice a strain value of 0.0005 during relatively short times, 1.5 hours in saline ice and 0.5 hours in fresh ice. Hence, the fresh ice experiment results in a higher strain and temperature gradient.

The exponential decay in temperature in the figure below displays the effects of Newton's law of cooling, where the rate of cooling is proportional to the temperature difference of, in this case, the ice, and its surroundings, the water freezing at the surface.

The strain-temperature plot shows that fresh ice experiences stronger hysteresis effects. The slopes of the fresh and saline strain-temperature curves are similar, especially during cooling, which occurs from -5°C to -9°C for both fresh and saline ice samples.
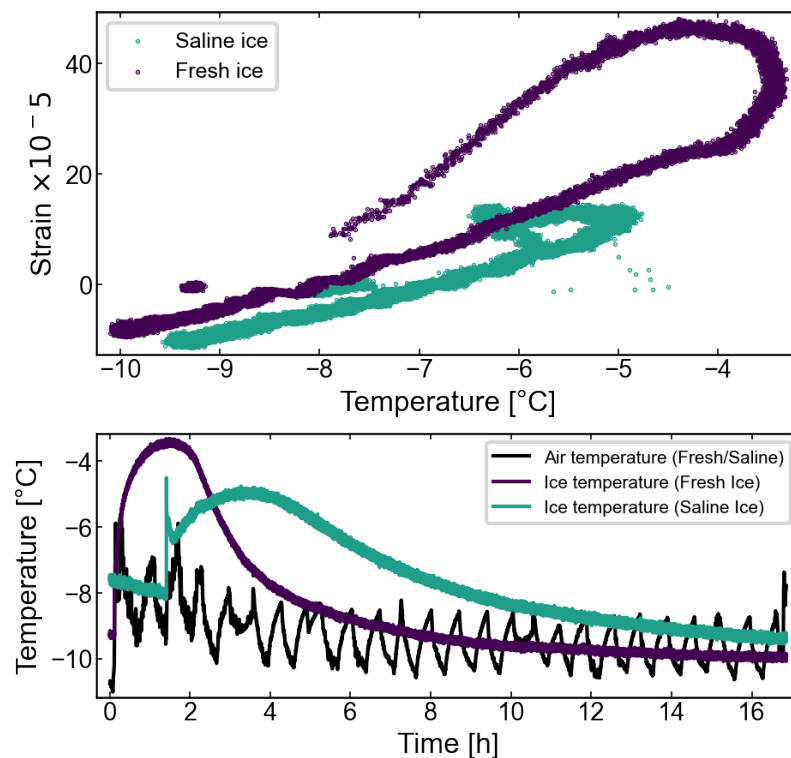
Figure 4.7: Fresh ice and saline ice flooding experimental comparison.

At the end of the tests, strain returns back to the zero level in fresh ice after five hours, and only four hours for saline ice. The salinity of the saline ice sample pool was measured again after the test to be 21.1 ppt, meaning that some salts penetrated into the ice block since the salinity decreased from the original value of 31.7 ppt.

The difference in the strain and ice temperature results for the saline and fresh ice can be explained by the distinct thermodynamic properties of fresh and saline ice, and by the difference in the freezing of fresh and seawater in the pools. When seawater freezes, slush forms in the water during cooling. Whereas freshwater transforms just into ice during cooling. Saline ice, consisting of small grains, acts as a more viscous material compared to fresh ice, which could explain the lower values of strain.

It is possible that the water from the pool experiments penetrated into the hole housing the thermistor string, influencing the temperature results, causing the large jump in the temperature plot in Figure 4.7. Therefore these results do not indicate that the ice temperature changed as rapidly as depicted in the figure. In addition, the water on the ice surface of these tests may influence the creep of the screws and the brackets securing the FBG strain sensor. Therefore it is necessary to repeat this experiment in future work to ensure accurate results.

4.4. Fieldwork in Svea

Results of the fieldwork performed from March to April 2021 are presented in this section. These experiments aimed to compare the thermal stresses in confined fresh and sea ice. The laboratory experiments were unconfined, with no thermal stresses, only thermal strains. However, in the fieldwork, confinement limits strains and influences the thermal stresses. Pressure sensors were installed in the ice in both a freshwater lake and a saline lagoon (Vallunden lake) in close proximity; data logging stations were located approximately 250 m from each other. Thus the two locations experienced the same weather conditions, which is highlighted by the similar temperature-time relations in Figure 4.9 and Figure 4.10. Vallunden lake is connected to the fjord via a narrow straight with a 20 m width and length of 100 m, which freezes during winter months [21].

The salinity profile of the sea ice in Vallunden lake is displayed in Figure 4.8. The difference in the salinity profiles at the bottom layer of the ice can be attributed to either warmer weather preceding

the ice core extraction on March 17th, causing the ice to halt growth, or due to the ice-water interface layer not being properly captured, as the high saline bottom layer displayed in the April 27th results represents a more typical salinity profile for sea ice.
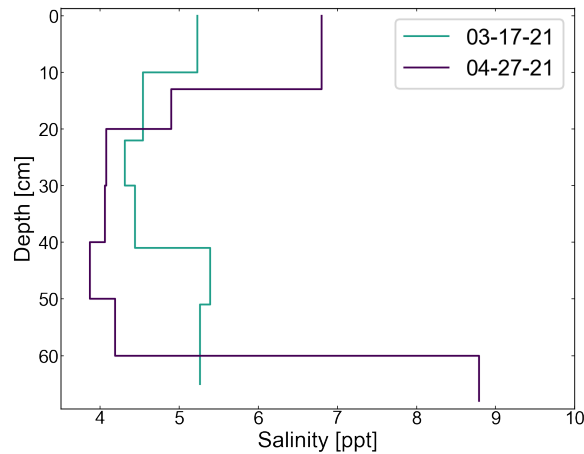

Figure 4.8: The salinity of sea ice on Vallunden saline lake.

Two pressure sensors were installed at each location, where one sensor was deeper than the other (17 cm and 35 cm below the ice surface). Figures 4.9-4.10 demonstrate the entire duration of stress and temperature data for both sites. Temperature data was measured by both the top and bottom pressure sensors and internally from the datalogger. Measured temperature data is also compared to the weather data achieved from the Sveagruva weather station.
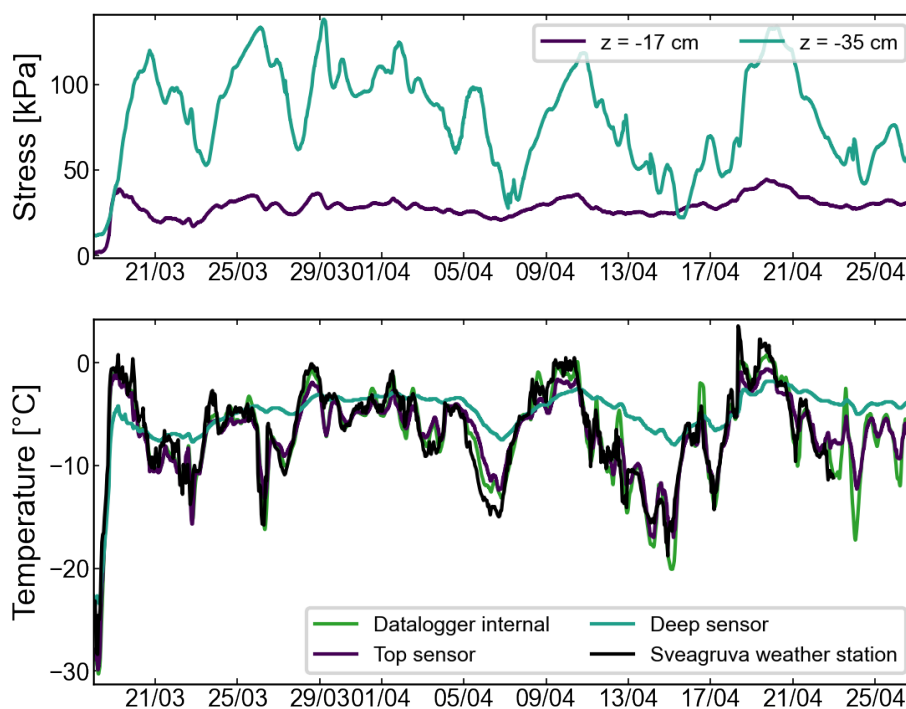

Figure 4.9: Strain and temperature time series data for the freshwater lake fieldwork.
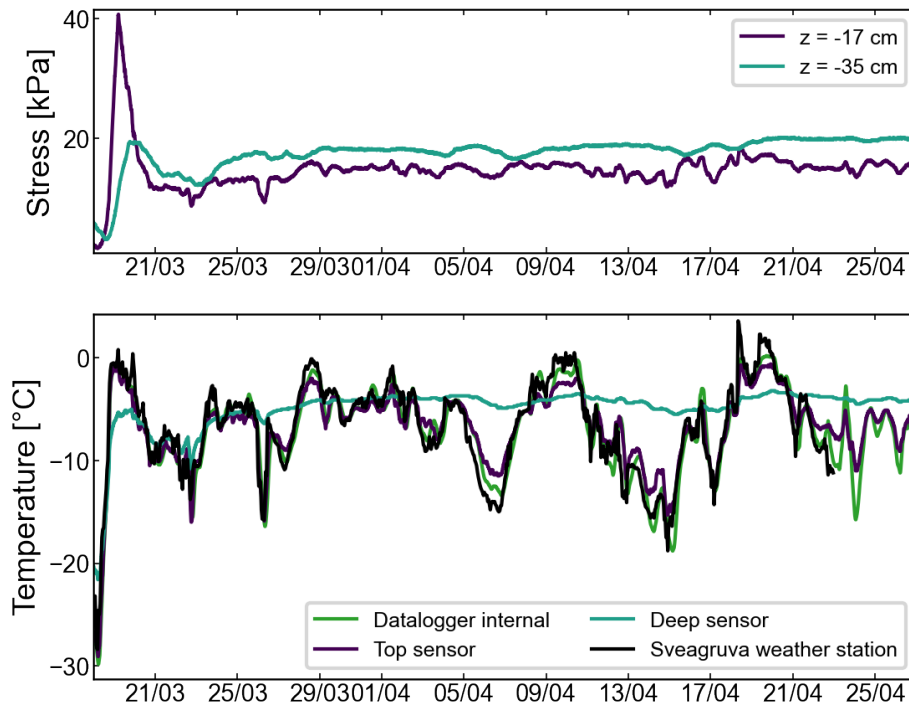
Figure 4.10: Strain and temperature time series data for the Vallunden saline lake fieldwork.

The beginning of the stress and temperature data for fresh and sea ice is enlarged in Figure 4.11-Figure 4.12 to demonstrate the warming event that took place during the beginning of the data collection period. The first two days of measurements were not included due to large amounts of noise in the data. For the freshwater lake stress-time data, the pressure sensor in the deepest layer recorded the highest stress values, whereas, for the saline lagoon stress-time data, the top sensor recorded the higher values for stress.
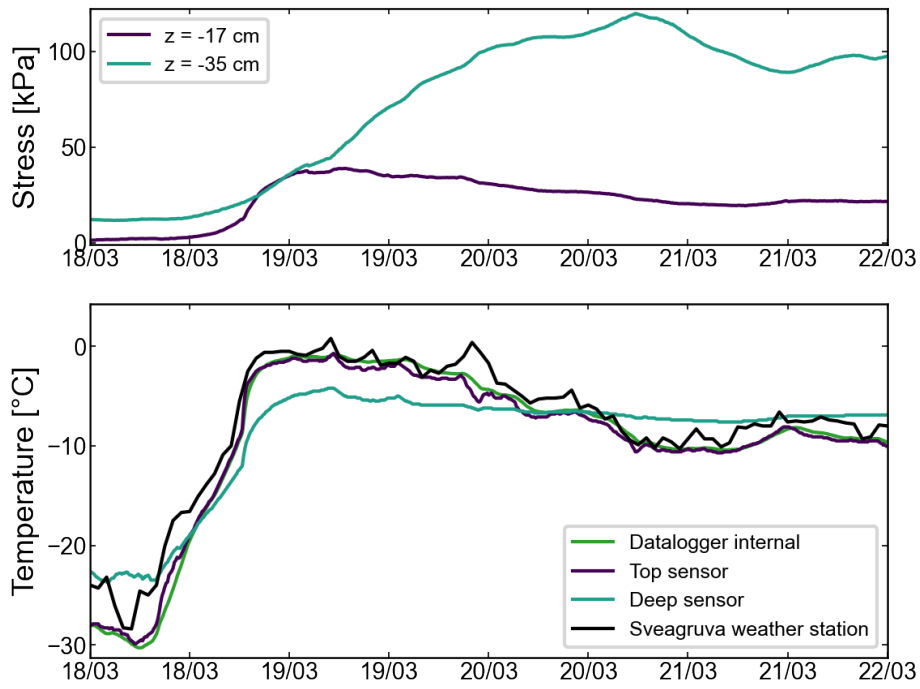
Figure 4.11: Beginning of data collection for the freshwater lake fieldwork.
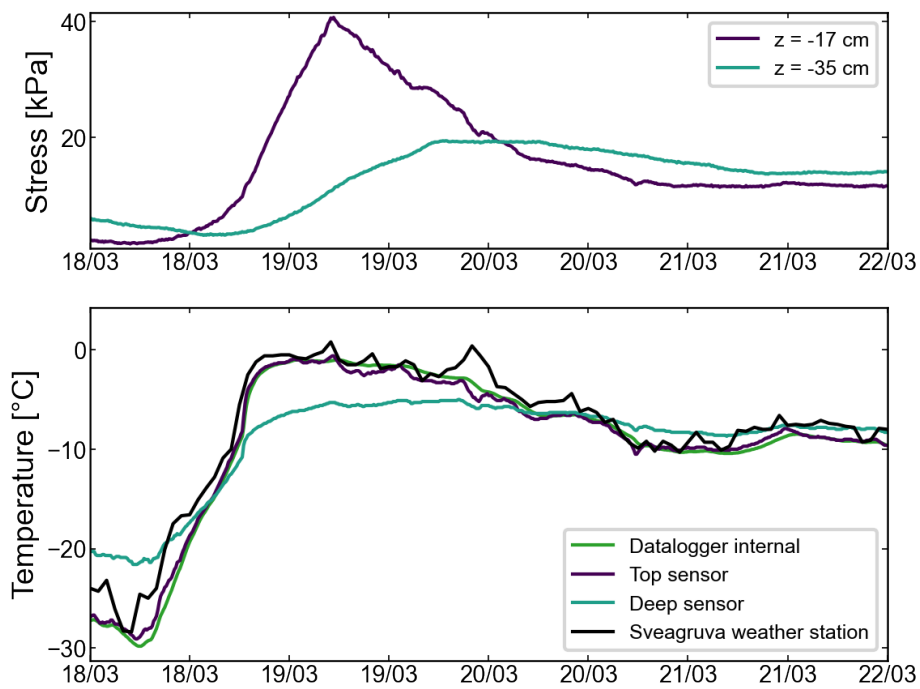

Figure 4.12: Beginning of data collection for the Vallunden saline lake fieldwork.

Figure 4.13-Figure 4.14 enlarge the data after the initial peak in stress, to closely examine the stress values after the maximum measurements occurred.
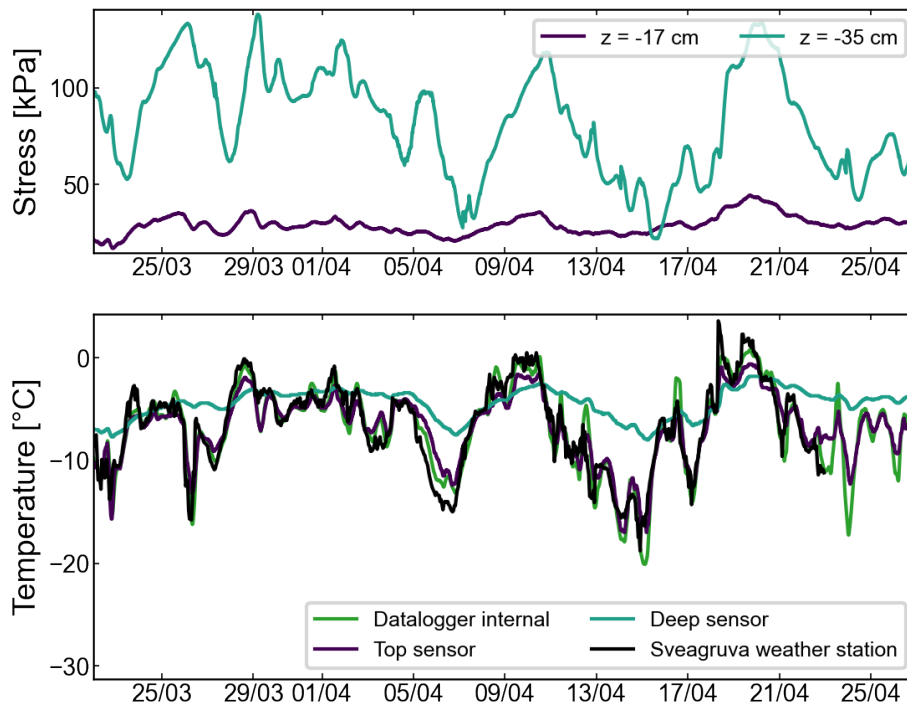
Figure 4.13: Fresh ice fieldwork enlarged stress and temperature temporal data.
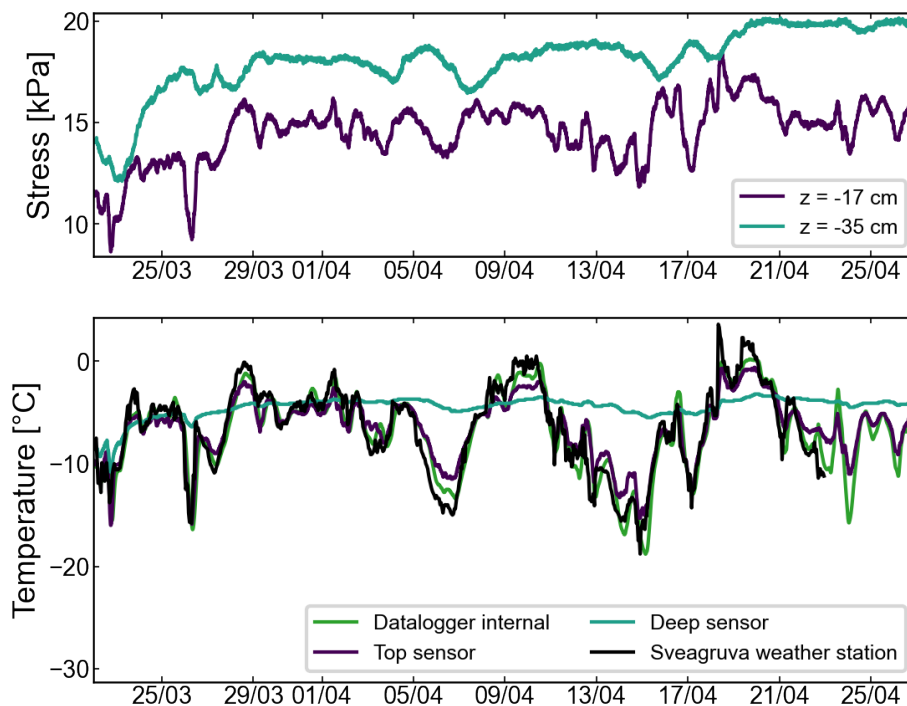
Figure 4.14: Sea ice fieldwork enlarged stress and temperature temporal data.

The results from the fieldwork yield higher stress values in the freshwater lake. There is a strong correlation between the weather station measured air temperature data to stresses, representing the dependence of ice deformations on temperature. For both fresh and sea ice, stress increased with depth. This can be explained by plate bending stresses, as the lower sensor is farthest away from the

neutral axis of the ice.

In the fresh ice results, there is a synchronous change at different depths in the ice. When stresses at the bottom sensor increase, they also increase at the top sensor. In sea ice, however, when stresses increase at the bottom sensors, they tend to decrease on the top sensor, as illustrated from Figure 4.13-Figure 4.14. In other words, in the top layers of sea ice compression would occur, however in the bottom layers expansion would occur. This finding is consistent with the Svea columnar sea ice block on the table experiment. Negative thermal expansion occurred in the lower depths in the ice sample, while positive thermal expansion occurred in the upper layers.

4.5. COMSOL Simulation Results

The COMSOL simulations were performed to replicate experiments consisting of the air temperature change fresh ice tests. The simulation represented the fresh ice sample with the same geometry and material properties. Ice surface temperature measured from the thermistor strings was used as an input in the model and applied to all faces of the ice block in order to simulate the controlled air temperature change that took place during each experiment.

The purpose of the model is to confirm accuracy in the measurements as the effective coefficient of thermal expansion for fresh ice is well-studied, accepted in literature to be $5.27 \times 10^{-5} 1/°C$ at 0°C [9].

In the numerical simulations, temperature data from thermistor string sensor 5, which corresponds to ice surface temperature, was applied as a boundary condition to all faces of the ice block.

Strain plotted over time for the experimental air temperature change fresh ice experiment, that took place on 02/09/21, against the numerical simulation results, is displayed in Figure 4.15a. This test corresponded to sample 01B1 from Table 3.1. The comparison with the COMSOL simulations yields the result that strain is under-predicted in the numerical simulation results. Alongside is the strain plotted against mean ice temperature in Figure 4.15b. Hysteresis can be observed in both the numerical simulation results and the experimental results, but in the COMSOL results the hysteresis is reversed, strain values increase over the cyclic runs of the tests whereas the experimental results strain decreases over time.
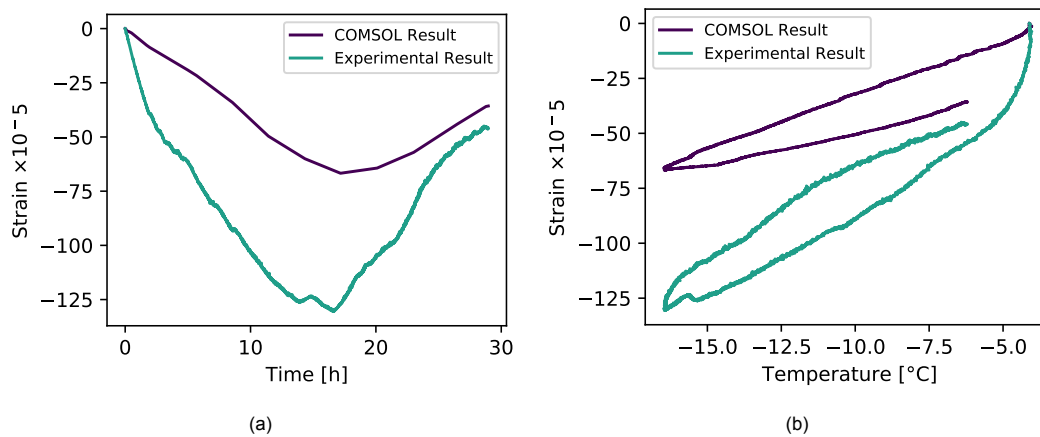

Figure 4.15: (a) Strain over time for the numerical model (purple) and cold laboratory experiment (blue) that took place on 02/09/21 using fresh ice. (b) Strain plotted against mean ice temperature for both the experimental and numerical simulation results.

The COMSOL model results for the fresh ice air temperature change experiment that occurred on 02/10/21 yield the following comparison to the experimental results, displayed in Figure 4.16. Strain is again underpredicted in the COMSOL model and the strain-temperature plot yields a slightly different slope, corresponding to different ECTE values from the model and the lab results.
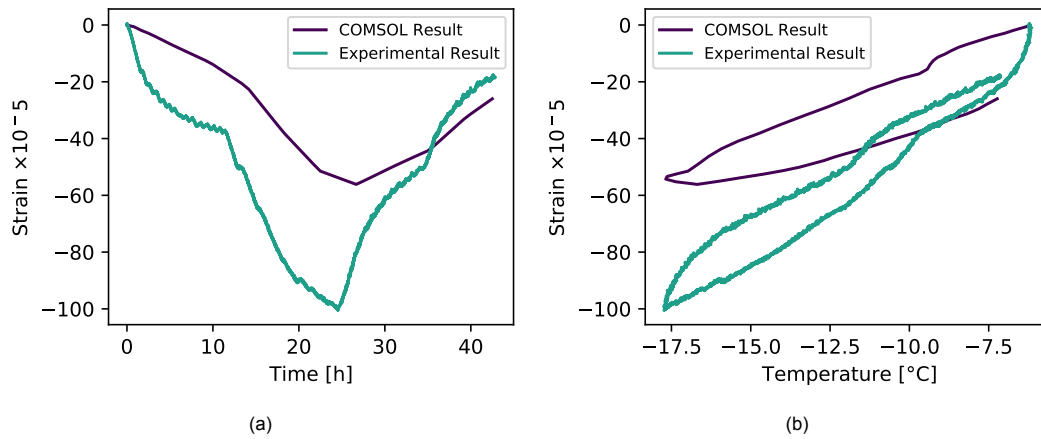
Figure 4.16: (a) Strain over time for the numerical model and experiment that took place on 02/10/21 using fresh ice. (b) Strain plotted against mean ice temperature for both the experimental and numerical simulation results.

The COMSOL model results for the fresh ice air temperature change experiment that occurred on 02/12/21 yield the following comparison to the experimental results, displayed in Figure 4.17.

Figure 4.17: (a) Strain over time for the numerical model simulation and experiment taking place on 02/12/21 for fresh ice. (b) Strain plotted against mean ice temperature for the model prediction and experimental result.

The COMSOL model results for the fresh ice air temperature change experiment that occurred on 02/22/21 yield the following comparison to the experimental results, displayed in Figure 4.18.
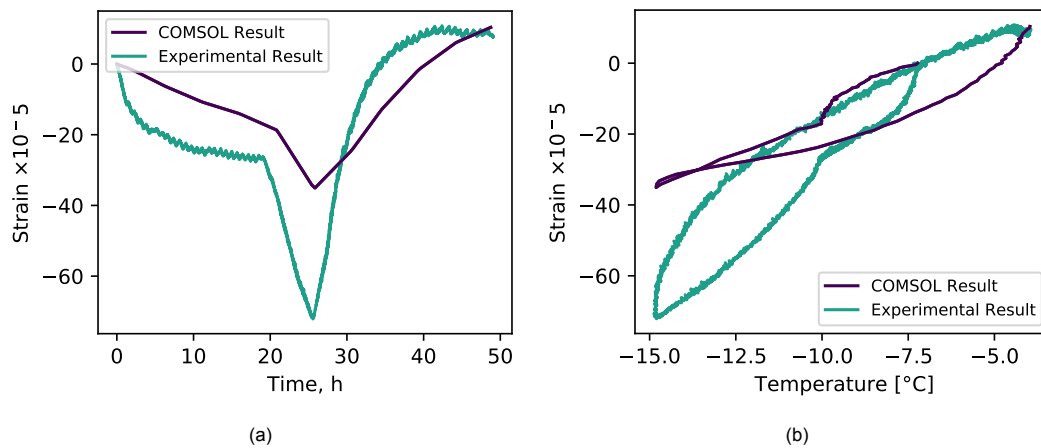
Figure 4.18: (a) Strain over time for the numerical model simulation and experiment taking place on 02/22/12 for fresh ice. (b) Strain plotted against mean ice temperature, the average of thermistor string sensors 5-12.

The COMSOL model results for the fresh ice air temperature change experiment that occurred on 01/28/21 yield the following comparison to the experimental results, displayed in Figure 4.19. This comparison was based on fresh ice sample 01A1, which had smaller dimensions than the previous comparisons made with COMSOL.
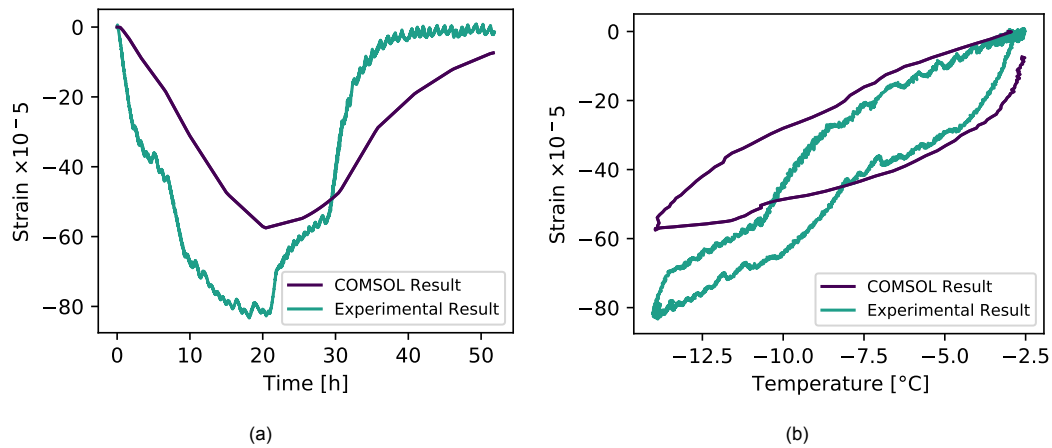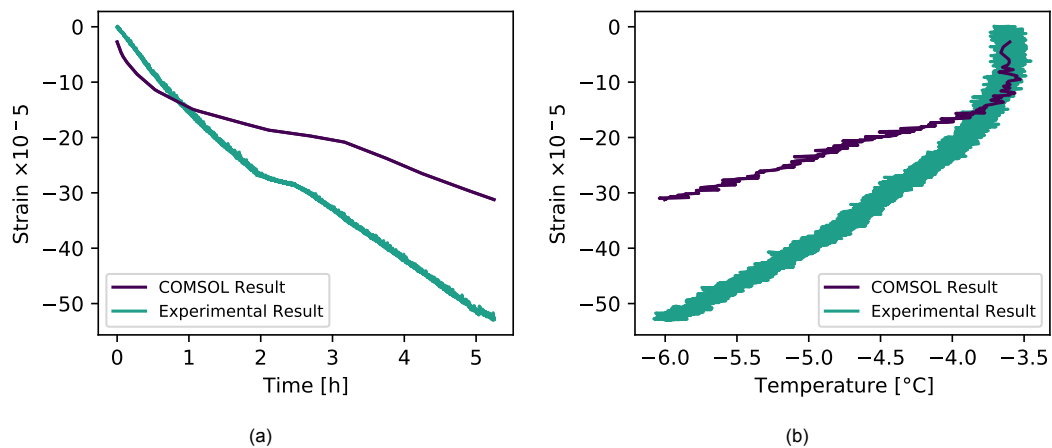

Figure 4.19: (a) Strain over time for the numerical model simulation and experiment taking place on 01/28/12 for fresh ice. (b) Strain plotted against mean ice temperature, the average of thermistor string sensors 5-12.

The experiments used in this comparison with the COMSOL numerical simulations for fresh ice, where the air temperature was changed while the ice sample rested on the table, yielded ECTE values that are consistent with the literature, where the mean values are reported in Table 4.1. Therefore, the difference in results from the model and experiments yields the conclusion that this COMSOL model does not accurately represent the experiments taking place. Therefore, further simulation comparison with other types of ice and other types of experiments were not performed, since the model is lacking the fundamental comparison capabilities with the already known case of fresh ice expanding under controlled air temperature cases. Future work should aim to identify the cause of the underestimation of thermal strain values in the COMSOL fresh ice model.

5

Conclusions and Recommendations

This work aimed to characterize the difference between fresh and sea ice thermal deformations when boundary conditions consisted of various thermal actions, namely air temperature change, floating in liquid, and flooding at the ice surface. Quantitative comparisons were able to be achieved through ECTE analysis for the non-floating, air temperature change experiments, where ECTE is a constant characterizing material behavior under thermal action. The linear coefficient of thermal expansion for sea ice depends on the properties of sea ice, including the permeability, salinity, and ice temperature [16]. Optic fiber sensors based on Fiber Bragg Grating (FBG) enabled strain and temperature measurements on the ice surface during the cold laboratory experiments. Fieldwork completed in a freshwater lake and saline lagoon with the same meteorological conditions enabled a comparison of fresh and sea ice thermal stresses to be performed. Geokon pressure cells accompanied by a datalogger were utilized to measure thermal stresses in the upper layer of the sea ice and fresh ice during the deployment of the equipment from March to April 2021.

5.1. Conclusions

In the thermal expansion air experiments, we found that fresh ice resulted in an ECTE value less than 10% lower than that for granular saline ice, which is within the uncertainty bounds of the experiment. Therefore, a significant difference cannot be concluded between the thermal expansion of columnar fresh ice and granular saline ice samples, when the ice is exposed to air temperature change. Columnar sea ice displayed the highest mean value for ECTE, however, a significant difference cannot be concluded due to large error margins. The range of temperatures for which the ice deforms was wider for fresh ice than saline ice tests when the same air temperatures were applied to the ice samples, which was concluded to be due to the higher specific heat capacity in saline ice.

The thin section images from each ice sample compared in this analysis, columnar fresh ice, granular spray ice, and columnar sea ice, demonstrate strong differences in crystalline structures. Granular saline ice is more plastic than columnar ice. The experiments reveal that granular saline ice demonstrates smaller hysteresis than fresh ice. Svea columnar sea ice experiments showed the largest hysteresis of all tests.

In the floating experiments, we qualitatively observed a higher strain-temperature slope, indicating a larger ECTE for granular saline ice. A full understanding of this phenomenon is not yet undertaken, however, this observation would be an interesting basis for further unconfined floating ice experiments.

Negative ECTE values were found both in the columnar sea ice air change experiments and the floating granular saline ice experiments. In the columnar sea ice tests, negative values were more common in deeper depths of the ice sample during heating. In the floating saline ice tests, negative ECTE was also observed during the higher temperatures at the end of the test, during heating. This atypical thermal behavior likely stems from brine migration in sea ice with high salinity.

In the flooding experiments, thermal actions were initiated by the latent heat release during water crystallization on the ice surface for granular saline ice and fresh ice samples. The air temperature was held constant. A significant difference was not found between fresh and granular saline ice strain-temperature slopes, which were especially similar during the cooling phase of the surface water freez-

ing. The fresh ice sample deformed with a greater temperature range than saline ice and showed a stronger hysteresis in results.

The main conclusions drawn from the fieldwork in Svea were that thermal stresses increased over the ice layer depth for both fresh ice and sea ice, and fresh ice experienced larger stresses by roughly one order of magnitude.

5.2. Recommendations

Floating and flooding experiments should be repeated to further define the difference between fresh and columnar sea ice thermal deformations due to these thermal actions. Floating experiments should be performed with columnar sea ice to see if this test would also result in a higher ECTE value than fresh ice. Flooding experiments give an answer to a practical problem of when water gets on top of the ice surface due to rain, melted snow, or tidal flooding, and how the ice will expand or react to this latent heat. This experiment was only able to be performed one time due to the timely preparations required for this type of experiment, and thus more iterations should occur to compare to the results achieved in this report. In future iterations of this experiment, the amount of water added to the pools should be of the same weight, in order for the differences in deformations to be properly compared under the same boundary conditions.

In future experiments, more emphasis should be put on measuring sea ice density before, after, and during tests, to study the brine migration and how it affects thermal expansion.

In addition, it would be interesting to calculate in future work how the thermal deformations recorded in these experiments would translate to loadings on offshore structures, which is a possible application of this work.

Lastly, future work in COMSOL modelling should identify the cause of the underestimation of thermal strain values in the COMSOL fresh ice model. Then, other tests can be modelled in COMSOL, such as the floating ice tests, to aid in further understanding the experimental results.

Bibliography

[1] ISO 19906-2010 Petroleum and natural gas industries. Technical report.

[2] Theodore L Bergman, Adrienne S Lavine, Frank P Incropera, and David P DeWitt. *Introduction to heat transfer*. John Wiley & Sons, 2011.

[3] T. R. Butkovich. Thermal expansion of ice. *Journal of Applied Physics*, 30(3):350–353, 1959. ISSN 00218979. doi: 10.1063/1.1735166.

[4] International Electrotechnical Commission et al. Wind energy generation systems-part 3-1: Design requirements for fixed offshore wind turbines. *International standard IEC*, pages 61400–3, 2019.

[5] Gordon FN Cox. Thermal expansion of saline ice. *Journal of Glaciology*, 29(103):425–432, 1983.

[6] Yu P Doronin and DE Kheisin. Sea ice. 1977.

[7] Oloufemi Fakorede, Zoé Feger, Hussein Ibrahim, Adrian Ilinca, Jean Perron, and Christian Masson. Ice protection systems for wind turbines in cold climate: characteristics, comparisons and analysis. *Renewable and Sustainable Energy Reviews*, 65:662–675, 2016. ISSN 18790690. doi: 10.1016/j.rser.2016.06.080. URL http://dx.doi.org/10.1016/j.rser.2016.06.08 0.

[8] Kenneth M Golden, Hajo Eicken, AL Heaton, J Miner, DJ Pringle, and J Zhu. Thermal evolution of permeability and microstructure in sea ice. *Geophysical research letters*, 34(16), 2007.

[9] M Jakob, S Erk, Z Ges Ka, et al. Warmedehnung des eises zwischen 0 und -253. *Z Ges. Kalte-Ind*, 35:125–130, 1928.

[10] Jerome B. Johnson and Ronald C. Metzner. Thermal Expansion Coefficients For Sea Ice. *Journal of Glaciology*, 36(124):343–349, 1990. ISSN 0022-1430. doi: 10.3189/0022143907937013 27.

[11] Raman Kashyap. *Fiber bragg gratings*. Academic press, 2009.

[12] SJ La Placa and B Post. Thermal expansion of ice. *Acta Crystallographica*, 13(6):503–505, 1960.

[13] Ben Lishman and Aleksey Marchenko. An investigation of relative thermal expansion of ice and steel. In *22nd IAHR International Symposium on Ice*. London South Bank University, 2014.

[14] Kathleen Yardley Lonsdale. The structure of ice. *Proceedings of the Royal Society of London. Series A. Mathematical and Physical Sciences*, 247(1251):424–434, 1958.

[15] Sveinung Løset, Karl N Shkhinek, Ove Tobias Gudmestad, and Knut V Høyland. *Actions from ice on Arctic offshore and coastal structures*. 2006. ISBN 5811407033.

[16] F Malmgren. On the properties of sea-ice: Norwegian north polar expedition with the maud, 1918-1925, sci. *Res*, 1(5):67, 1927.

[17] A Marchenko, T Thiel, and S Sukhorukov. Measurements of thermally induced deformations in saline ice with fiber bragg grating sensors. In *Proc. 21st IAHR Int. Symp. on Ice 'Ice Research for a Sustainable Environment*, 2012.

[18] A Marchenko, D Wrangborg, and T Thiel. Using distributed optical fiber sensors based on fbgs for the measurement of temperature fluctuations in saline ice and water on small scales. In *Proceedings of the International Conference on Port and Ocean Engineering under Arctic Conditions, POAC*, 2013.

[19] Aleksey Marchenko. Thermo-mechanical loads of confined sea ice on structures. *Philosophical Transactions of the Royal Society A: Mathematical, Physical and Engineering Sciences*, 376 (2129), 2018. ISSN 1364503X. doi: 10.1098/rsta.2017.0341.

[20] Aleksey Marchenko and Ben Lishman. The influence of closed brine pockets and permeable brine channels on the thermo-elastic properties of saline ice. *Philosophical Transactions of the Royal Society A: Mathematical, Physical and Engineering Sciences*, 375(2086), 2017. ISSN 1364503X. doi: 10.1098/rsta.2015.0351.

[21] Aleksey Marchenko, Aleksey Shestov, Evgeny Karulin, Eugene Morozov, Marina Karulina, Pyotr Bogorodskii, Sergey Muzylev, D. Onishchenko, and A. Makshtas. Field studies of sea water and ice properties in svalbard fjords. volume 1, 01 2011.

[22] Aleksey Marchenko, Ben Lishman, David Wrangborg, and Torsten Thiel. Thermal Expansion Measurements in Fresh and Saline Ice Using Fiber Optic Strain Gauges and Multipoint Temperature Sensors Based on Bragg Gratings. *Journal of Sensors*, 2016, 2016. ISSN 16877268. doi: 10.1155/2016/5678193.

[23] Adolf K Y Ng, Changmin Jiang, Paul Larson, and Barry Prentice. Climate Change and Its Impacts : Opening Up the Arctic Seas for Maritime Transport. (January), 2018. doi: 10.1016/B978-0-1 2-811067-6.00010-9.

[24] Office of energy efficiency & renewable energy. Offshore wind market report: 2021 edition, 2000.

[25] A Othonos and K Kalli. Fiber bragg gratings: Fundamentals and applications in telecommunications and sensing. norwood: Artech house, 1999.

[26] O. Pettersson. On the Properties cf Water and Ice. *Vega-expeditionens vetenskapliga iakttagelser (ed. AE Nordenskiöld)*, 2:247–323, 1883.

[27] Elton Roy Pounder. *The physics of ice*. Elsevier, 2013.

[28] RW Powell. Thermal conductivities and expansion coefficients of water and ice. *Advances in physics*, 7(26):276–297, 1958.

[29] Aydin Rajabzadeh, Richard C Hendriks, Richard Heusdens, and Roger M Groves. Classification of composite damage from fbg load monitoring signals. In *Sensors and Smart Structures Technologies for Civil, Mechanical, and Aerospace Systems 2017*, volume 10168, page 1016831. International Society for Optics and Photonics, 2017.

[30] K Röttger, A Endriss, Jörg Ihringer, S Doyle, and WF Kuhs. Lattice constants and thermal expansion of h2o and d2o ice ih between 10 and 265 k. *Acta Crystallographica Section B: Structural Science*, 50(6):644–648, 1994.

[31] Peter Schwerdtfecer. The thermal properties of sea ice. *Journal of Glaciology*, 4(36):789–807, 1963.

[32] R.L. Thoman, J. Richter-Menge, and Druckenmiller M.L. Arctic report card 2020, 2000.

[33] David Wrangborg, Aleksey Marchenko, and Dmitry Murashkin. Measurement of loads exerted by sea ice on the quay at kapp amsterdam on svalbard. In *Proceedings of the International Conference on Port and Ocean Engineering Under Arctic Conditions*, 2015.

[34] Li Zhou, Shifeng Ding, Ming Song, Junliang Gao, and Wei Shi. A Simulation of Non-Simultaneous Ice Crushing Force for Wind Turbine Towers with Large Slopes. 2019.

A
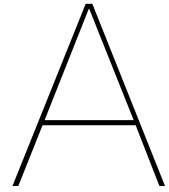
Appendix A

The following plots demonstrate the temperature profile, temperature gradient, and strain response for each experiment. The temperature gradient inside the ice samples appeared only when the laboratory air temperature was changed, otherwise, it was more constant. The temperature gradient is displayed over time, which is indicated by the color gradient (time begins at the color purple and ends at the color yellow). In plots where the temperature gradient is less linear, it is possible that the thermistor string was pushed out of the ice sample, which happened more often during floating tests. The thermistors deepest in the ice samples, which are more insulated from the air itself, generally show the largest divergence from the value of the air temperature.

The procedure for determining the effective coefficient of thermal expansion (ECTE) from the laboratory results involves a linear curve-fitting mechanism that determines the slope of the strain/temperature data, which corresponds to the ECTE. The temperature in the following plots represents mean ice temperature, the average of thermistor string sensors 5-12. The linear selection of the strain-temperature slope was based on when the temperature gradient was also the most constant with respect to time. When the equation of the line is displayed on the strain-temperature plot, the only significant value is the slope of this equation, which corresponds to the ECTE of each test.

A.1. Fresh ice on table, air temperature change experiments
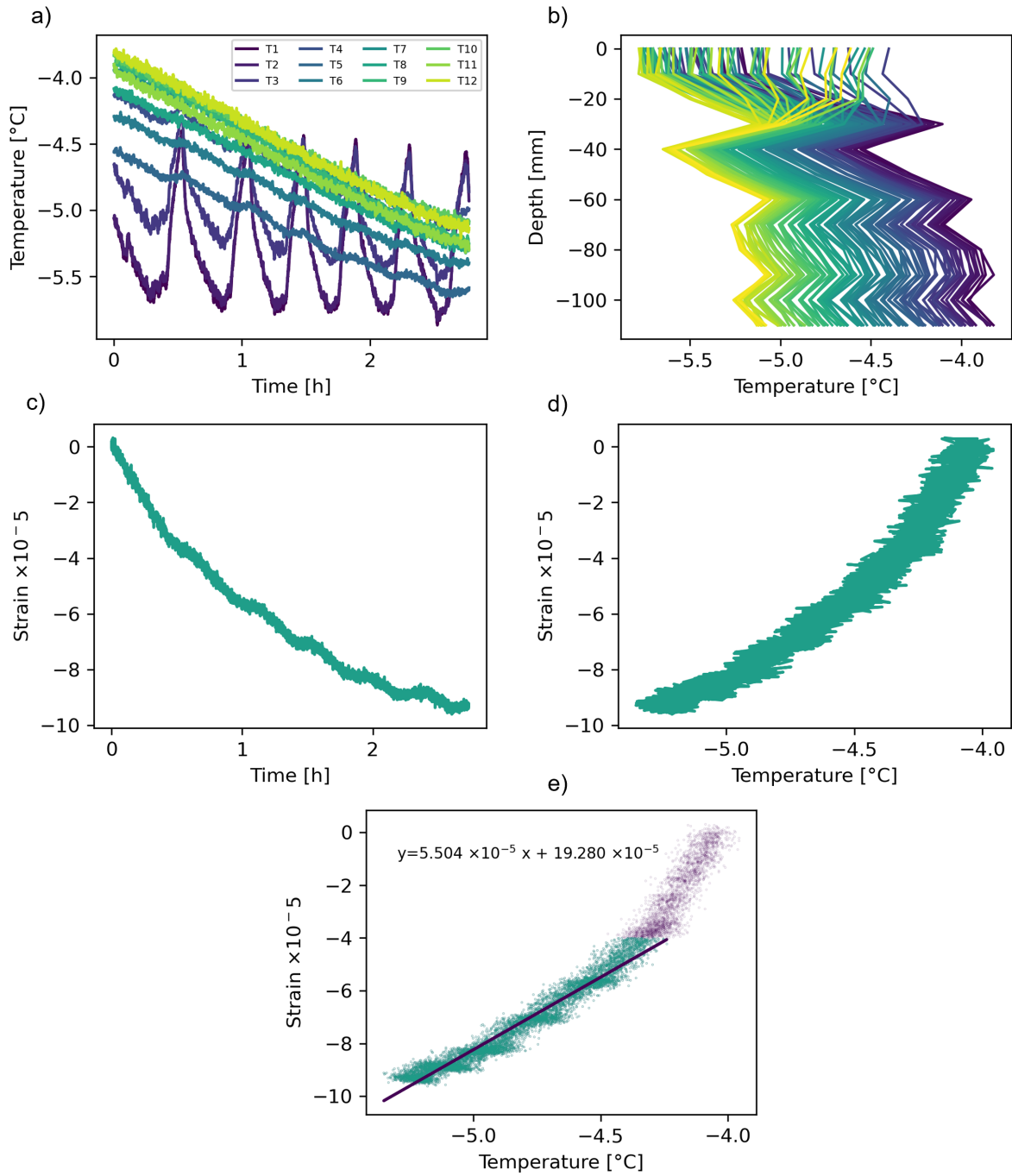
Figure A.1: The first part of **Experiment E01**, fresh ice on the table, sample 01A1. (a) Temperature profile during cooling (b) Temperature gradient displays strong variance near the ice surface, which may have been due to the thermistor string being pushed out of the ice sample during the test and measuring the air temperature. (c) Strain over time (d) Strain over mean ice temperature (e) Strain over mean ice temperature ECTE calculation. The slope of the line equates to the ECTE value for the experiment.
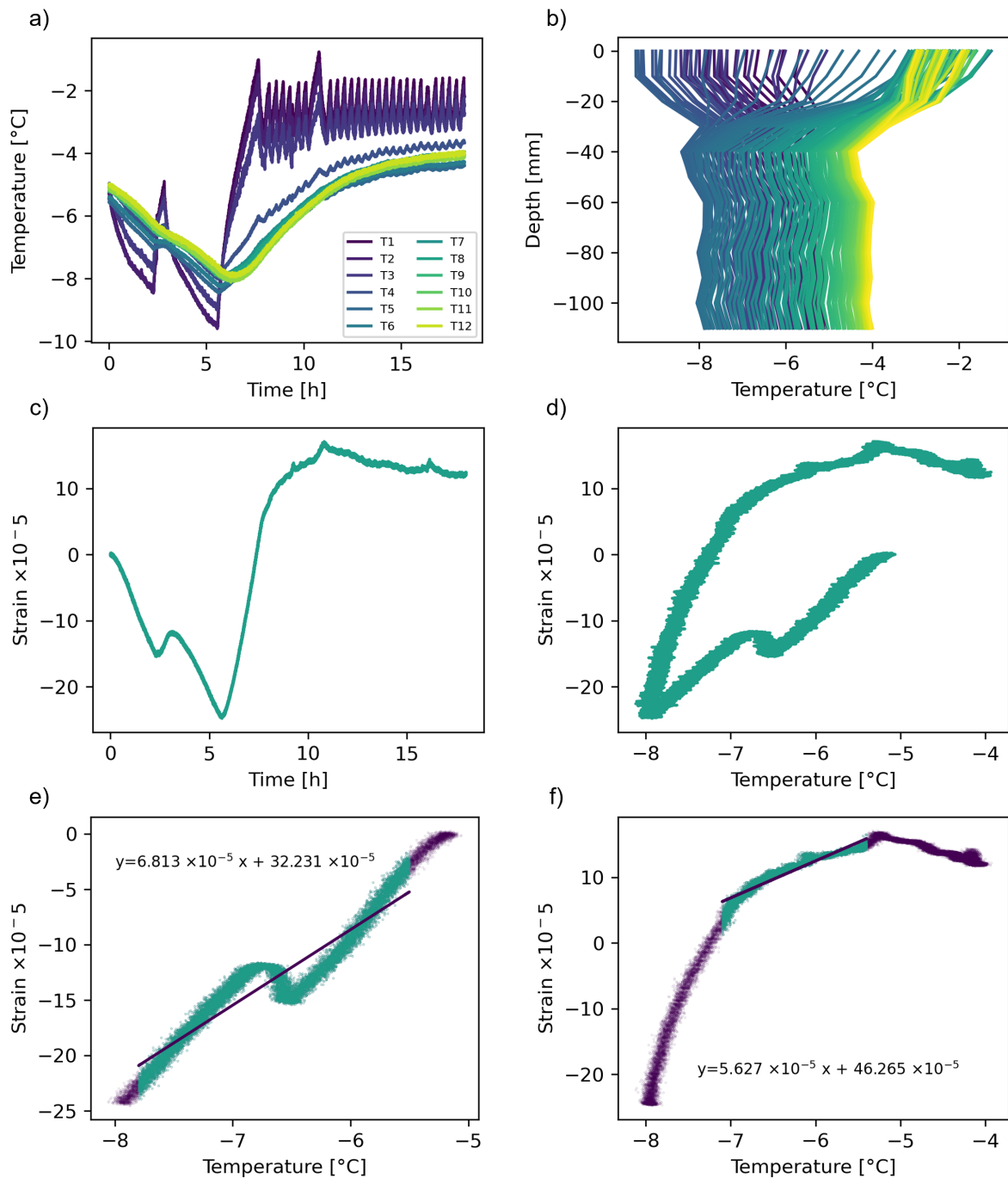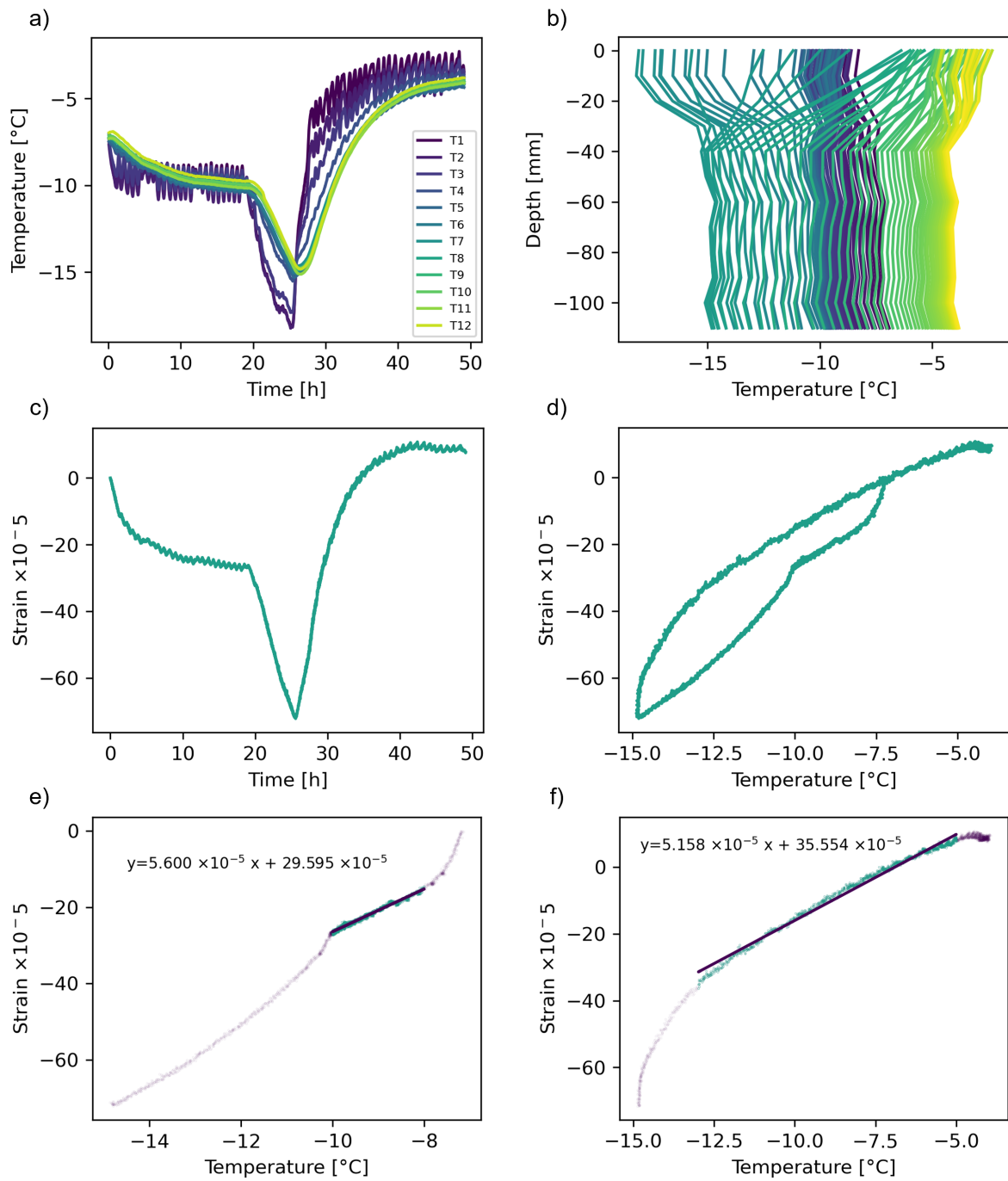
Figure A.2: Part two of **Experiment E01**, fresh ice on the table, sample 01A1. (a) The temperature profile of cooling then heating (b) Temperature gradient (c) Strain over time (d) Strain over mean ice temperature (e-f) Strain over mean ice temperature ECTE calculation. The slope of the line equates to the ECTE value for the experiment.
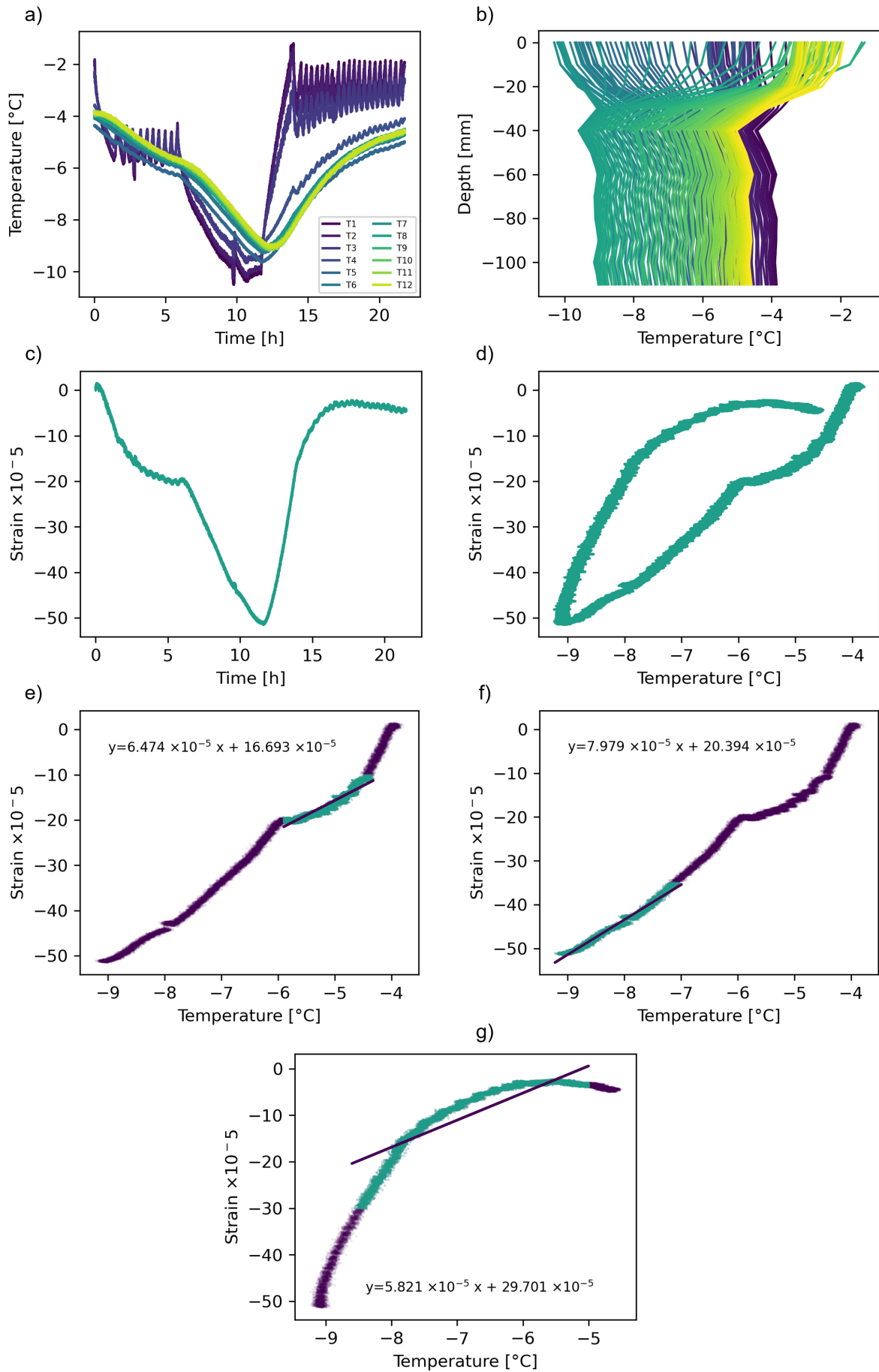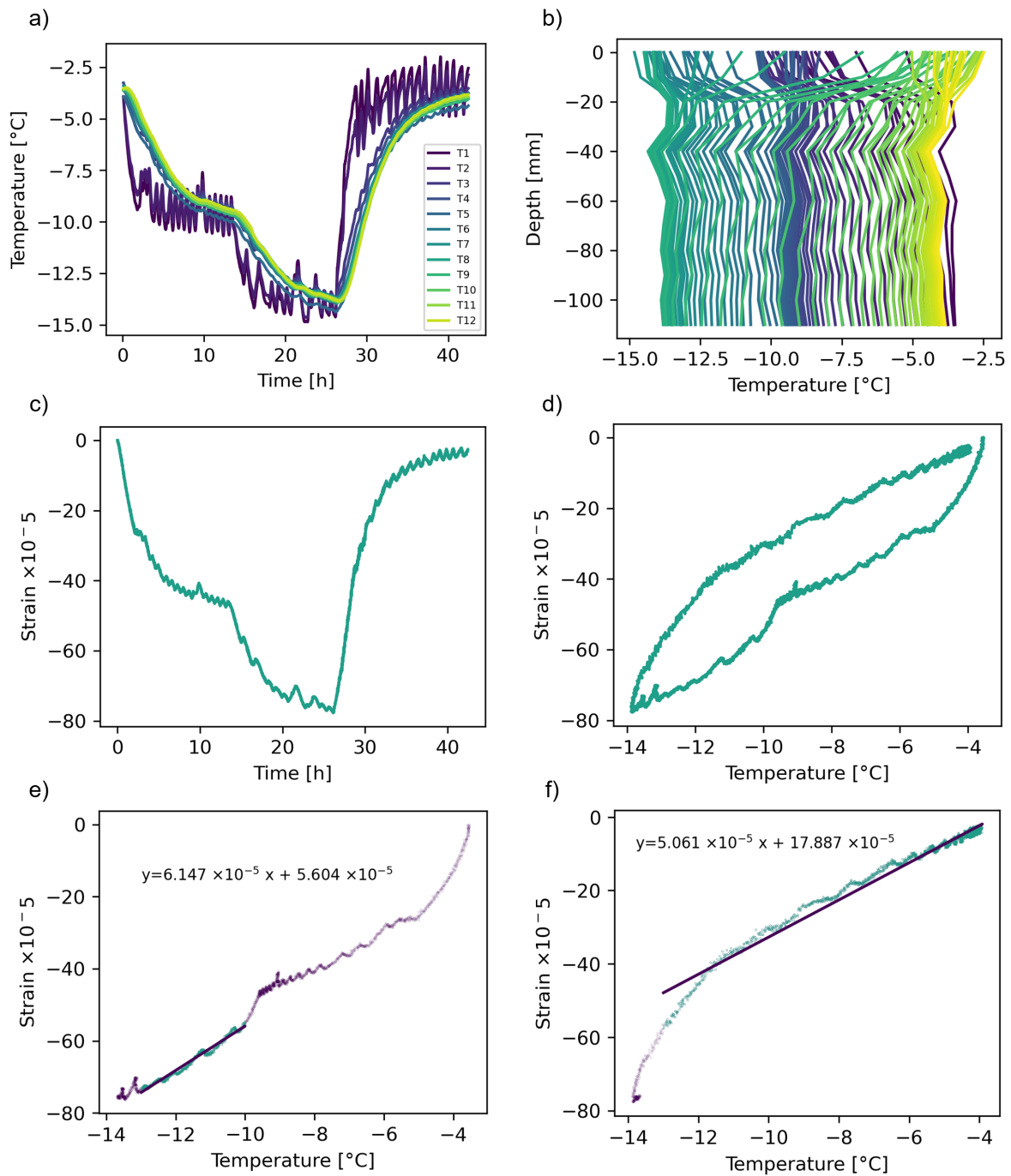
Figure A.3: **Experiment E02**, fresh ice on the table, sample 01A1. (a) Temperature profile, cooling then heating (b) Temperature gradient (c) Strain over time (d) Strain over mean ice temperature (e-g) Strain over mean ice temperature ECTE calculation. The slope of the line equates to the ECTE value for the experiment.
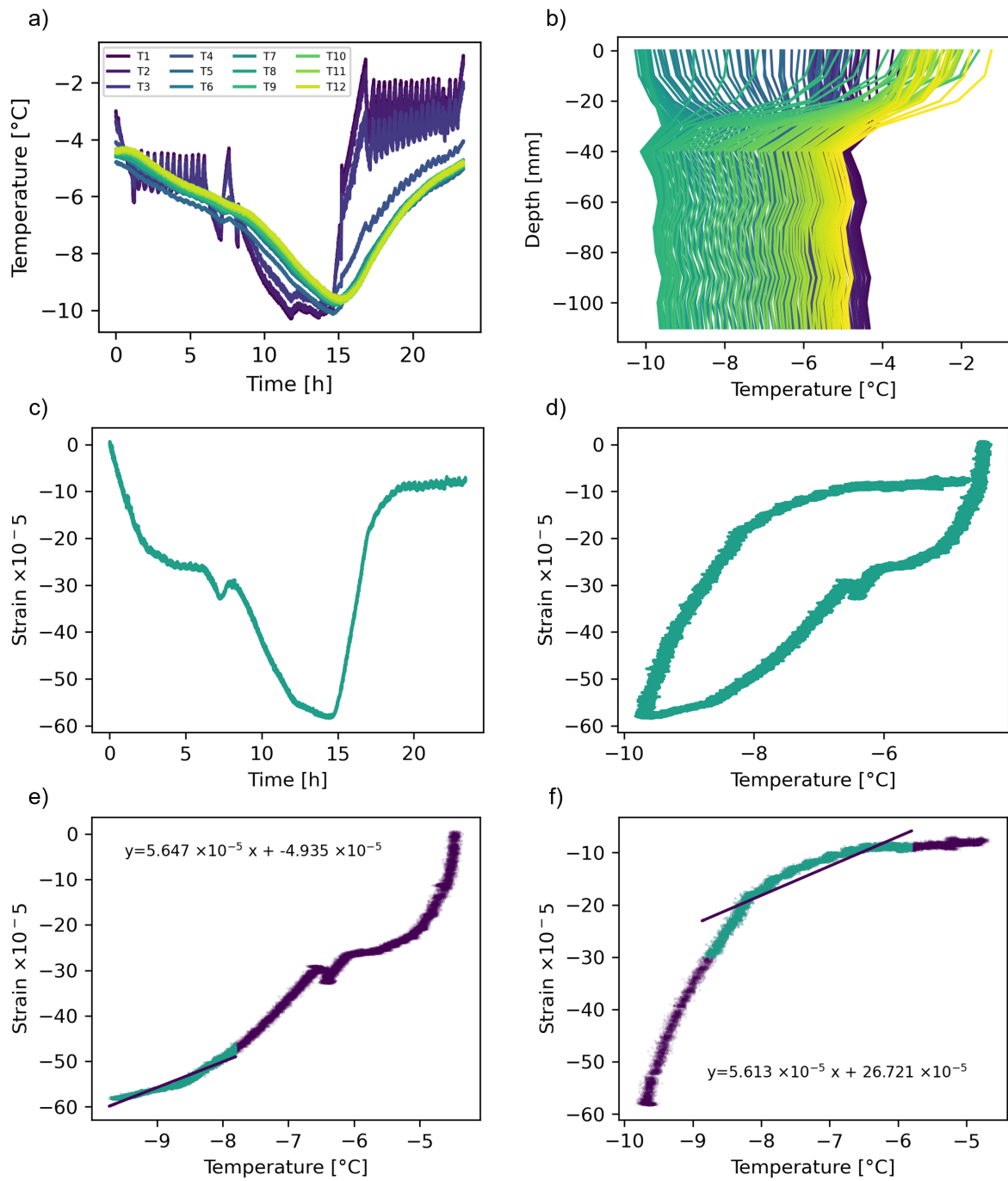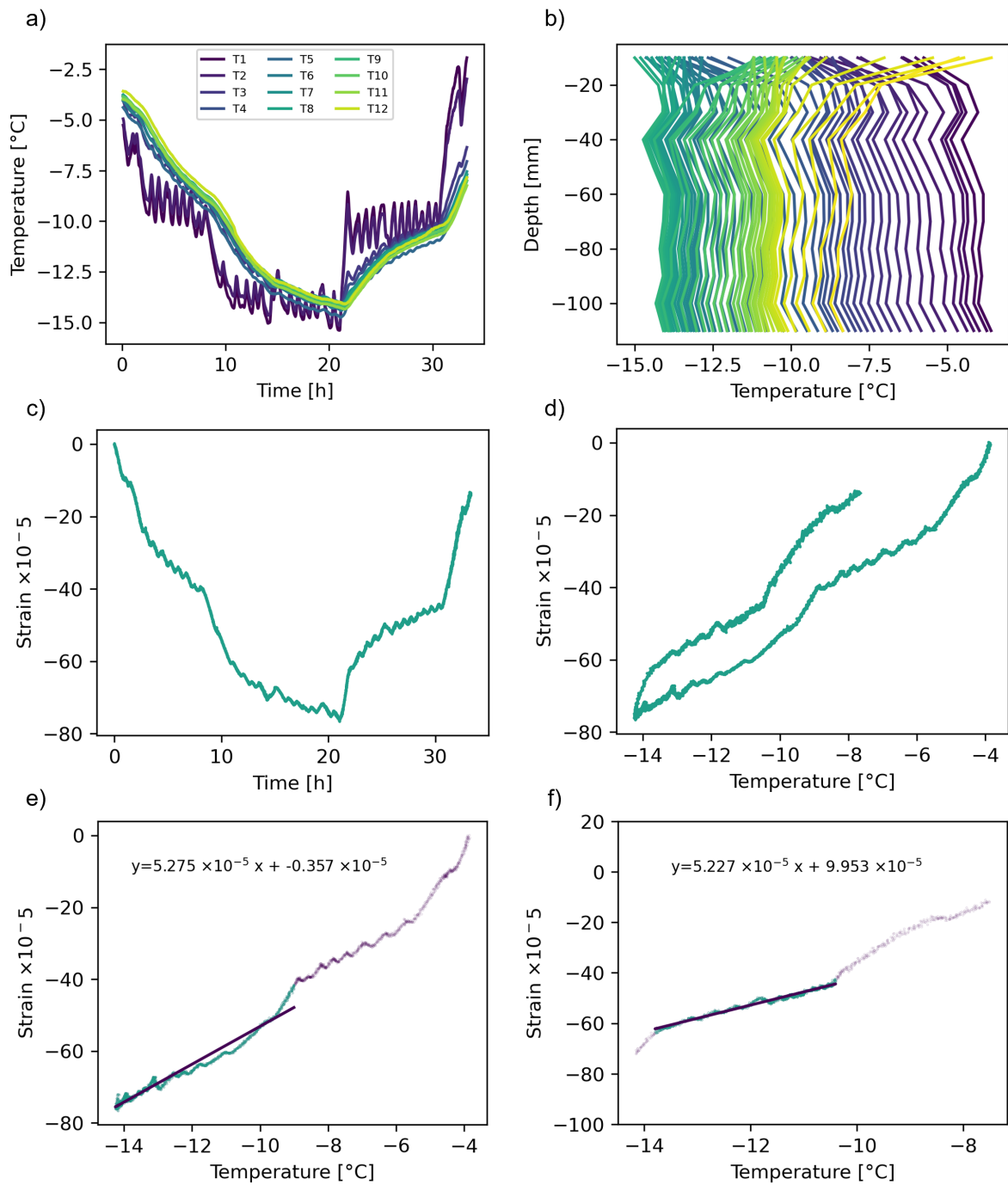
Figure A.4: **Experiment E03**, fresh ice on the table, sample 01A1. (a) Temperature profile, cooling then heating (b) Temperature gradient (c) Strain over time (d) Strain over mean ice temperature (e-f) Strain over mean ice temperature ECTE calculation. The slope of the line equates to the ECTE value for the experiment.
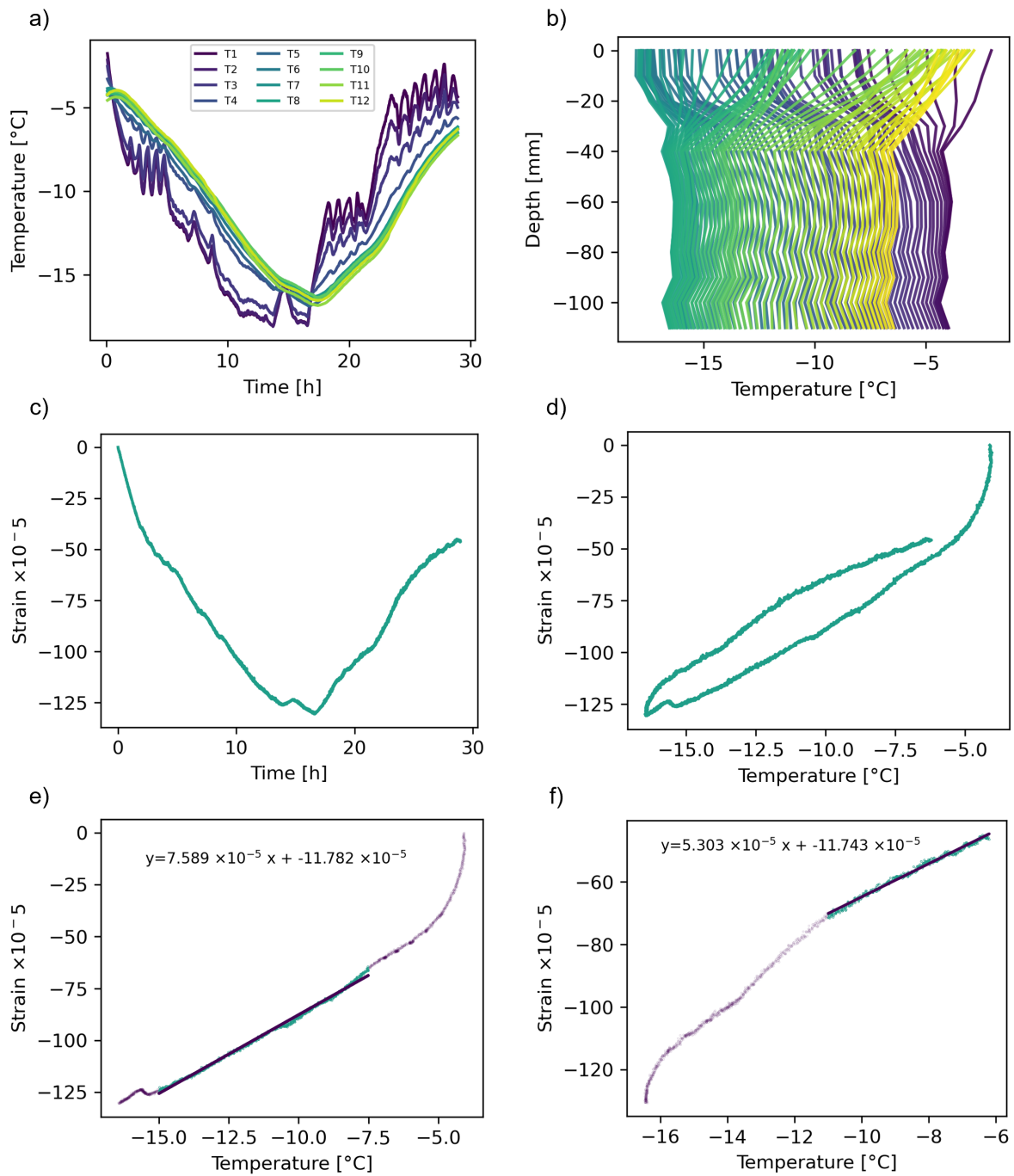
Figure A.5: **Experiment E04**, fresh ice on the table, sample 01B1. (a) Temperature profile, cooling then heating (b) Temperature gradient (c) Strain over time (d) Strain over mean ice temperature (e-f) Strain over mean ice temperature ECTE calculation. The slope of the line equates to the ECTE value for the experiment.
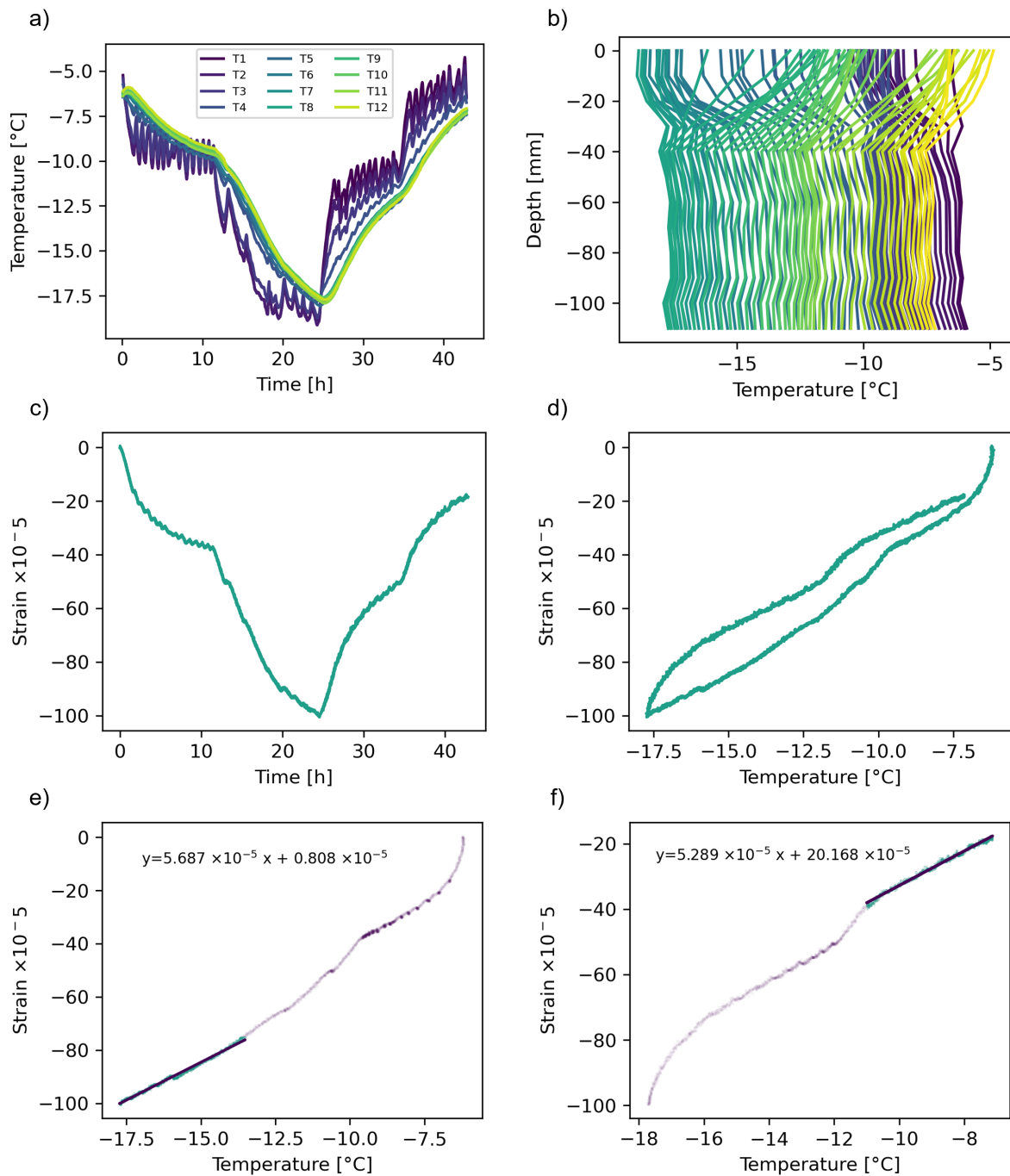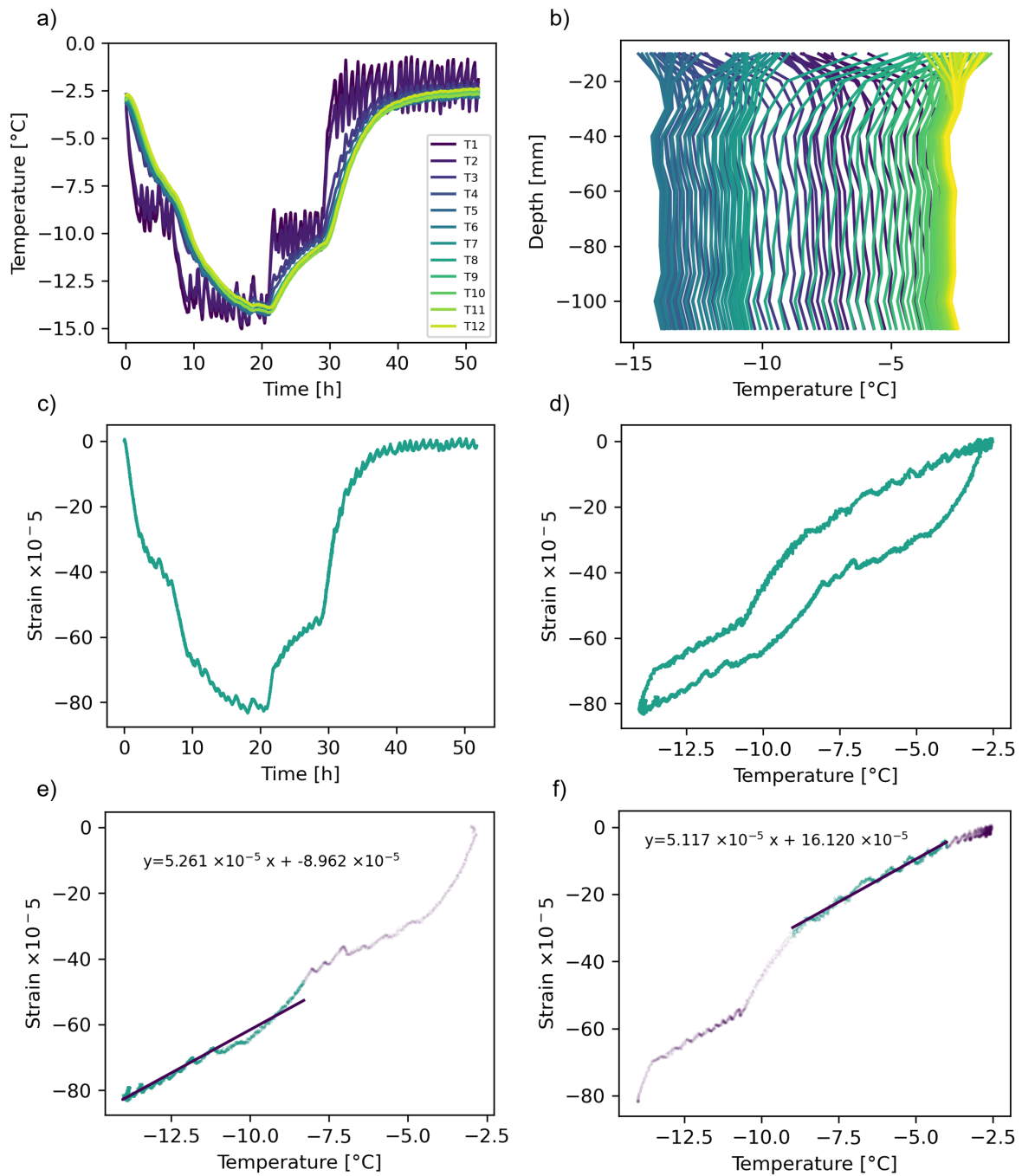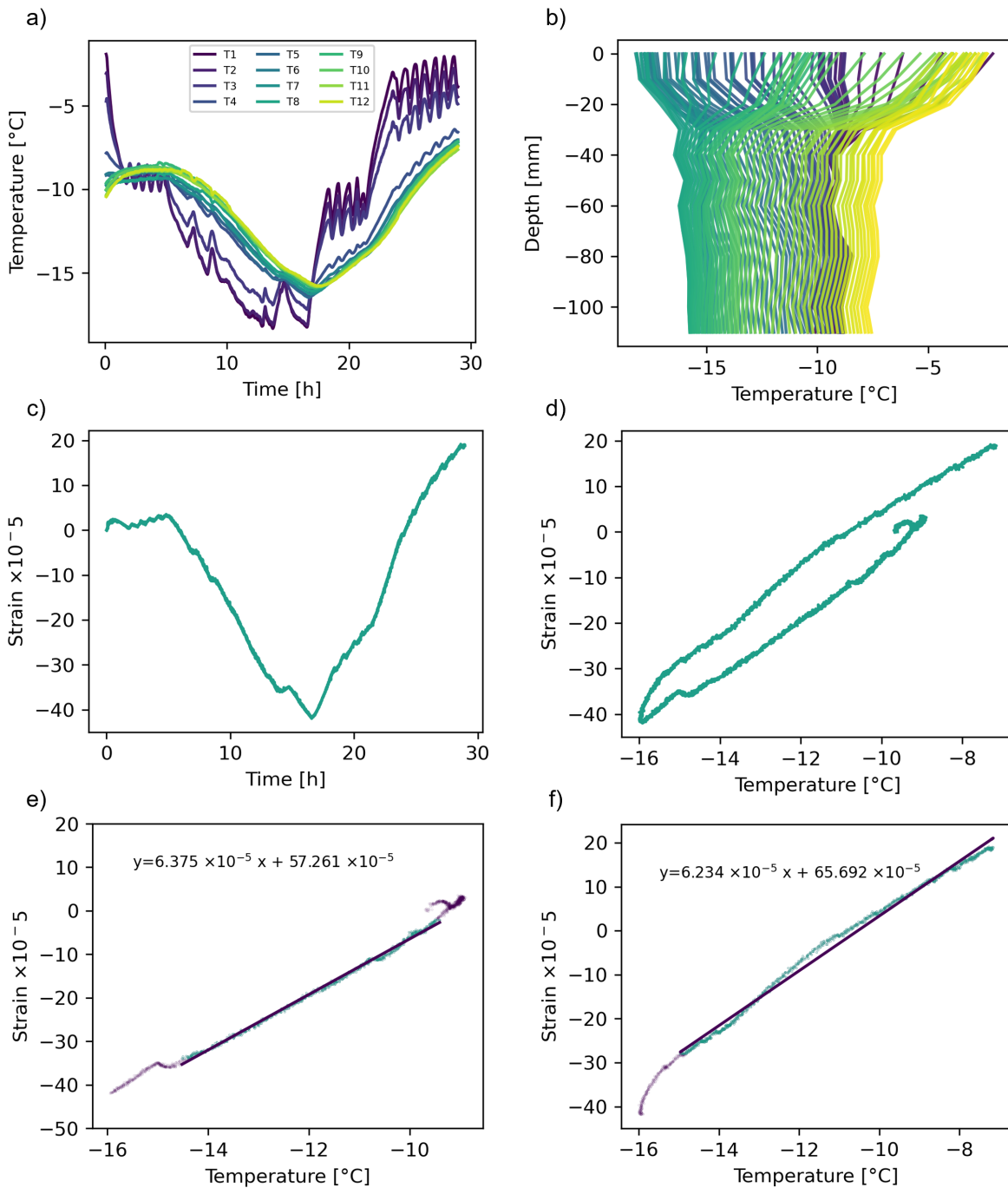
Figure A.6: **Experiment E05**, fresh ice on the table, sample 01B1. (a) Temperature profile, cooling then heating (b) Temperature gradient (c) Strain over time (d) Strain over mean ice temperature (e-f) Strain over mean ice temperature ECTE calculation. The slope of the line equates to the ECTE value for the experiment.

Figure A.7: **Experiment E06**, fresh ice on the table, sample 01B1. (a) Temperature profile, cooling then heating (b) Temperature gradient (c) Strain over time (d) Strain over mean ice temperature (e-f) Strain over mean ice temperature ECTE calculation. The slope of the line equates to the ECTE value for the experiment.
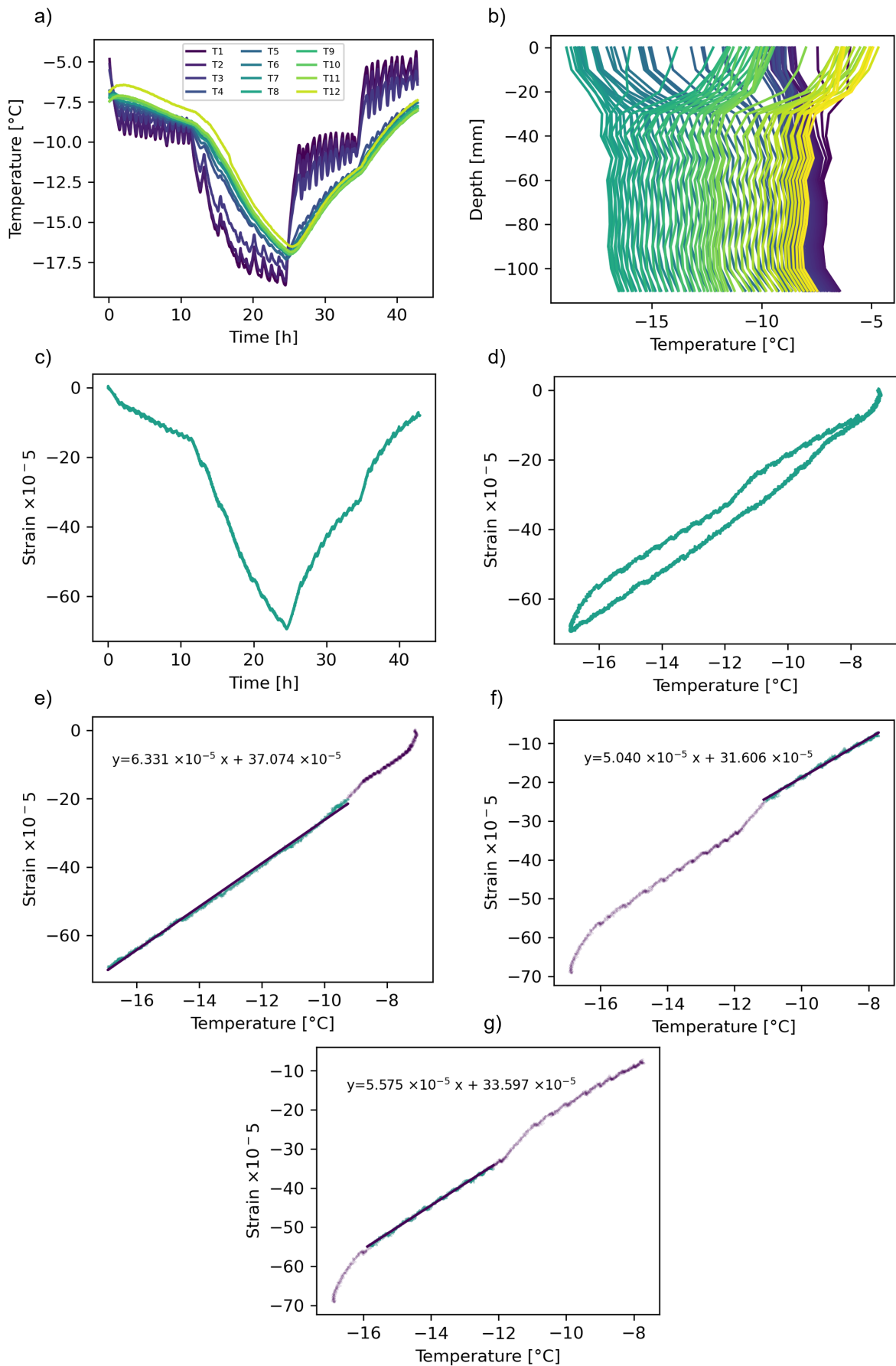
Figure A.8: **Experiment E07**, fresh ice on the table, sample 01B1. (a) Temperature profile, cooling then heating (b) Temperature gradient (c) Strain over time (d) Strain over mean ice temperature (e-f) Strain over mean ice temperature ECTE calculation. The slope of the line equates to the ECTE value for the experiment.

Figure A.9: **Experiment E08**, fresh ice on the table, sample 01B1. (a) Temperature profile, cooling then heating (b) Temperature gradient (c) Strain over time (d) Strain over mean ice temperature (e-f) Strain over mean ice temperature ECTE calculation. The slope of the line equates to the ECTE value for the experiment.
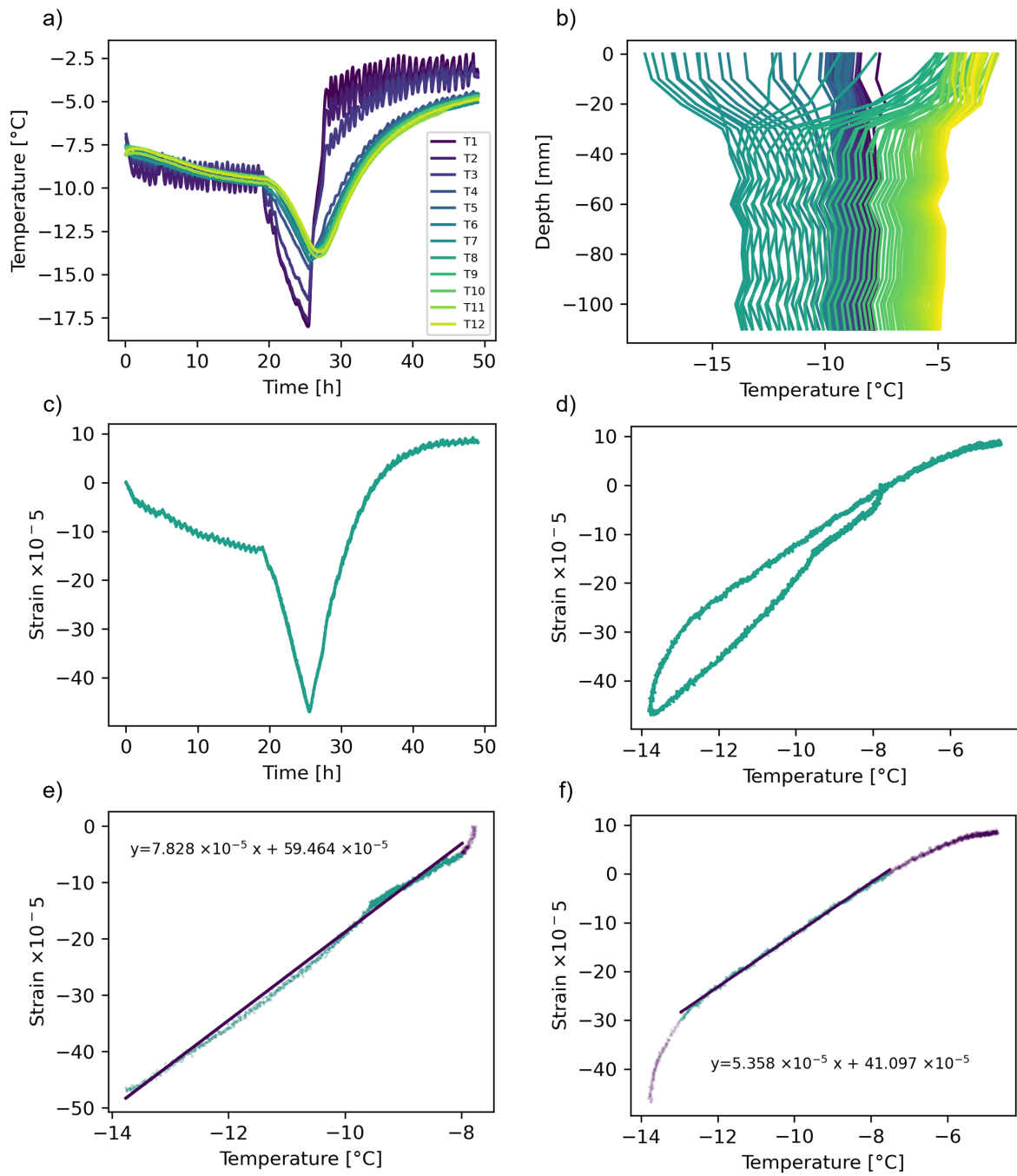
Figure A.10: **Experiment E09**, fresh ice on the table, sample 01B1. (a) Temperature profile, cooling then heating (b) Temperature gradient (c) Strain over time (d) Strain over mean ice temperature (e-f) Strain over mean ice temperature ECTE calculation. The slope of the line equates to the ECTE value for the experiment.

## A.2. Granular saline ice on table, air temperature change experiments

Figure A.11: **Experiment E10**, granular saline ice on the table, sample 02A1. (a) Temperature profile, cooling then heating (b) Temperature gradient (c) Strain over time (d) Strain over mean ice temperature (e-f) Strain over mean ice temperature ECTE calculation. The slope of the line equates to the ECTE value for the experiment.
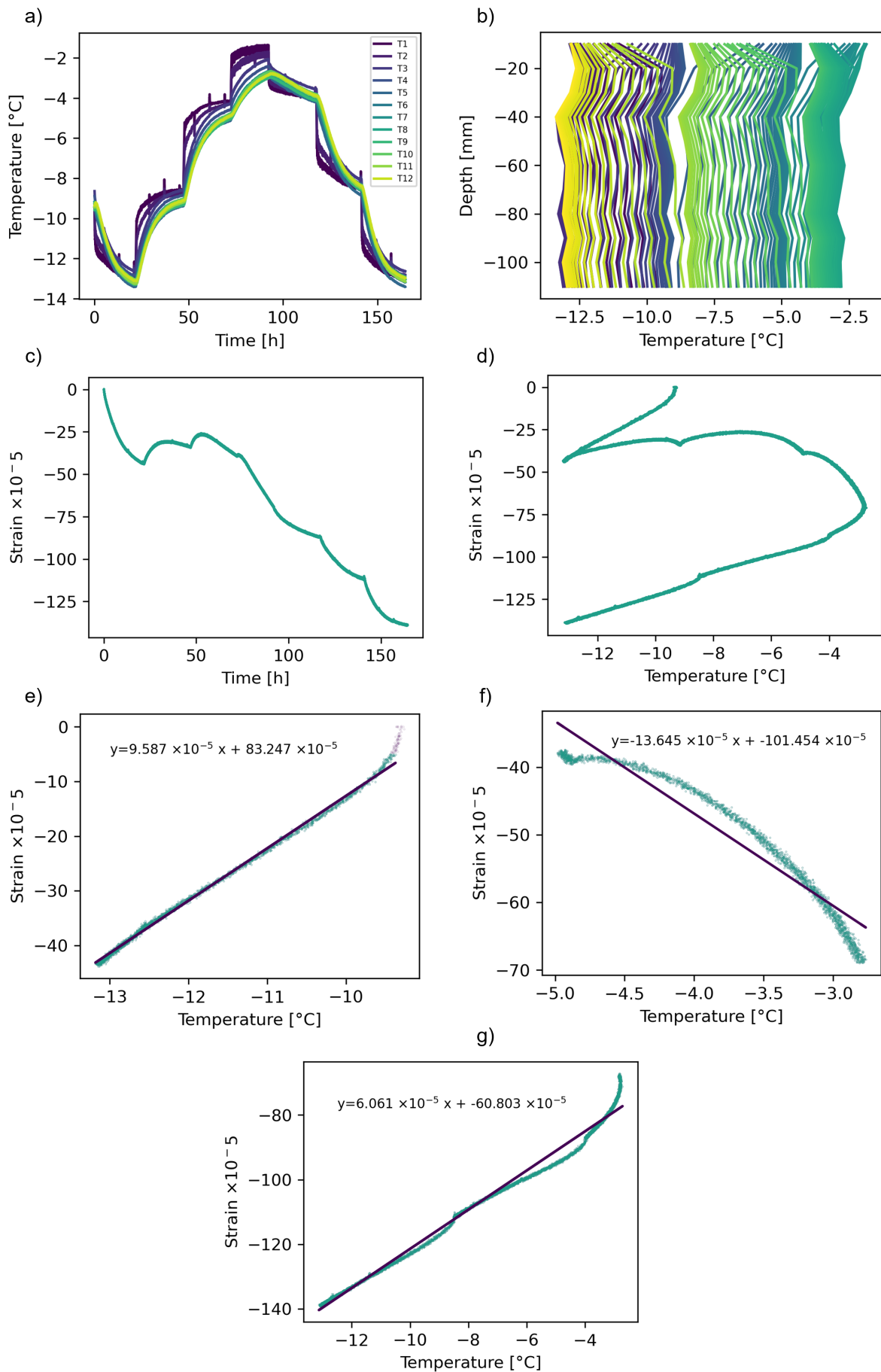
Figure A.12: **Experiment E11**, granular saline ice on the table, sample 02A1. (a) Temperature profile, cooling then heating (b) Temperature gradient (c) Strain over time (d) Strain over mean ice temperature (e-g) Strain over mean ice temperature ECTE calculation. The slope of the line equates to the ECTE value for the experiment.
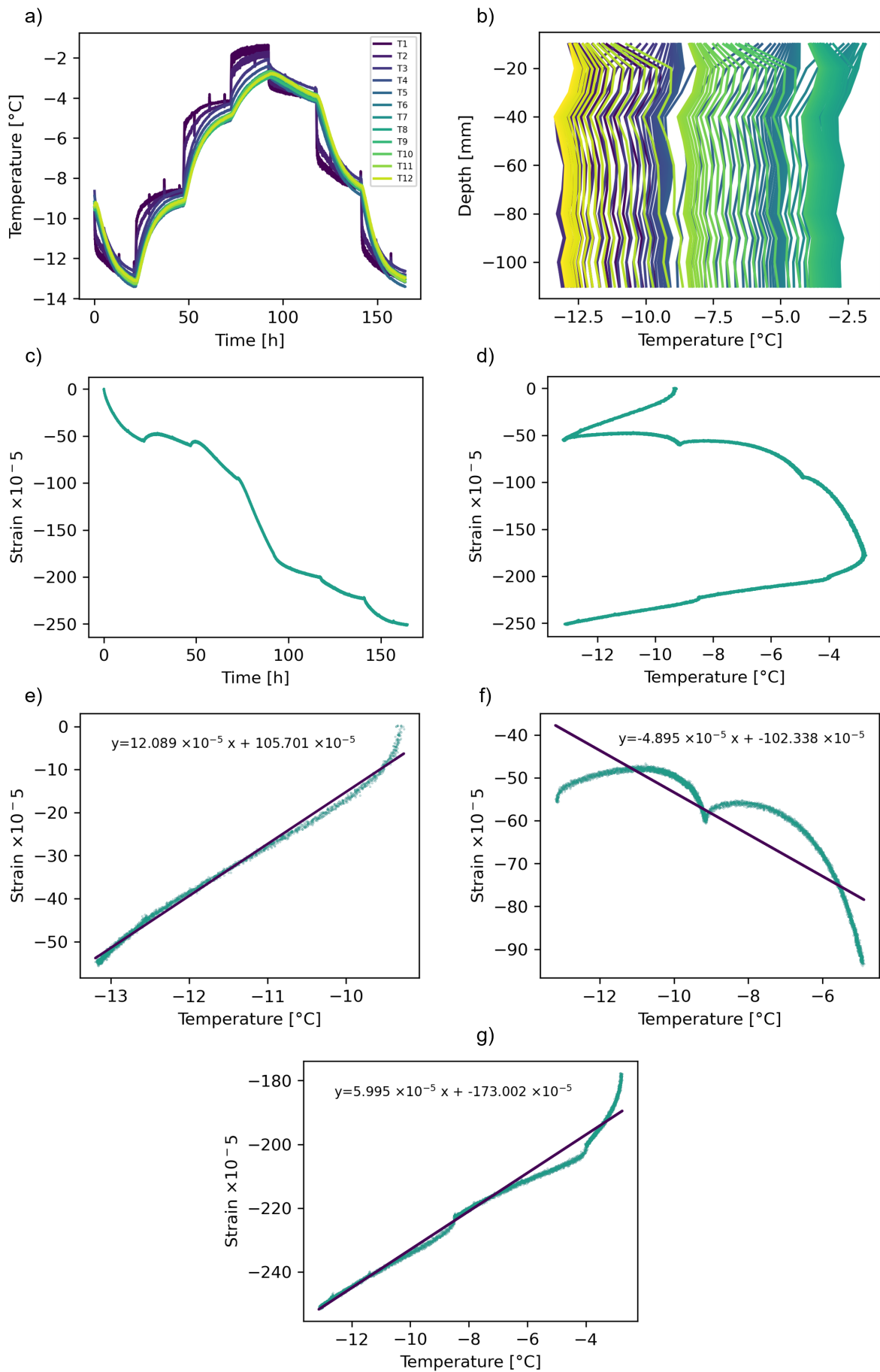
Figure A.13: **Experiment E12**, granular saline ice on the table, sample 02A1. (a) Temperature profile, cooling then heating (b) Temperature gradie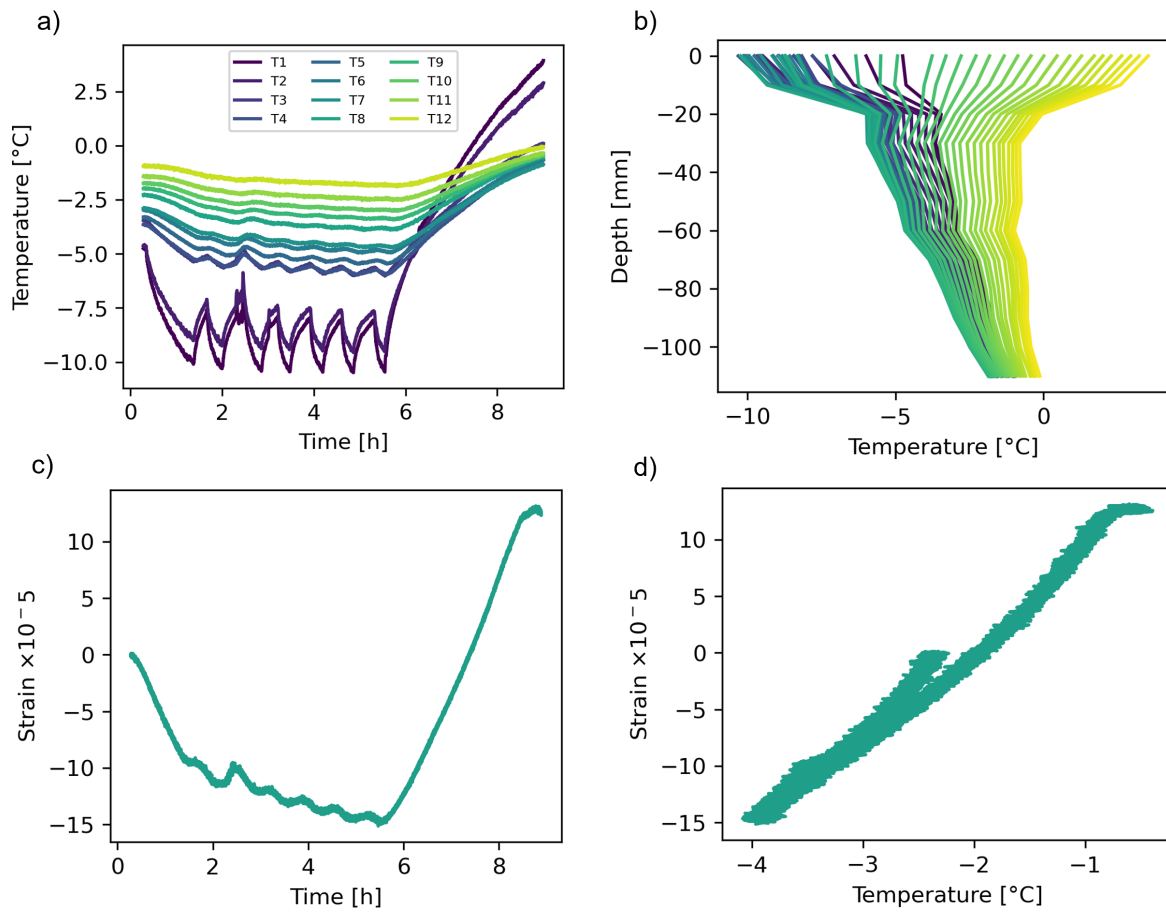nt (c) Strain over time (d) Strain over mean ice temperature (e-f) Strain over mean ice temperature ECTE calculation. The slope of the line equates to the ECTE value for the experiment.

A.3. Svea columnar sea ice on table, air temperature change experiments
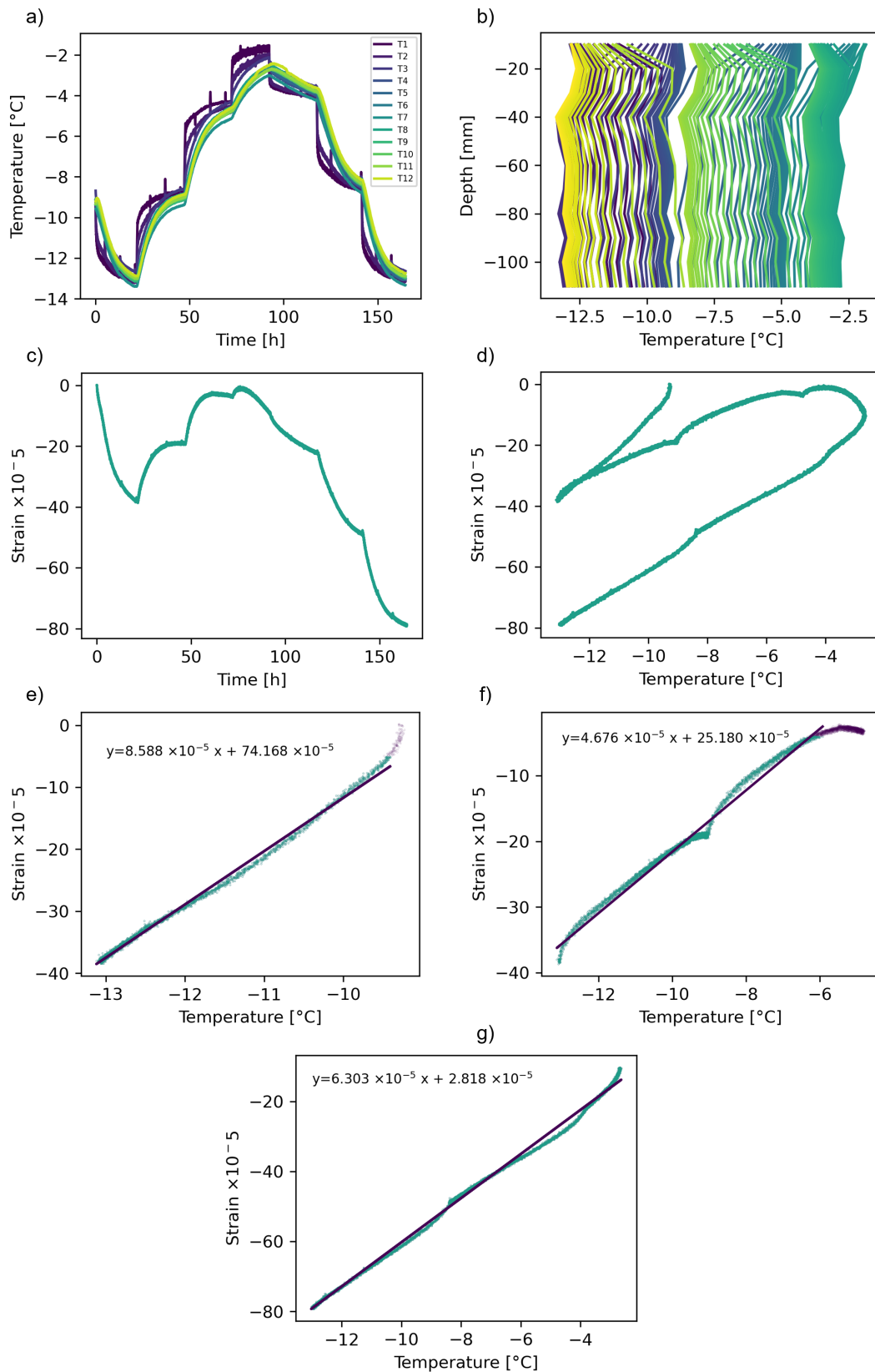
Figure A.14: **Experiment E13**, Svea ice on the table, sample 03A1, depth of 10 cm below the ice surface. (a) Temperature profile, cooling then heating then cooling (b) Temperature gradient (c) Strain over time (d) Strain over mean ice temperature (e-g) Strain over mean ice temperature ECTE calculation. The slope of the line equates to the ECTE value for the experiment.

Figure A.15: **Experiment E13**, Svea ice on the table, sample 03A1, depth of 20 cm below the ice surface. (a) Temperature profile, cooling then heating then cooling (b) Temperature gradie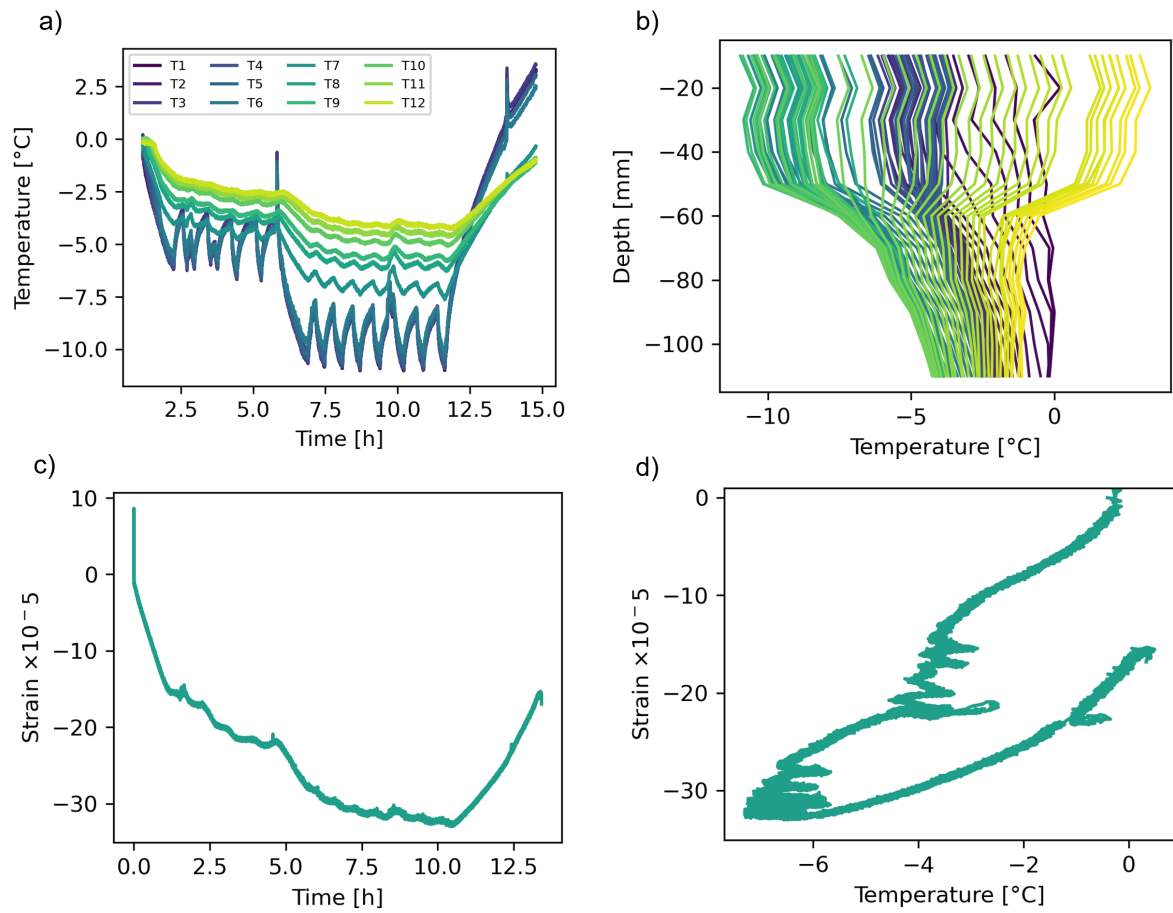nt (c) Strain over time (d) Strain over mean ice temperature (e-g) Strain over mean ice temperature ECTE calculation. The slope of the line equates to the ECTE value for the experiment.

Figure A.16: **Experiment E13**, Svea ice on the table, sample 03A1, depth of 30 cm below the ice surface. (a) Temperature profile, cooling then heating then cooling (b) Temperature gradient (c) Strain over time (d) Strain over mean ice temperature (e-g) Strain over mean ice temperature ECTE calculation. The slope of the line equates to the ECTE value for the experiment. Negative ECTE values were found in this test.

A.4. Floating fresh ice
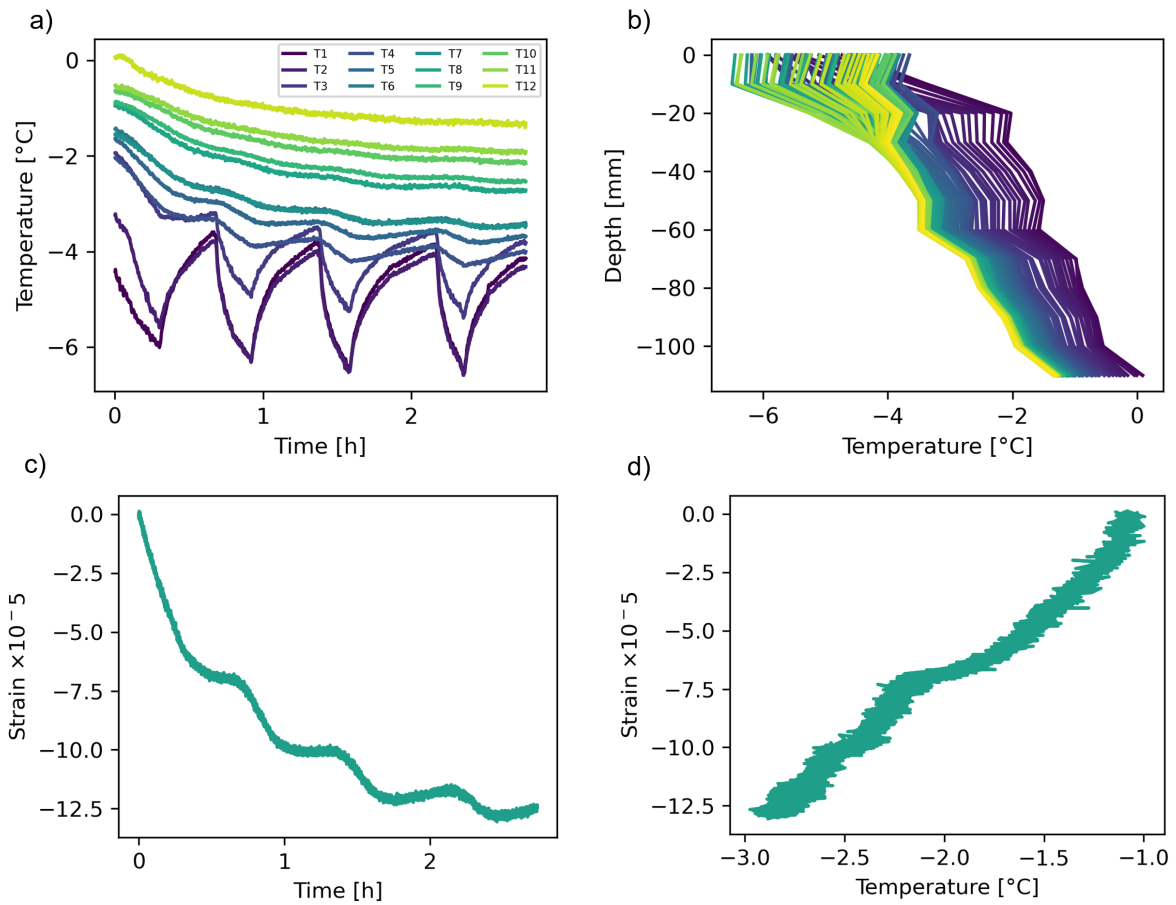
Figure A.17: **Experiment E14**, Floating fresh ice, sample 01B1. (a) Temperature profile, cooling (b) Temperature gradient (c) Strain over time (d) Strain over mean ice temperature

Figure A.18: **Experiment E15**, Floating fresh ice, sample 01B1. (a) Temperature profile, cooling then heating (b) Temperature gradient (c) Strain over time (d) Strain over mean ice temperature
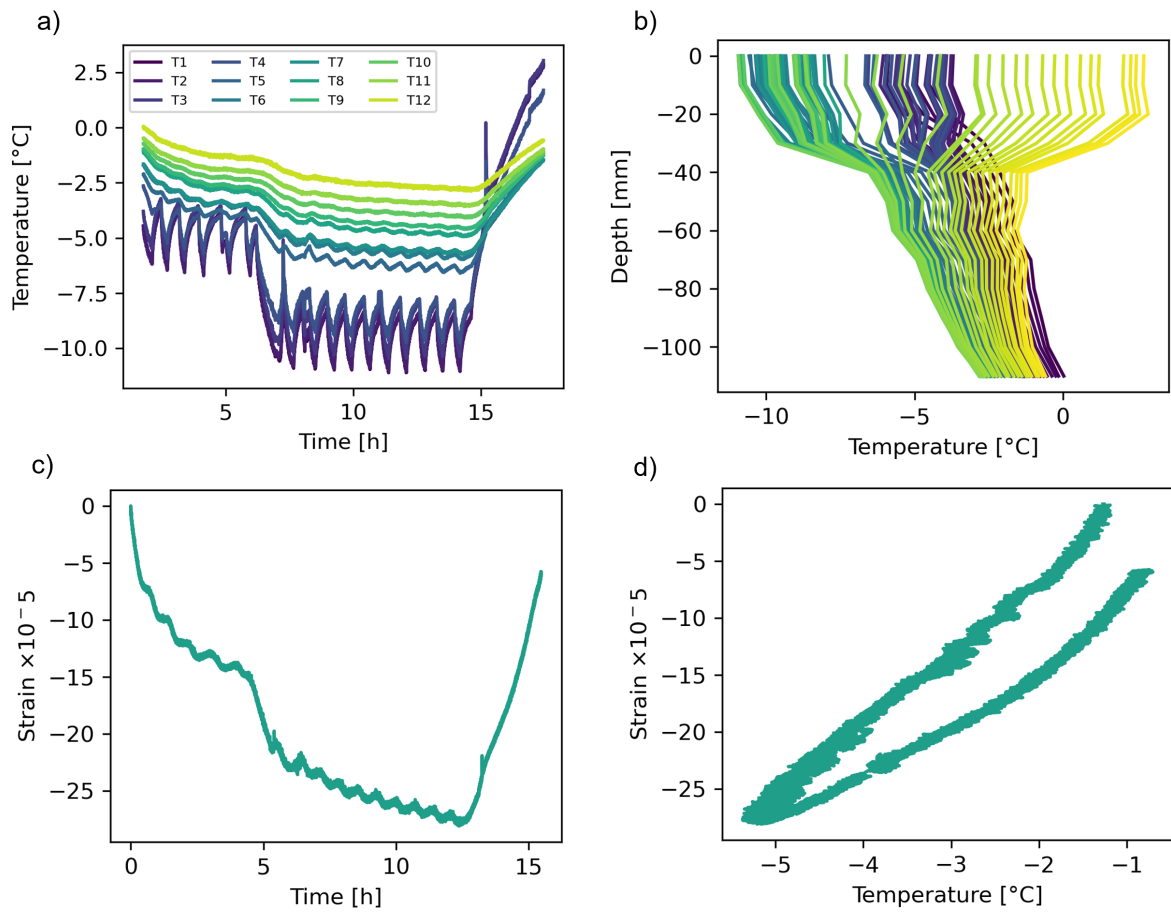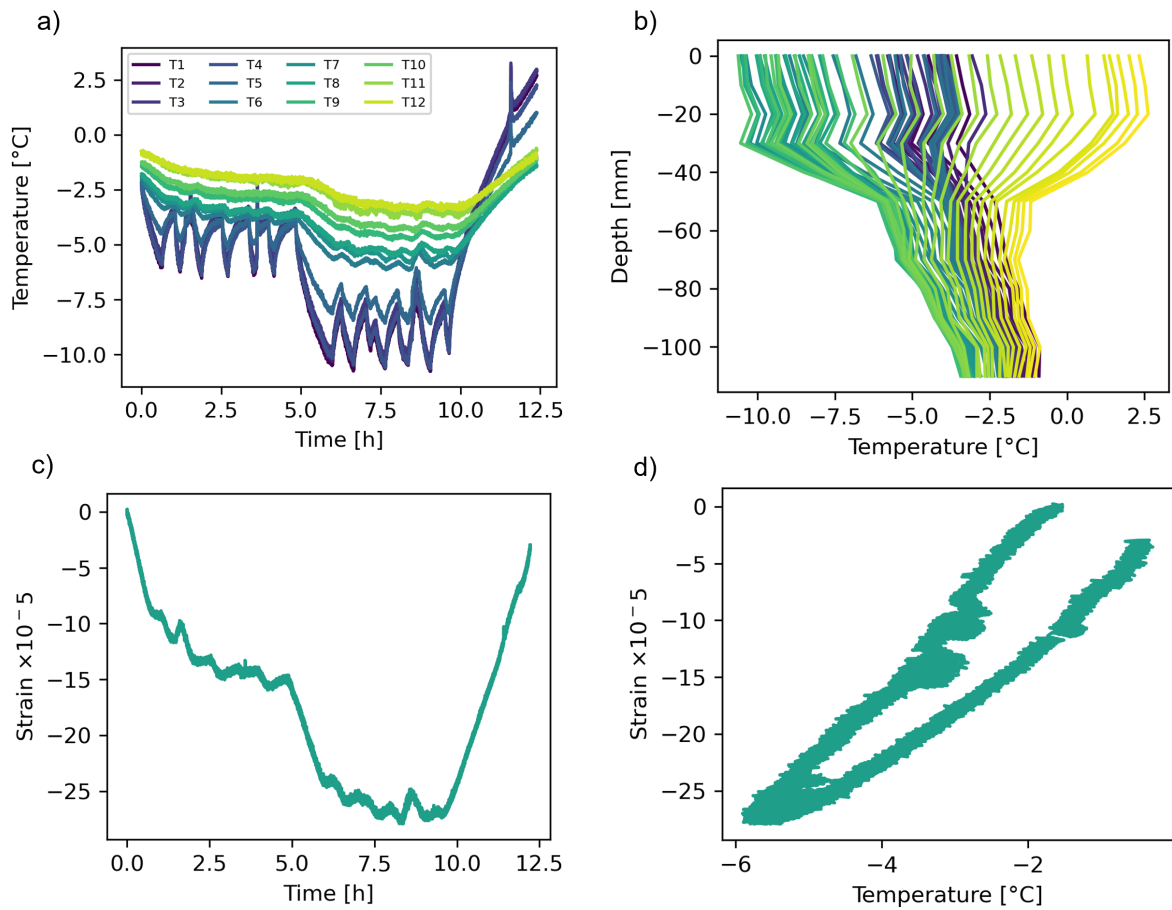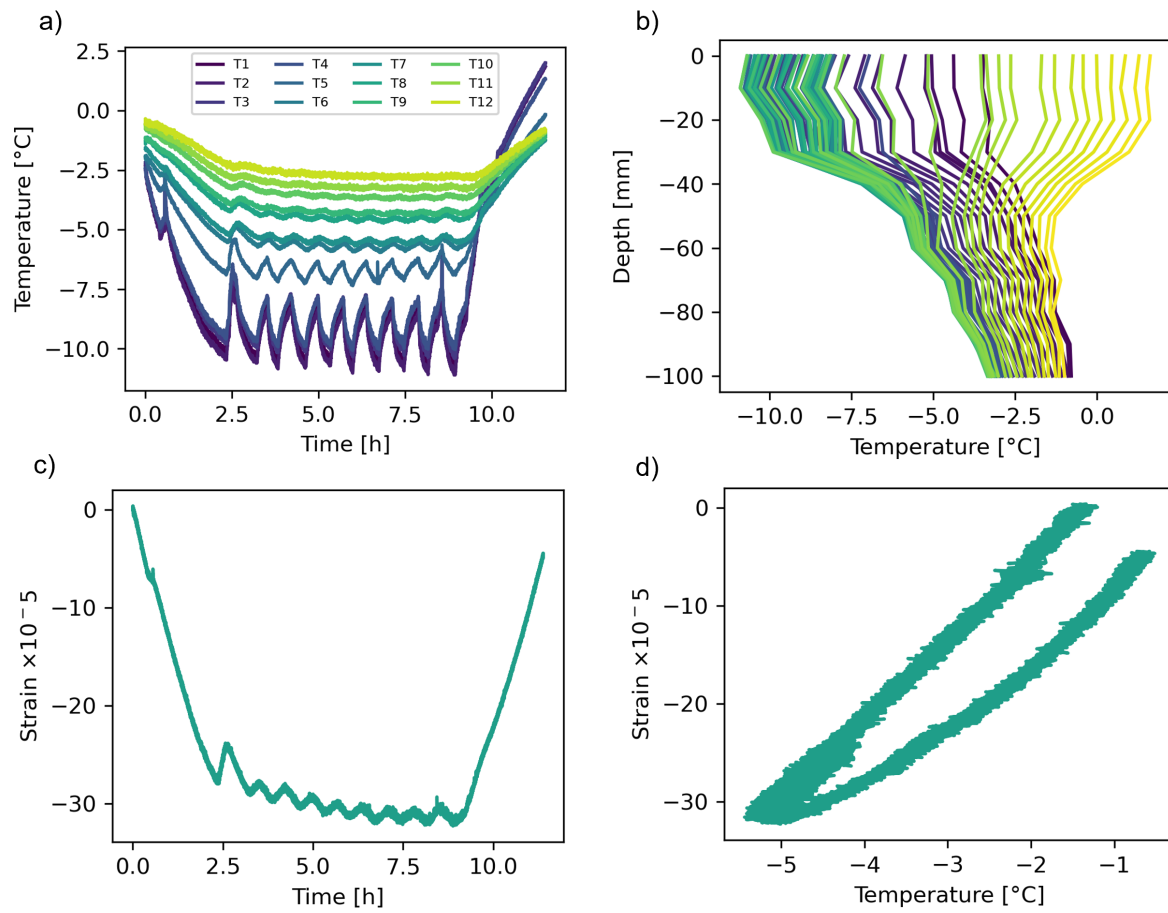
Figure A.19: **Experiment E16**, Floating fresh ice, sample 01B1. (a) Temperature profile, cooling then heating (b) Temperature gradient (c) Strain over time (d) Strain over mean ice temperature

Figure A.20: **Experiment E17**, Floating fresh ice, sample 01B1. (a) Temperature profile, cooling then heating (b) Temperature gradient (c) Strain over time (d) Strain over mean ice temperature
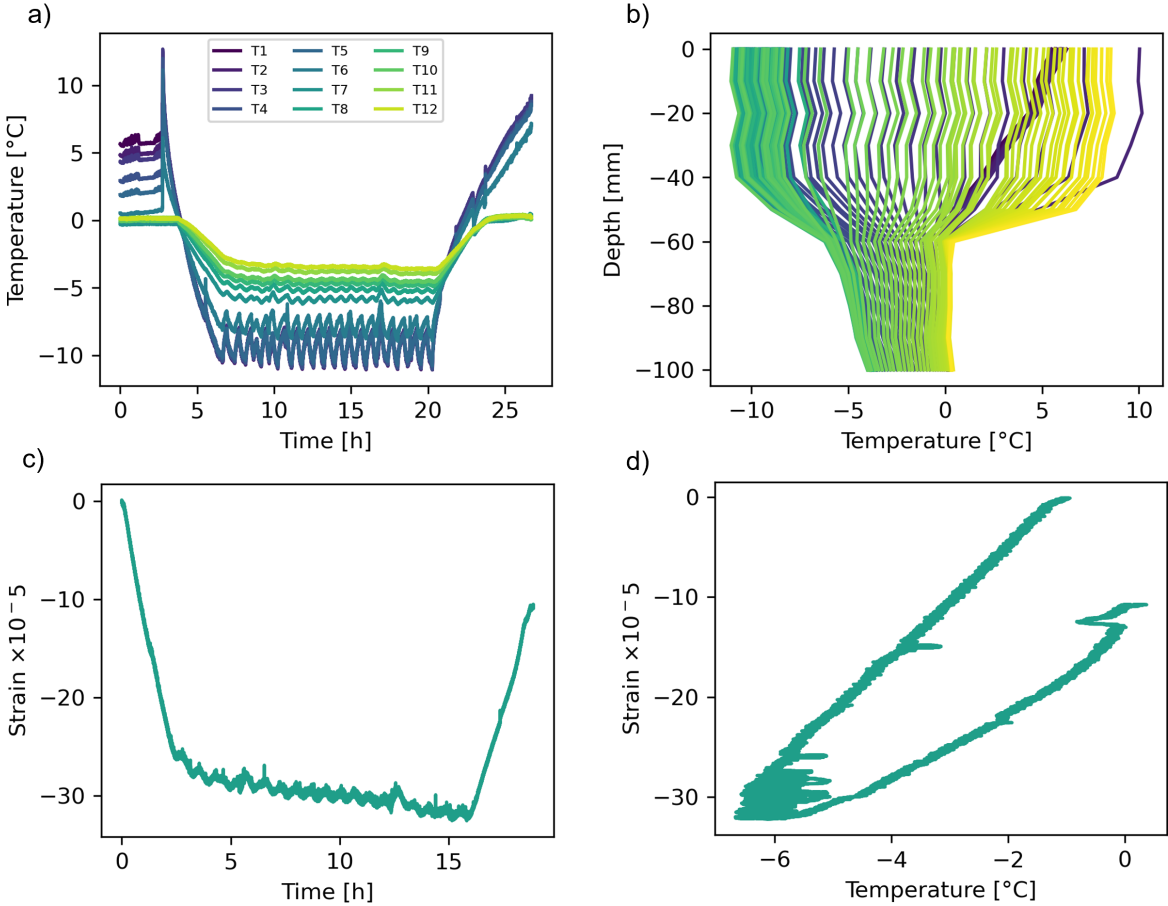
Figure A.21: **Experiment E18**, Floating fresh ice, sample 01B1. (a) Temperature profile, cooling then heating (b) Temperature gradient (c) Strain over time (d) Strain over mean ice temperature (TS5 to TS12)

Figure A.22: **Experiment E19**, Floating fresh ice, sample 01B1. (a) Temperature profile, cooling then heating (b) Temperature gradient (c) Strain over time (d) Strain over mean ice temperature

Figure A.23: **Experiment E20**, Floating fresh ice, sample 01B1. (a) Temperature profile, cooling then heating (b) Temperature gradient (c) Strain over time (d) Strain over mean ice temperature
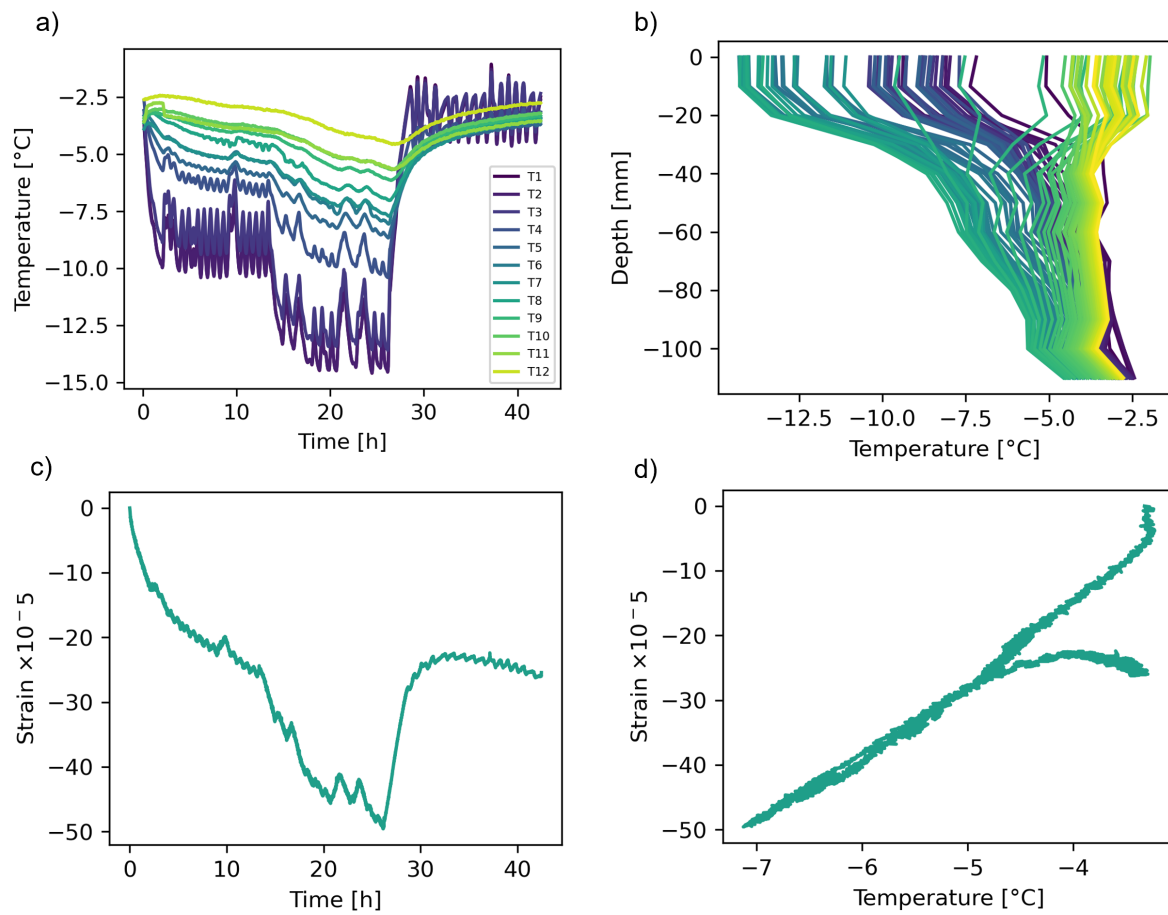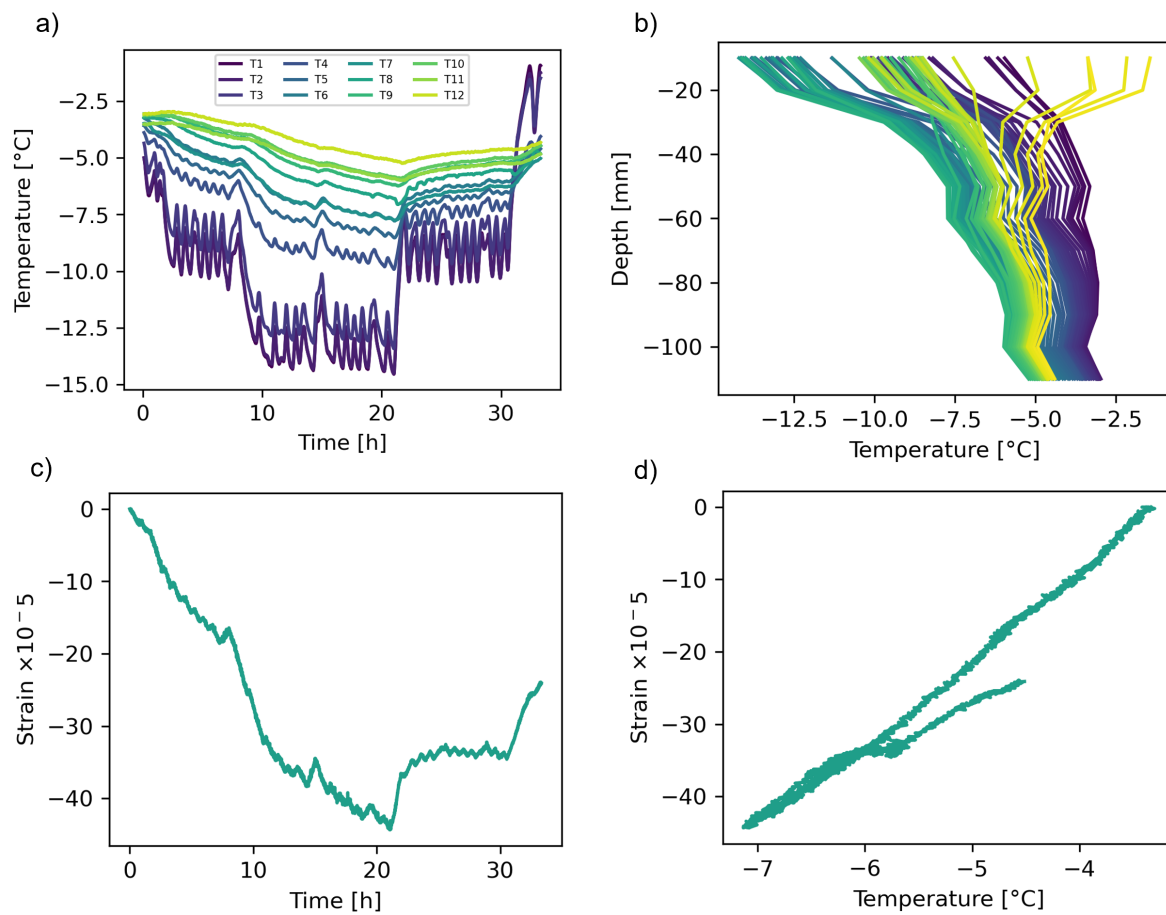
A.5. Floating granular saline ice

Figure A.24: **Experiment E21**, Floating granular saline ice, sample 02A1. (a) Temperature profile, cooling then heating (b) Temperature gradient (c) Strain over time (d) Strain over mean ice temperature

Figure A.25: **Experiment E22**, Floating fresh ice, sample 02A1. (a) Temperature profile, cooling then heating (b) Temperature gradient (c) Strain over time (d) Strain over mean ice temperature
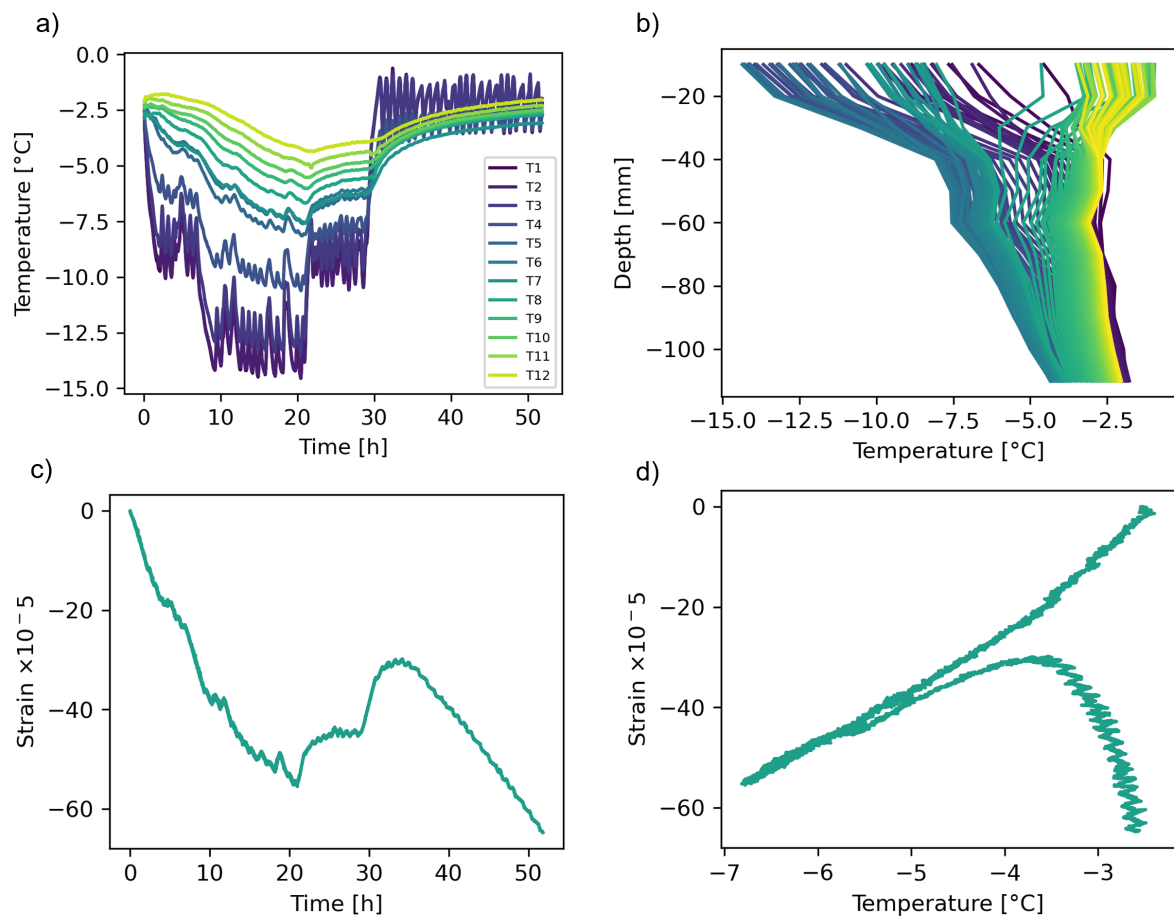
Figure A.26: **Experiment E23**, Floating fresh ice, sample 02A1. (a) Temperature profile, cooling then heating (b) Temperature gradient (c) Strain over time (d) Strain over mean ice temperature

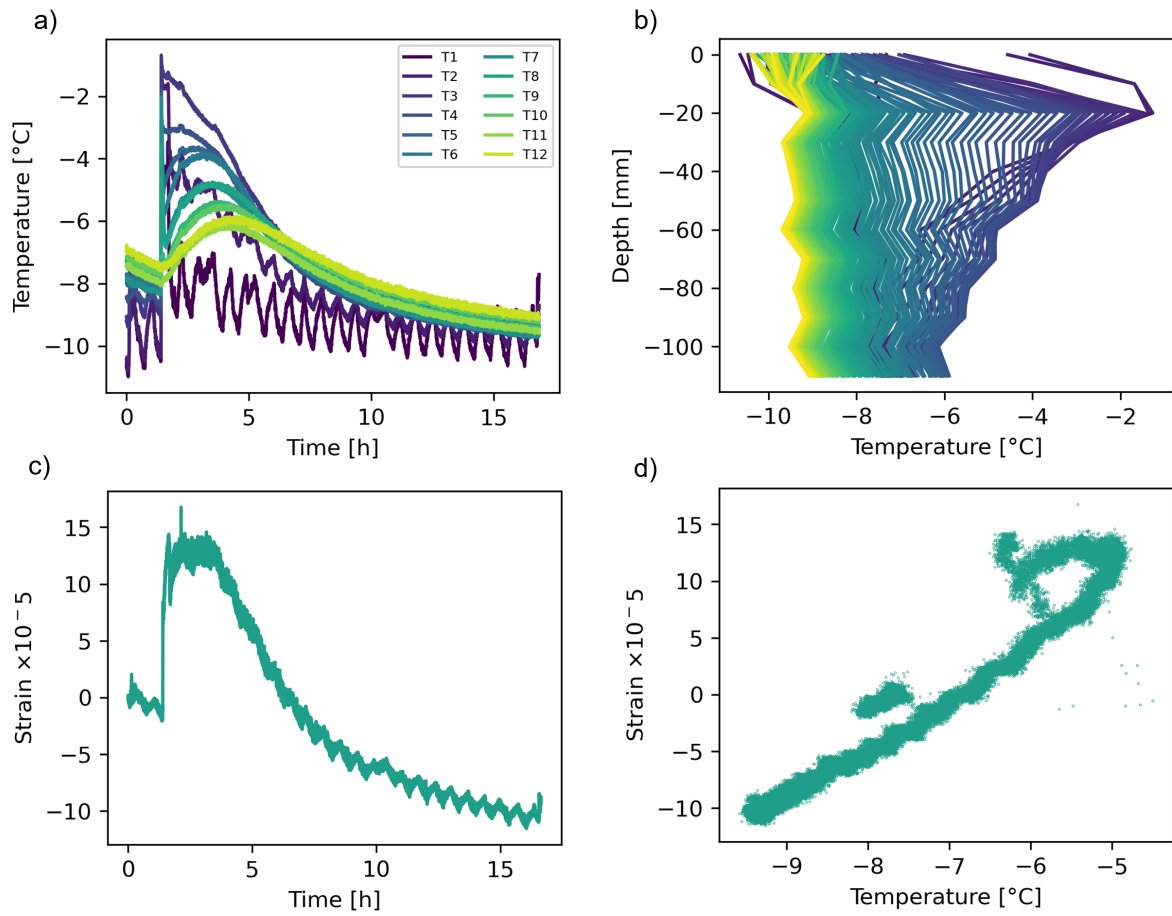## A.6. Flooding experiment: fresh and saline ice

Figure A.27: **Experiment E23**, Pool experiment with granular saline ice, sample 02A1. (a) Temperature profile (b) Temperature gradient (c) Strain over time (d) Strain over mean ice temperature
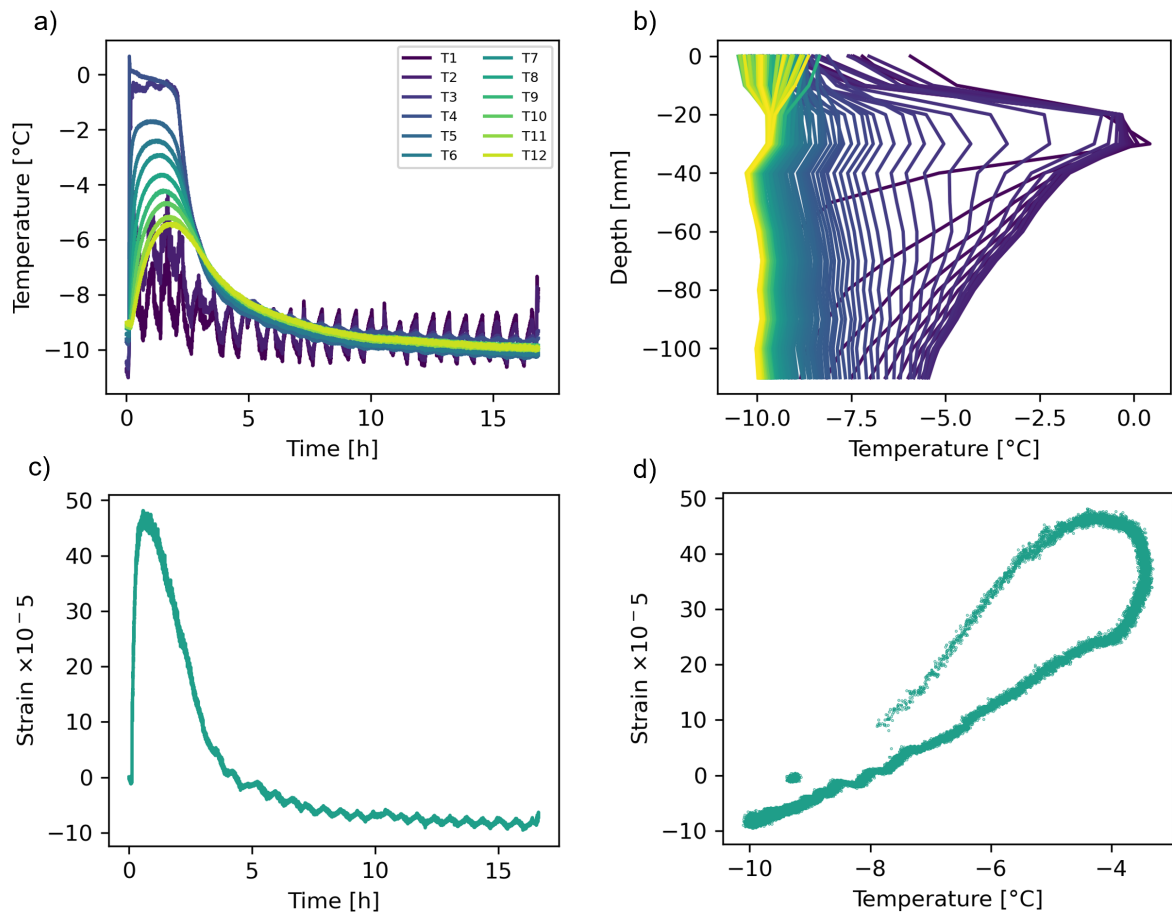
Figure A.28: **Experiment E24**, Pool experiment with fresh ice, sample 01B1. (a) Temperature profile (b) Temperature gradient (c) Strain over time (d) Strain over mean ice temperature